X-661-71-461

NASA TM X- 65753

GODDARD SPACE FLIGHT CENTER CONTRIBUTIONS TO THE TWELFTH INTERNATIONAL CONFERENCE ON COSMIC RAYS, HOBART, TASMANIA, 1971

NOVEMBER 1971

GSFC

GODDARD SPACE FLIGHT CENTER

GREENBELT, MARYLAND

GODDARD SPACE FLIGHT CENTER CONTRIBUTIONS TO THE TWELFTH INTERNATIONAL CONFERENCE ON COSMIC RAYS

HOBART, TASMANIA 1971

November, 1971

TABLE OF CONTENTS

THE COSMIC RAY PROTON AND HELIUM SPECTRA ABOVE 50 GeV

M. J. Ryan*, V. K. Balasubrahmanyan, and J. F. Ormes

Goddard Space Flight Center, Greenbelt, Md. 20771

Abstract

The primary cosmic ray proton and He spectra from 50 GeV to 2000 GeV have been measured by an ionization spectrometer flown on a balloon at an altitude of 6 gm cm^{-2} for 16 hours. The geometrical factor of the instrument was 300 cm^2 sterad and more than 5,000 events were observed. At low energies, the energies of individual events can be determined to within $\pm$30%. At higher energies, the cascade is not fully contained within the four mean free path thick spectrometer and the problems of estimating the energies of these events will be discussed. The proton spectrum continues with constant exponent $=-2.7\pm0.1$ up to energies greater than 1,000 GeV. This spectrum is in agreement with the results of Pinkau et al. (1969) at the low energies. However, there is no evidence for the spectral break at about 1,000 GeV as reported by Grigorov et al. (1969).

1. Introduction

In this paper we report measurements of the proton and helium energy spectra obtained at balloon altitudes using an ionization spectrometer of depth 4 m.f.p. and 2,500 cm^2 cross sectional area. An outline of the arrangement of the detectors is shown in Fig. 1. The major part of the spectrometer is the 7 iron modules each 0.5 proton m.f.p. (5 radiation lengths) thick. Notice that there are 3 plastic scintillators in each module so that an observed detector output of N particles is actually an average of the three sampling scintillators. This averaging helps to reduce fluctuations of the nuclear cascades but allowances must be made for this averaging when reconstructing shower curves in regions of rapid development.

Above the iron section are 12 tungsten modules each 1 radiation length thick, making a total of 0.48 proton m.f.p. of tungsten. An incident primary particle is identified in the charge module section which contains 2 plastic scintillators, a Cerenkov counter and a CsI scintillator. A wire grid spark chamber containing 4 X-Y planes defines the particle trajectory and is helpful in rejecting background events.

All detector outputs are normalized to a single particle output defined as the mean energy loss of a single muon which passes through the entire spectrometer. In the proton mode the spectrometer is triggered by an energy release $>$ 50 GeV in the first five iron modules. Fig. 2 shows 4 events obtained during the balloon flight. The frequent independent sampling of this spectrometer allows a good estimate of the first interaction point of the incoming particles. For protons an interaction is defined to have occurred in the first detector whose output is greater than 3 particles provided that the following 2 detectors have outputs greater than 5 particles. For He nuclei the corresponding particle numbers are 7, 10, and 10. Basically the definition requires that a neutral pion of energy $>$ 0.5 GeV be produced at that point.

*NAS/NRC Research Associate

The ability to specify the first interaction point removes a major source of fluctuation in shower development, but the remaining fluctuations in nuclear disintegration energy and in cascade development limit the estimation of the energy of individual events to $\pm 25\%$. A more serious problem is that for large energy primaries the nuclear cascade is not contained within the 4 m.f.p. depth of the spectrometer and some energy escapes out the bottom as suggested by curves 2 and 4 of Fig. 2.

2. Calibration and Energy Estimation

The spectrometer was calibrated with 10, 15 and 20 GeV protons from A.G.S. at the Brookhaven National Laboratory. The total calorimeter output formed by summing the seven iron modules was found to be directly proportional to the incident proton energy. The excellent energy resolution obtainable with this type of instrument is shown in Fig. 3. The observed output implies that at these low energies 60% of the incident energy is being sampled by the scintillators. However, these energies are lower than those of the cosmic rays of interest and so a similar instrument will be calibrated at the National Accelerator Laboratory later this year. This should provide accurate calibration up to proton energies of 500 GeV. Theoretical and Monte Carlo calculations (1), (2) show that the total output of an infinitely deep absorber will be directly proportional to the incident energy up to energies of at least 10^4 GeV. To estimate the energy escaping out the bottom of our finite depth instrument we have extrapolated the mean shower curves shown in Fig. 4.

The lowest curve is that obtained with 17.6 GeV/c protons at Brookhaven. The flight data curves are constructed for events which interacted in the first iron module and penetrated the bottom of the spectrometer. They are grouped according to the sum over seven modules. The extrapolated curves indicate that the fraction of energy escaping increases from 3% at 40 GeV to 22% at 40 GeV. The correction for high energy events has been estimated from

$$C = 8.3 \ln E_7 - 28 \qquad (1)$$

where E_7 is the energy obtained by summing over all 7 modules.

In order to increase the effective geometry factor, we have also used those events which exited after 5 iron modules i.e., 3 m.f.p. To estimate the energies of these events we have used a weighted mean of modules 4 and 5 and extrapolated assuming that the showers are exponentially absorbed with an attenuation length of 240 gm cm^{-2}(3). A cross check of this method has been made using those events which exited beyond the 7th module, and it is found that the energy estimates using 5 and 7 modules are in good agreement.

We have also investigated using the number of particles at shower maximum as an energy estimator but the dispersion within groups of events is much larger. The number at maximum increases as $E^{0.8}$. Similar corrections have been estimated for He at the same energy/nucleon.

4. Energy Spectra

Using the corrections outlined above, we obtain the primary energy spectra shown in Fig. 5. We have included data from 12 hours of flight at an altitude of 6 gm cm^{-2}. The sensitive live time was 68% and the geometrical factor was

330 cm^2 ster. The fluxes shown have been corrected to the top of the atmosphere (x 1.15), for particles which interact beyond module 3 (x 1.30) for spark chamber inefficiency (x 1.2) and for backscattering (x 1.25). These corrections will be discussed in detail in a paper to be published.

The spectra show that the ratio of protons to the nuclei remains constant up to total energies of 3,000 GeV. We have checked the influence of backscatter (< 25% at 17.6 GeV/c) on our spectra by observing that the spectrum has the same slope for the groups of events which interact in the first, second, and third modules. The loss of events due to backscattering of multiple particles into the charge module from a depth of 1.5 m.f.p. should be small due to the large thicknesses of material and the small solid angle (.60 sterad) into which high energy products would have to be backscattered.

Our measurements do not give any evidence for the change in slope of the proton spectrum observed by Grigorov in the region of 1,000 GeV. If the proton spectrum continues with constant exponent to above 10^{13} eV then the observed spectra at mountain altitudes suggest that there is a change in the proton air nuclei cross section at those energies. It is hoped that these discrepancies will be resolved by the spectrometer similar to the one described above, which is being designed for the High Energy Astronomy Satellite.

5. References

Grigorov, N.L., V.E. Nestorov, I.D. Rapoport, I.A. Savenko, G.A. Skuridin, 1969, Proc. XI Int. Conf. on Cosmic Rays, 1, 518.

Jones, W.V., 1969, Phys. Rev. 187, 1868.

Jones, W.V., 1969, Proc. XIth Int. Conf. on Cosmic Rays.

Jones, L.W., et al., 1970, "Properties of Proton-Proton Interactions between 70 to 600 GeV", Proceedings of the XI Interamerican Seminar on Cosmic Rays, La Paz, Bolivia (to be published).

Kamata, K., et al., 1969, Proc. XIth Int. Conf. on Cosmic Rays, 3, 49.

Murzin, V.S., 1967, Progress in Elementary Particles and Cosmic Ray Physics, 9, North Holland Publishing Co., Amsterdam.

Pinkau, K., U. Pollvogt, W.K.H. Schmidt and R.W. Huggett, 1969, Proc. XIth Conf. on Cosmic Rays, 3, 291.

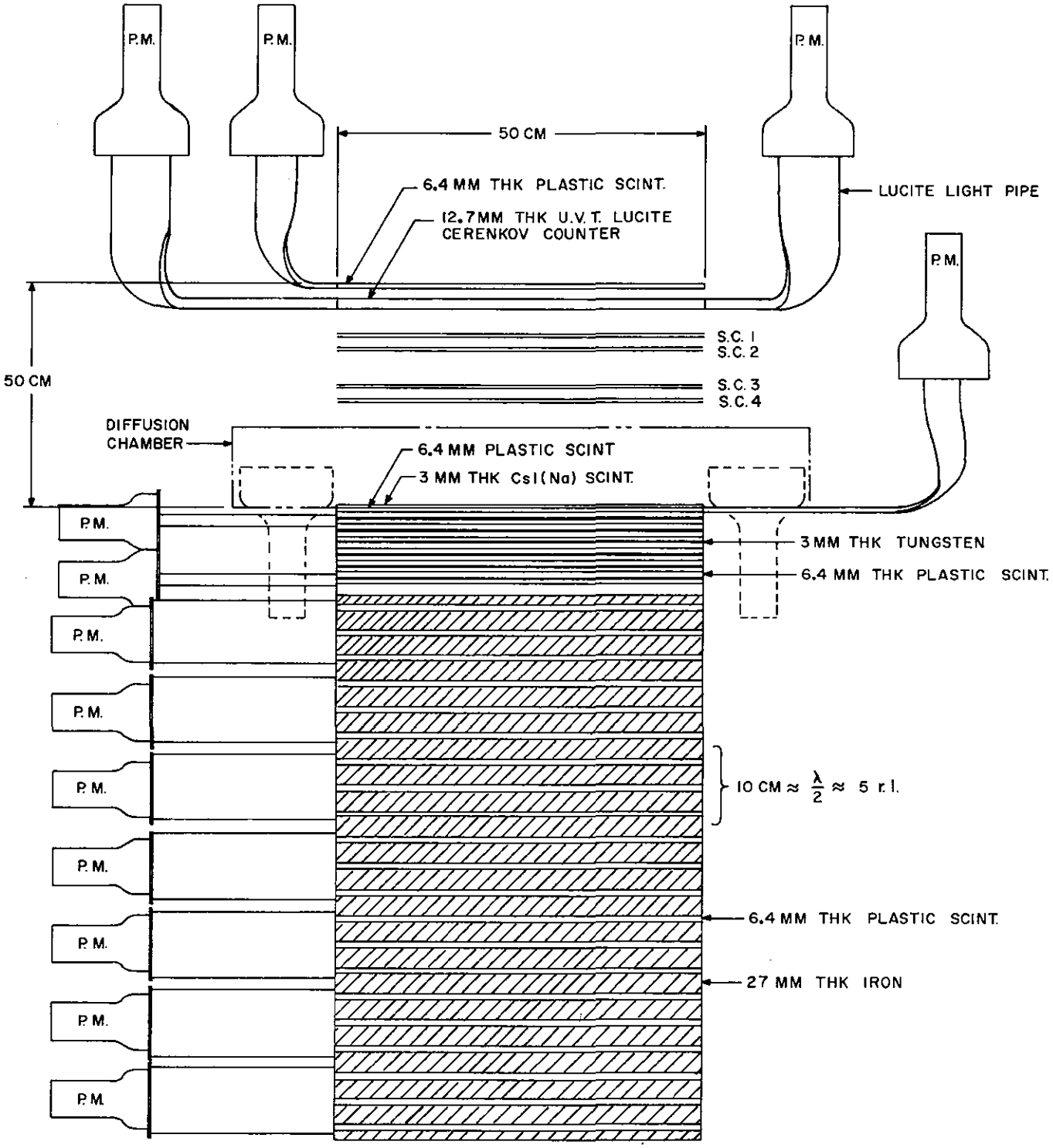

IONIZATION SPECTROMETER

Figure 1

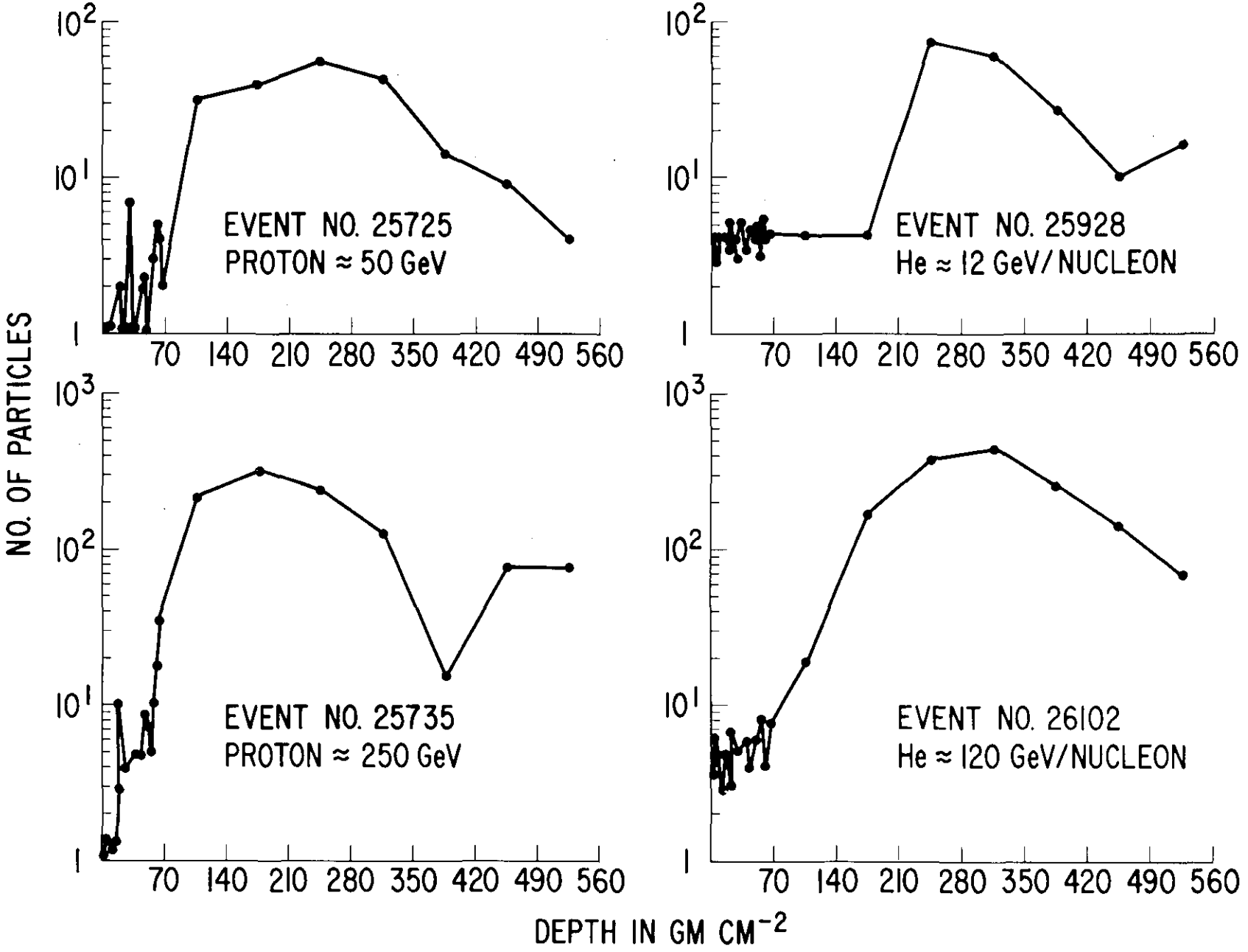
NO. OF PARTICLES
DEPTH IN GM CM^{-2}
EVENT NO. 25725
PROTON ≈ 50 GeV
EVENT NO. 25928
He ≈ 12 GeV/NUCLEON
EVENT NO. 25735
PROTON ≈ 250 GeV
EVENT NO. 26102
He ≈ 120 GeV/NUCLEON
10^3
10^2
10^1
1
70 140 210 280 350 420 490 560

Figure 2

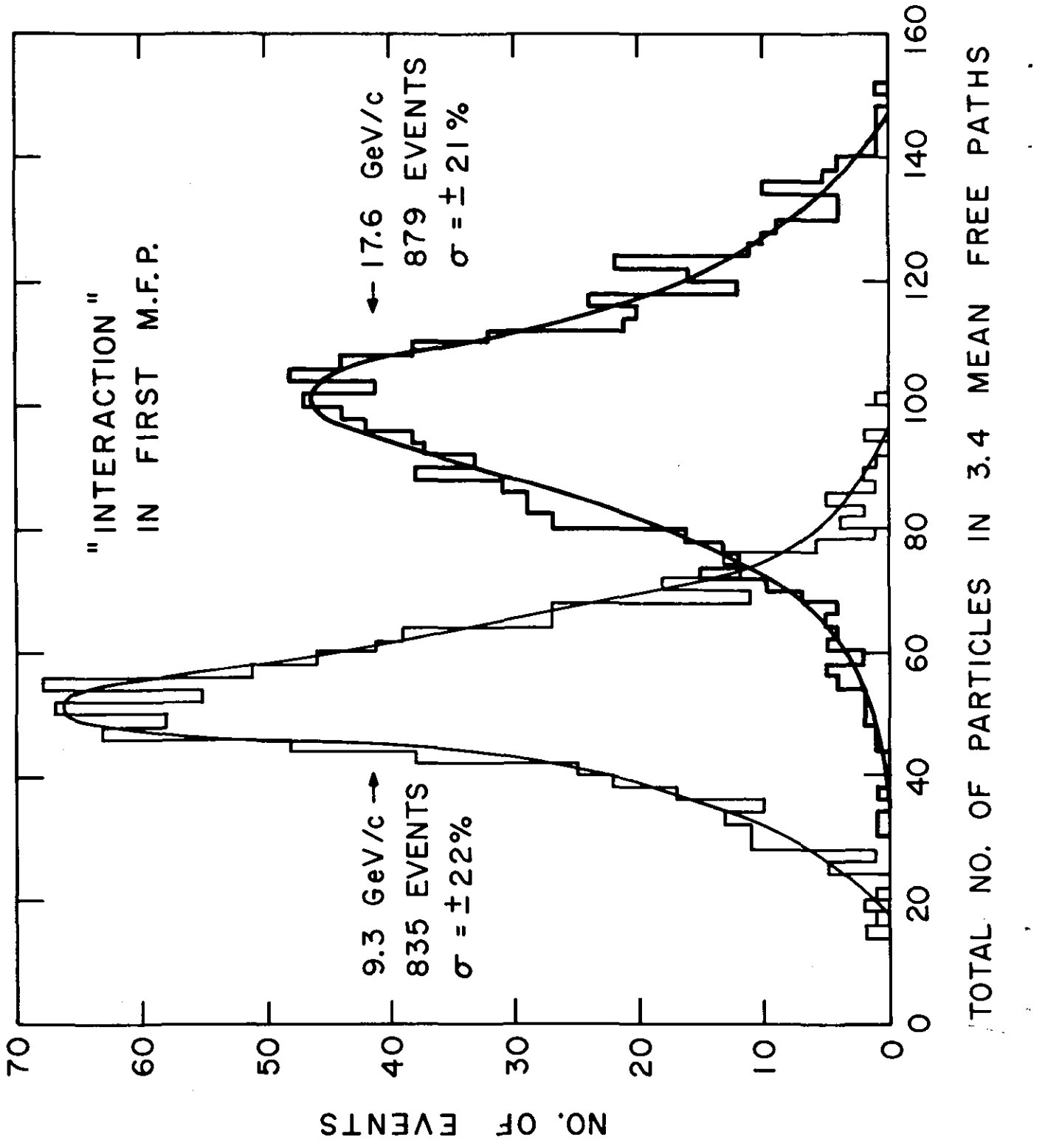
NO. OF EVENTS
TOTAL NO. OF PARTICLES IN 3.4 MEAN FREE PATHS
"INTERACTION"
IN FIRST M.F.P.
9.3 GeV/c →
835 EVENTS
σ = ±22%
← 17.6 GeV/c
879 EVENTS
σ = ± 21 %
0
10
20
30
40
50
60
70
0
20
40
60
80
100
120
140
160

Figure 3

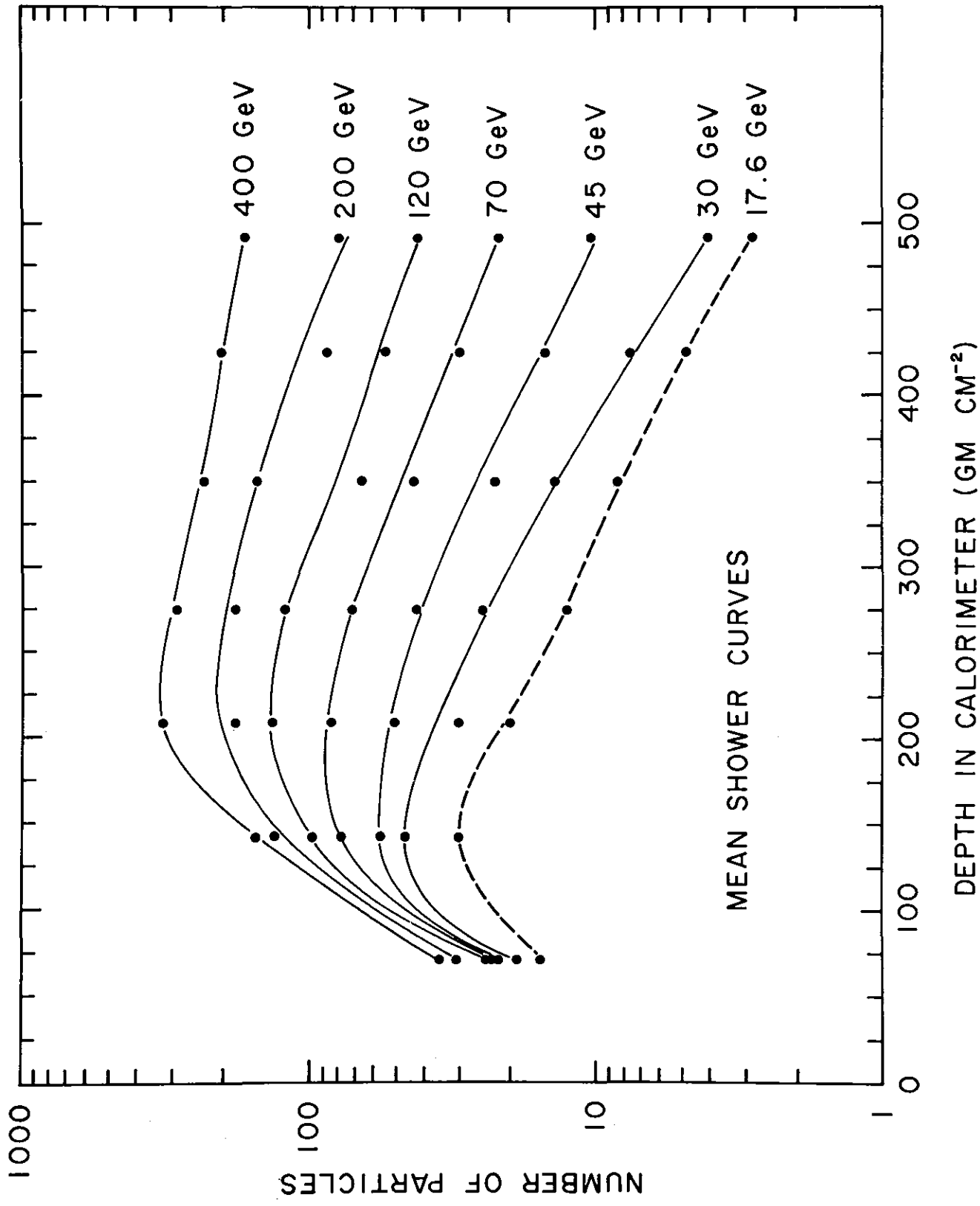
400 GeV
200 GeV
120 GeV
70 GeV
45 GeV
30 GeV
17.6 GeV
MEAN SHOWER CURVES
NUMBER OF PARTICLES
1000
100
10
1
0
100
200
300
400
500
DEPTH IN CALORIMETER (GM CM⁻²)

Figure 4

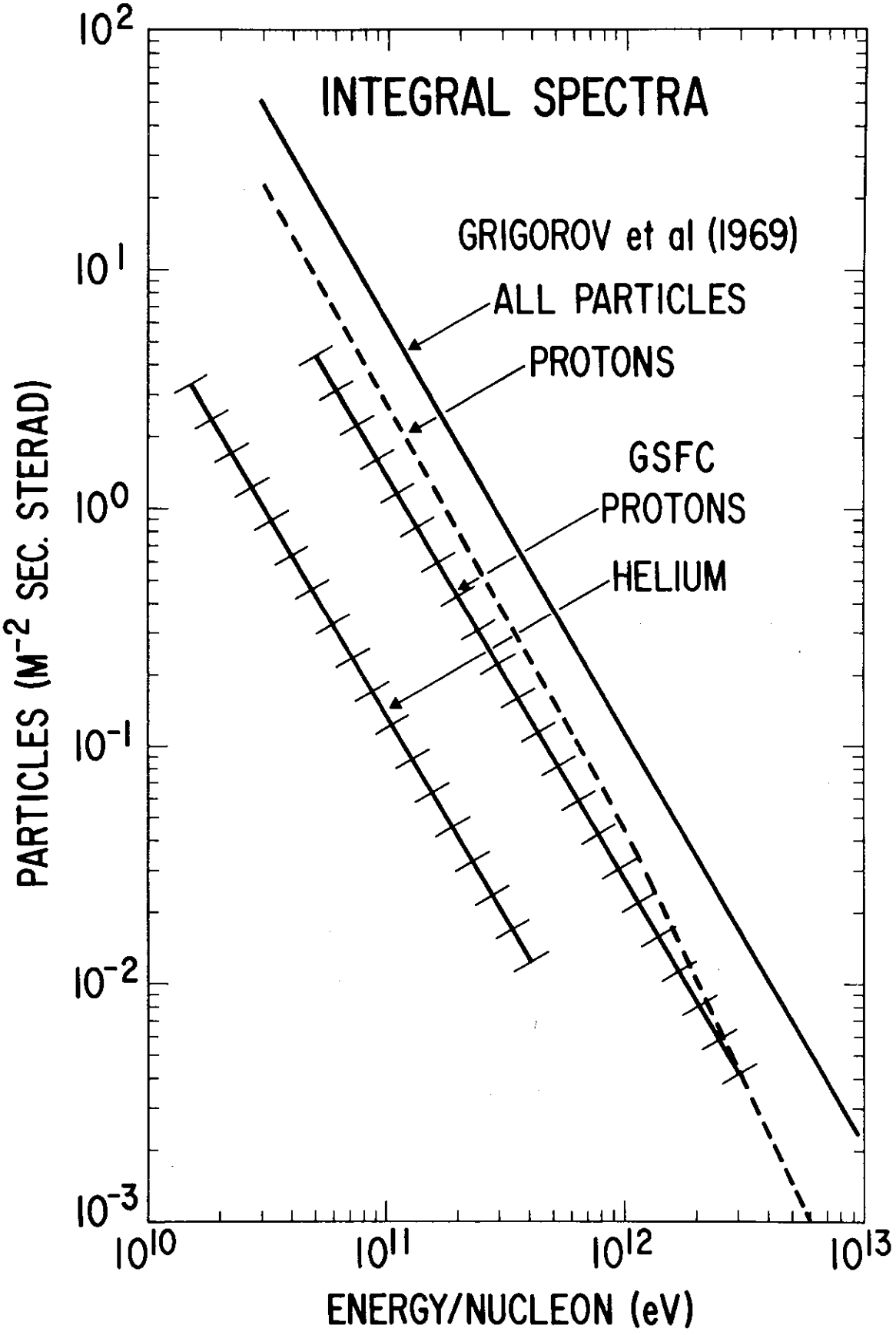
INTEGRAL SPECTRA
GRIGOROV et al (1969)
ALL PARTICLES
PROTONS
GSFC
PROTONS
HELIUM
PARTICLES (M^{-2} SEC. STERAD)
ENERGY/NUCLEON (eV)
10^2
10^1
10^0
10^{-1}
10^{-2}
10^{-3}
10^{10}
10^{11}
10^{12}
10^{13}

Figure 5

CHARGE COMPOSITION OF GALACTIC COSMIC RADIATION

J. F. Ormes, V. K. Balasubrahmanyan, and M. J. Ryan*

Goddard Space Flight Center, Greenbelt, Md. 20771

Abstract

Experimental results from the balloon borne ionization spectrometer flown in November 1970 have enabled the extension of the measurement of the energy spectra of cosmic rays to 10^{12} eV. The exposure factor for this flight was 1825 m^2-sr-sec and approximately 10,000 nuclei with $Z \geq 3$ have been observed. For nuclei with $Z \sim 6$, charges could be resolved to ± 0.2 units. The technique used for the measurement of energies of complex nuclei using an ionization spectrometer will be reported. Differential spectra of individual nuclei from lithium to oxygen and groups of nuclei with Z = 10-14, 15-19, 20-23, and 24-30 energy range 2×10^{10}eV to 10^{12}eV could be described in a power law representation with an exponent -2.6. The results indicate that the composition of galactic cosmic rays remain similar to that observed at lower energies. These results from direct measurements, provide evidence for the processes of source acceleration, and interstellar propagation remaining essentially energy independent up to 10^{12}eV.

1. Introduction

The charge composition of cosmic rays between 10^{10} and 10^{13} eV was measured with an ionization spectrometer flown on a balloon which was launched on 14 November 1970, the balloon floated at a ceiling altitude of 6 gm/cm^2 for 14 hours and provided an exposure factor of $\sim$ 1825 m^2ster.sec. More than 10,000 nuclei with $Z > 2$ were studied and provide measurements of the detailed charge composition to approximately 2000 GeV total energy.

2. Experimental Details

Figure 1 shows a diagram of the instrument flown.

It consists of three major components, a charge measuring module, a spark chamber for determining particle trajectories, and an ionization spectrometer for measuring total energy. The charge of an incoming particle was determined using two plastic scintillators, the Lucite Cerenkov counter and the CsI mosaic. As each detector has a large sensitive area of 50 cm x 50 cm, the spark chamber was used to apply corrections to eliminate the dispersion caused by the variation of response over the area of the detector and also due to the angle of incidence of the particles. These corrections are discussed in some detail in the paper by Ormes and Balasubrahmanyan (1969).

When using the spark chamber to correct for these geometric effects it is necessary to determine the track of the incident particle unambiguously. The spark chamber has four perpendicularly oriented wire planes

*NAS/NRC Research Associate

each with 200 wires spanning 50 cm. For each particle four (X,Y) measurements are available. As the experiment had as its objective, the study of singly charged particles such as protons and electrons and also Fe nuclei (Z = 26), the tracks of the incident particle had to be determined over an ionization range of 1 to 676. With the knock-on probability increasing as Z^2, heavier nuclei were invariably accompanied by knock-on electrons which cause confusion in determining the track of the incident heavy nucleus. A computer algorithm was developed to detect the tracks of heavy nuclei efficiently. For charges above Z=10 some error in angle may be caused by the knockons but the efficiency of finding a track is > 95% even at iron. Charge resolution obtained in this experiment is shown in Figure 2.

The charge-module was followed by the electron cascade section consisting of 12 tungsten plates of 6.13 gm/cm^2 (.04 mfp for protons and ~ 1 radiation unit for electrons) and plastic scintillators of .63 gm/cm^2 (.01 mfp for protons). In this section, electrons developed electro-magnetic cascades whereas protons had only a small probability of simulating electrons. The details of separating electrons from the copious background of protons is discussed in detail in a subsequent paper (Silverberg et al. 1971). The electron cascade sections were followed by a nuclear cascade section consisting of 7 modules of Fe each 1/2 mfp for protons. Each module had three plastic scintillators distributed inside the iron viewed by a single photo tube. Since a sample of the number of particles in the cascade is taken every 1.5 radiation lengths, the fluctuations due to low energy electron cascades are decreased.

3. Energy Measurement

Most of the heavy nuclei interact in the tungsten modules or the first iron module allowing the whole spectrometer to absorb their energy. However using the whole spectrometer greatly reduces the available geometry. In order to "calibrate" the spectrometer response at various thicknesses the following procedure was followed. First the energy normalization was obtained using the energy loss of a sea level muon. Carbon nuclei selected from the spark chamber tracks such that they go through the entire spectrometer were calculated using 3,4,5,6, and 7 Fe modules. In Figure (3), the correlation of the energy of a particle determined with 3,4,5, and 6 modules with the energy determined using all 7 modules is shown. It can be seen that there is a good correlation between the energies determined by a subset of modules to that obtained using the entire spectrometer. However, as we go from 6 to 3 modules, the dispersion in the energy correlation increases. This gives an estimate of the error in determining the energy depending upon the "thickness" of the spectrometer as determined by the particle trajectory.

Figure (4) shows the estimated energy as a function of spectrometer depth. These curves represent average integral growth curves. These curves from 100 to 700 GeV show a tendency to saturate at the higher

module numbers and can be approximately expressed on the form

$$E_i = E_A[1 - \exp(-\frac{N_i}{N})] \qquad (1)$$

Where E_i is the energy estimated using N_i modules, E_A the asymptotic energy and N is the number of modules required to absorb .73 of the energy. N varies slowly with energy. This equation is consistent with a model where the energy is absorbed exponentially in a thick block of matter. Using expression (1), the asymptotic energy E_A can be estimated. For the results presented in this paper, energy was determined for particles which passed through at least the first three iron modules.

4. Results and Discussions

Figure (5) shows the results on the differential energy spectrum of Li, Be, B, C, N, and O nuclei are shown. The intensity of the different components have been corrected for spallation in the atmosphere and the detector and have been extrapolated to the top of the atmosphere. The spectra are all consistent within errors to a power law in total energy with an exponent ~ -2.7 and extend to $\sim$ 150 GeV/nucleon. The flattening at the lowest energy end of the spectrum is due to geomagnetic cutoff. (During the flight the balloon drifted from a geomagnetic cutoff of 5 GV to one of 3.5 GV).

Figure (6) shows the results on energy spectrum of L, M, LH, MH, VH groups of nuclei and all these nuclei have similar power law energy spectra in total energy with the exponent $\sim 2.7 \pm 0.1$. The errors shown in Figures (5) and (6) are statistical.

Von Rosenvinge et al. (1967) made measurements on composition up to 25 GeV/nucleon using the geomagentic cutoff at different locations, and, at the highest energy, a gas Cerenkov counter at different pressures as a threshold device. Our spectra and intensity are reasonable in agreement with these results. The intensities at 1.5 GeV/nucleon are about .10% below those of Von Rosenvinge (1969) which were obtained in 1966. The direction of the difference in intensities between the two experiments is consistent with an increasing solar modulation or it could be due to systematic effects.

Table (1) shows the results on the ratios of individual elements of light and medium groups and is in general agreement with the results of Lezniak et al. (1969), Dayton et al., O'Dell et al. (1969), and Webber & Ormes (1969).

Our results have shown that the charge composition at around 100 GeV/nucleon is essentially similar to that at low energies (Garcia-Munoz & Simpson, 1969; Teegarden et al., 1969). The implications of this on the photodisintegration phenomena in the immediate vicinity of a pulsar is discussed in a paper presented in this conference (Balasubrahmanyan, et al.).

TABLE 1

CHARGE RESOLUTION IN THE MEDIUM NUCLEI REGION

$\Delta Z = \pm 0.2$
L/M = 0.29 AT 7 gm/cm^2

No. of Boron Nuclei	1570
No. of Beryllium Nuelci	251
No. of Lithium Nuclei	496
No. of Carbon Nuclei	3505
No. of Nitrogen Nuclei	1281
No. of Oxygen Nuclei	3165

Li, Be, B = 1.98:1:6.25
C : N : O = 1.11:0.40:1

5. References

Balasubrahmanyan, V. K., Ormes, J. F., and Ryan, M. J., 1971. O. G. Session, Proc. 12th International Conf. Cosmic Rays.

Dayton, B., Lund, N., and Risbo, T. 1969. Proc. 11th International Conf. Cosmic Rays, 1, 375.

Garcia-Munoz, M., and Simpson, J. A. 1969. Proc. 11th International Conf. Cosmic Rays, 1, 317.

Lezniak, J. A., von Rosenvinge, T. T., and Webber, W. R. 1969. Proc. 11th International Conf. Cosmic Rays, 1, 375.

O'Dell, F. W., Shapiro, M. M., Silberberg, R., Stiller, B., Tsao, C. H., Durgaprasad, N., Fichtel, C. E., Guss, D. E., and Reames, D. V., 1969. Proc. 11th International Conf. Cosmic Rays, 1, 457.

Ormes, J. F., and Balasubrahmanyan, V. K. 1969. Proc. 11th International Conf. Cosmic Rays.

Silverberg, R. F., Ormes, J. F., Balasubrahmanyan, Ryan, M. 1961. O.G. Session, Proc. 12th International Conf. Cosmic Rays.

Teegarden, B. J., McDonald, F. B., and Balasubrahmanyan, V. K. 1969. Proc. 11th International Conf. Cosmic Rays, 1, 345.

von Rosenvinge, T. T., 1969. Ph.D. Thesis, University of Minnesota.

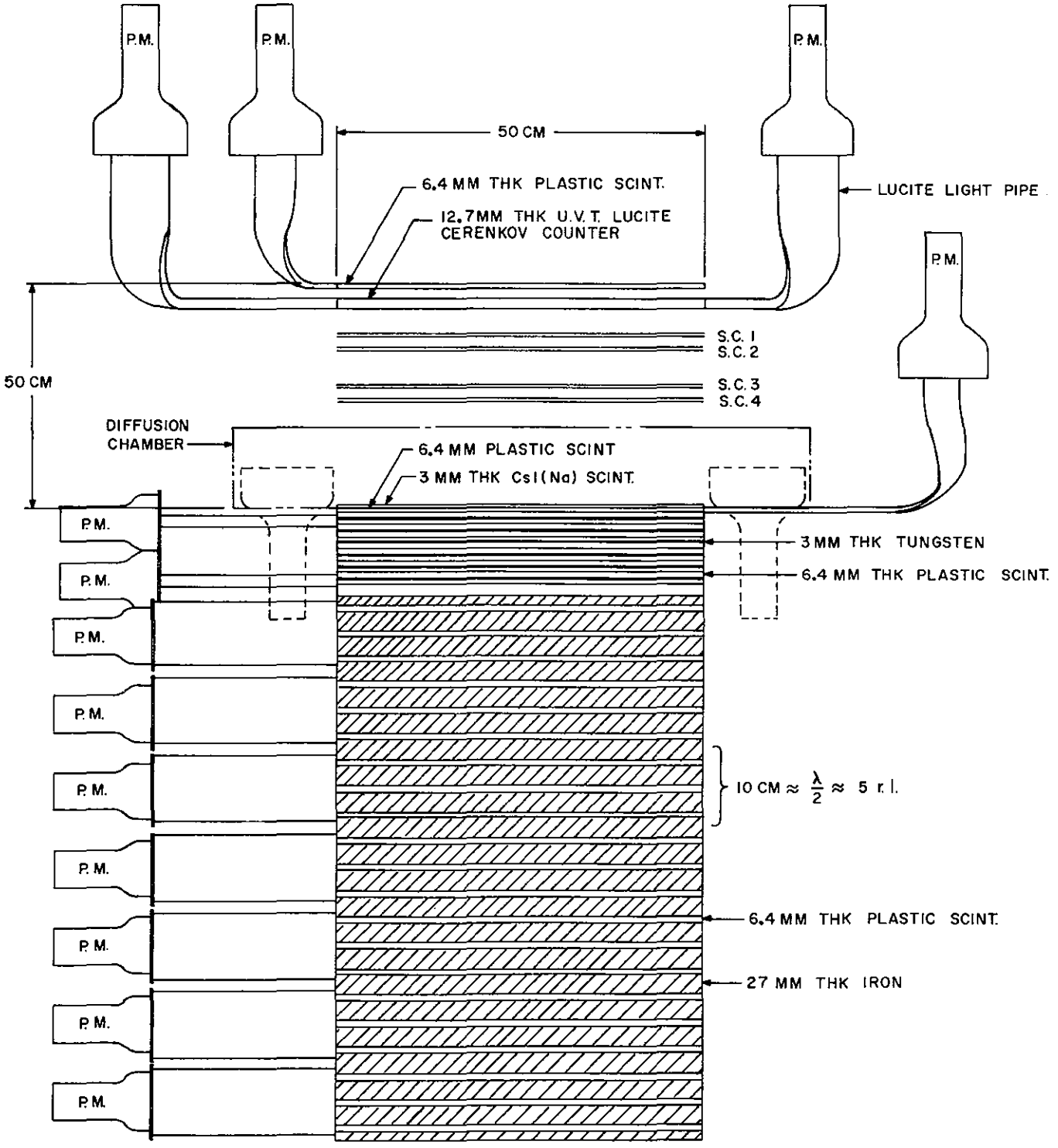

IONIZATION SPECTROMETER

FIGURE 1

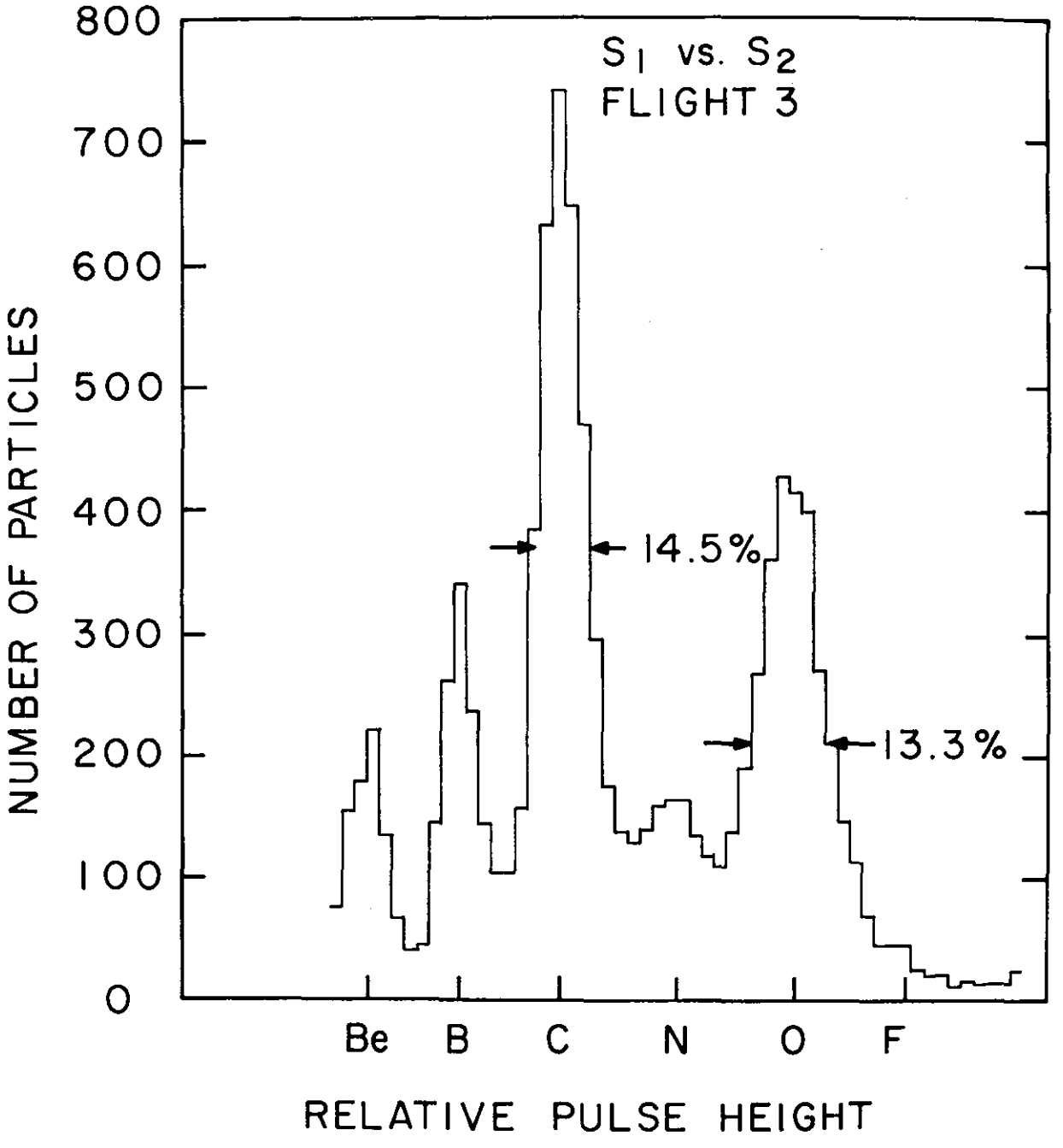
800
700
600
500
400
300
200
100
0
NUMBER OF PARTICLES
S1 vs. S2
FLIGHT 3
14.5%
13.3%
Be
B
C
N
O
F
RELATIVE PULSE HEIGHT

FIGURE 2

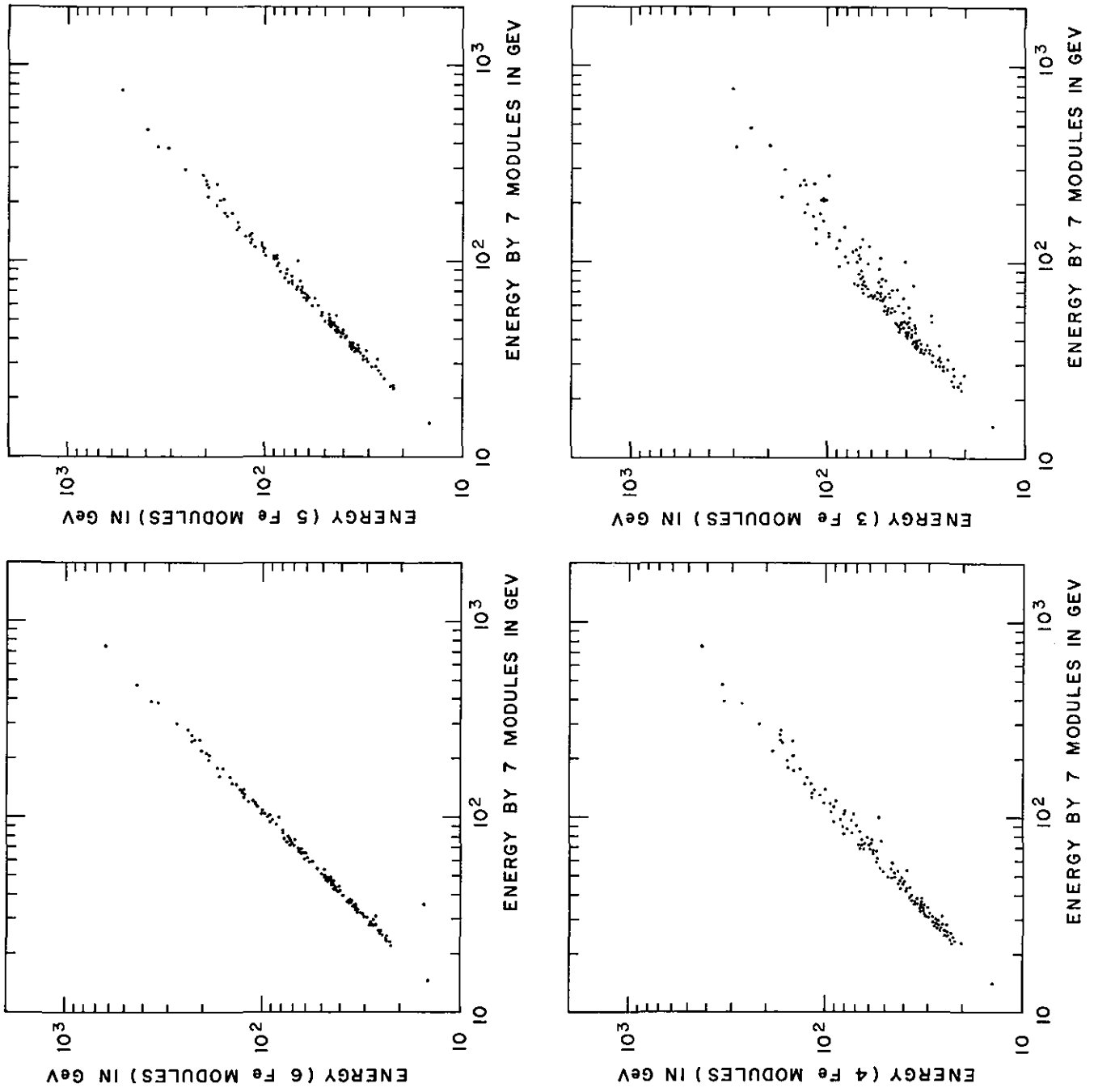
ENERGY (5 Fe MODULES) IN GeV
ENERGY BY 7 MODULES IN GEV
ENERGY (3 Fe MODULES) IN GeV
ENERGY BY 7 MODULES IN GEV
ENERGY (6 Fe MODULES) IN GeV
ENERGY BY 7 MODULES IN GEV
ENERGY (4 Fe MODULES) IN GeV
ENERGY BY 7 MODULES IN GEV
10
10^2
10^3

FIGURE 3

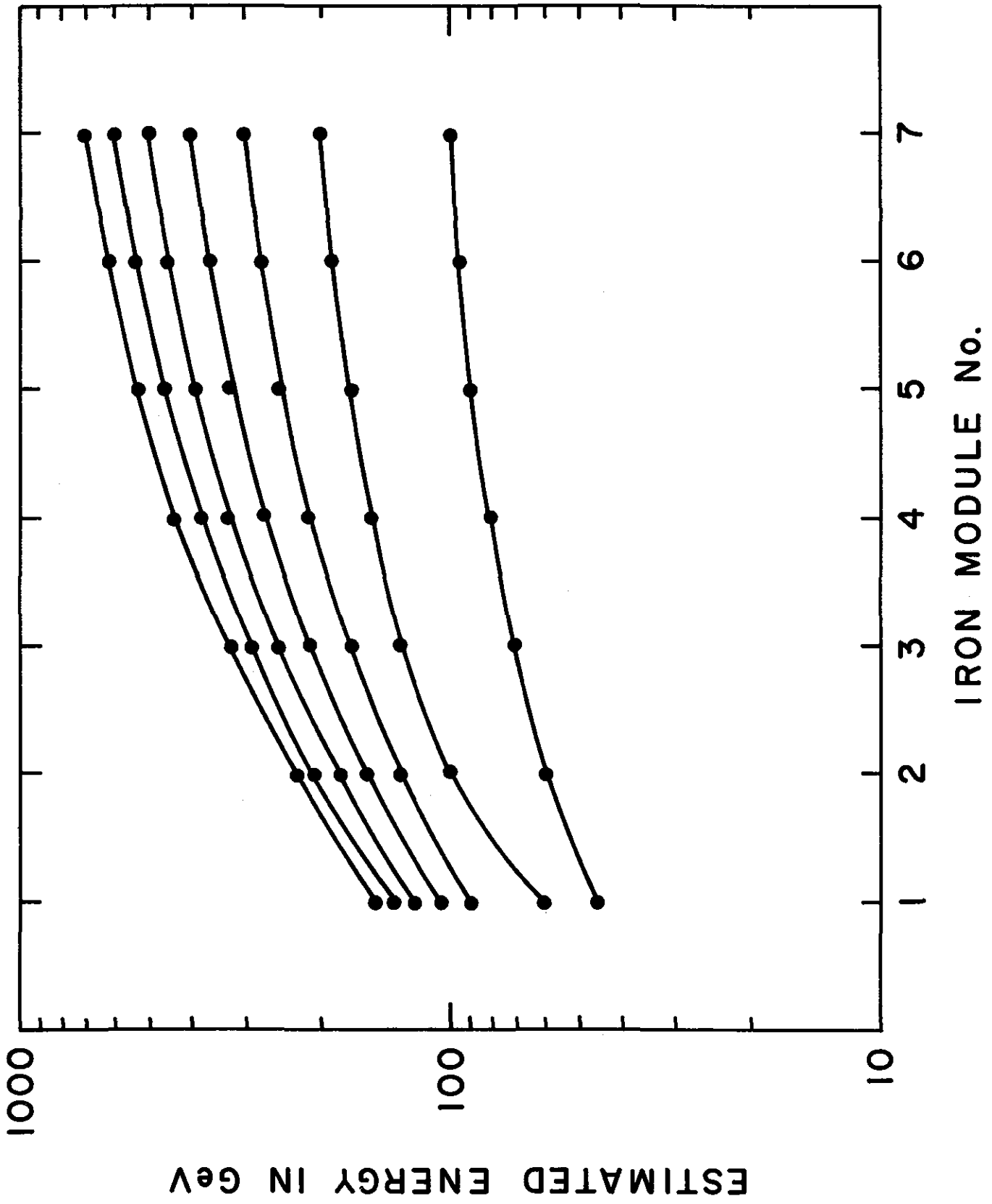

FIGURE 4

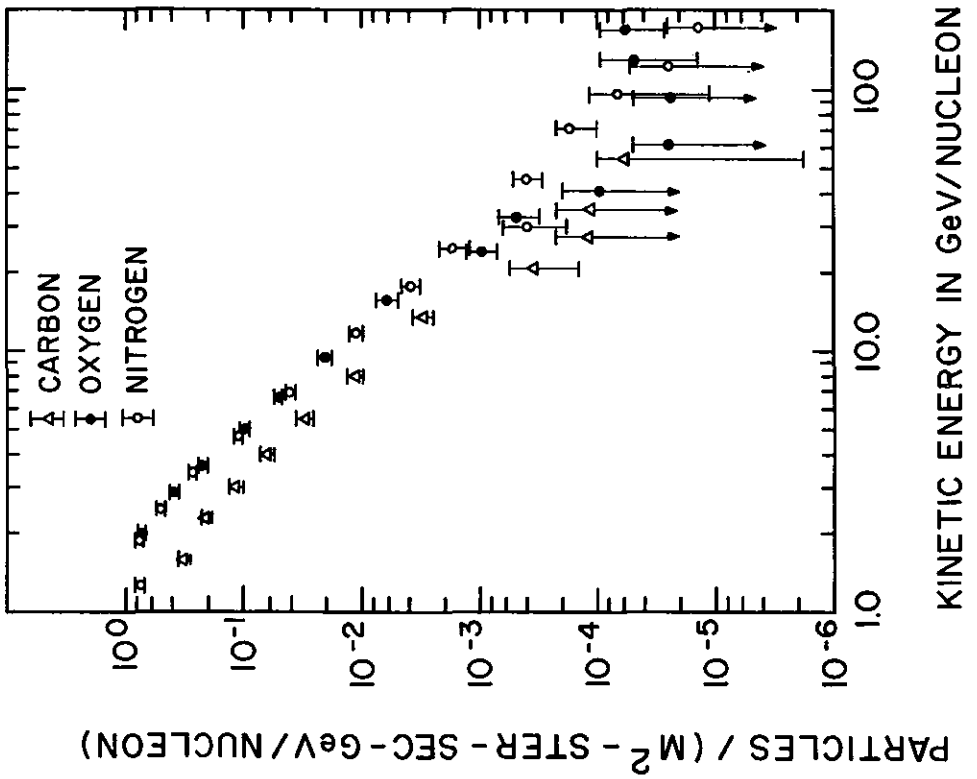
CARBON
OXYGEN
NITROGEN
10^0
10^{-1}
10^{-2}
10^{-3}
10^{-4}
10^{-5}
10^{-6}
1.0
10.0
100
PARTICLES / (M^2 - STER - SEC - GeV / NUCLEON)
KINETIC ENERGY IN GeV/NUCLEON

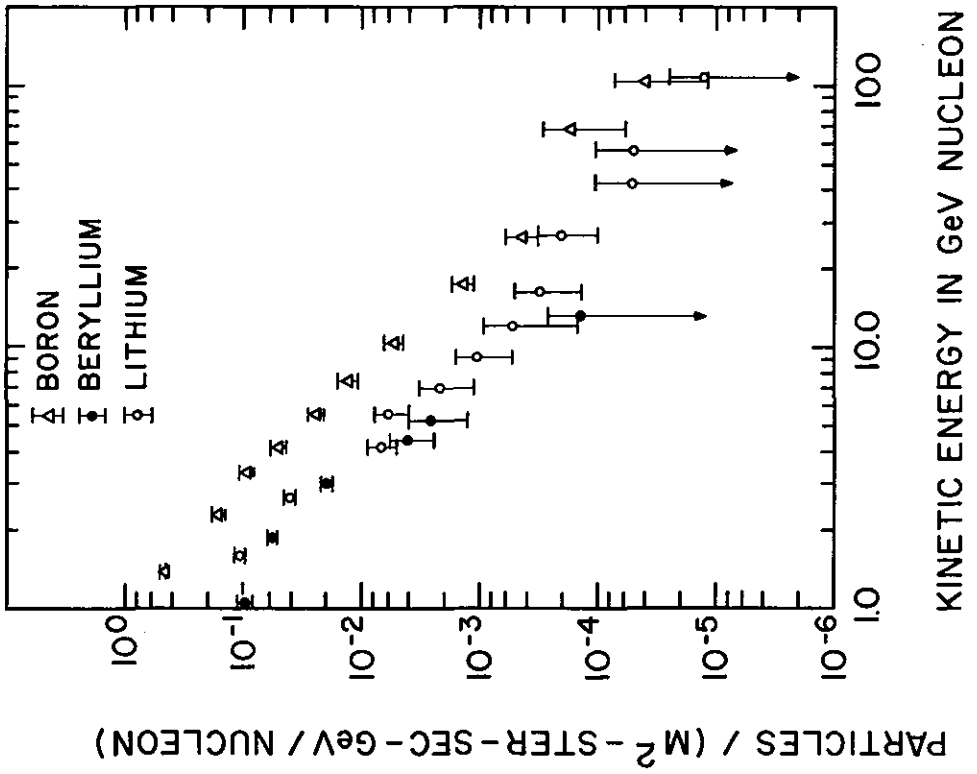
BORON
BERYLLIUM
LITHIUM
10^0
10^{-1}
10^{-2}
10^{-3}
10^{-4}
10^{-5}
10^{-6}
1.0
10.0
100
PARTICLES / (M^2 - STER - SEC - GeV / NUCLEON)
KINETIC ENERGY IN GeV NUCLEON

FIGURE 5

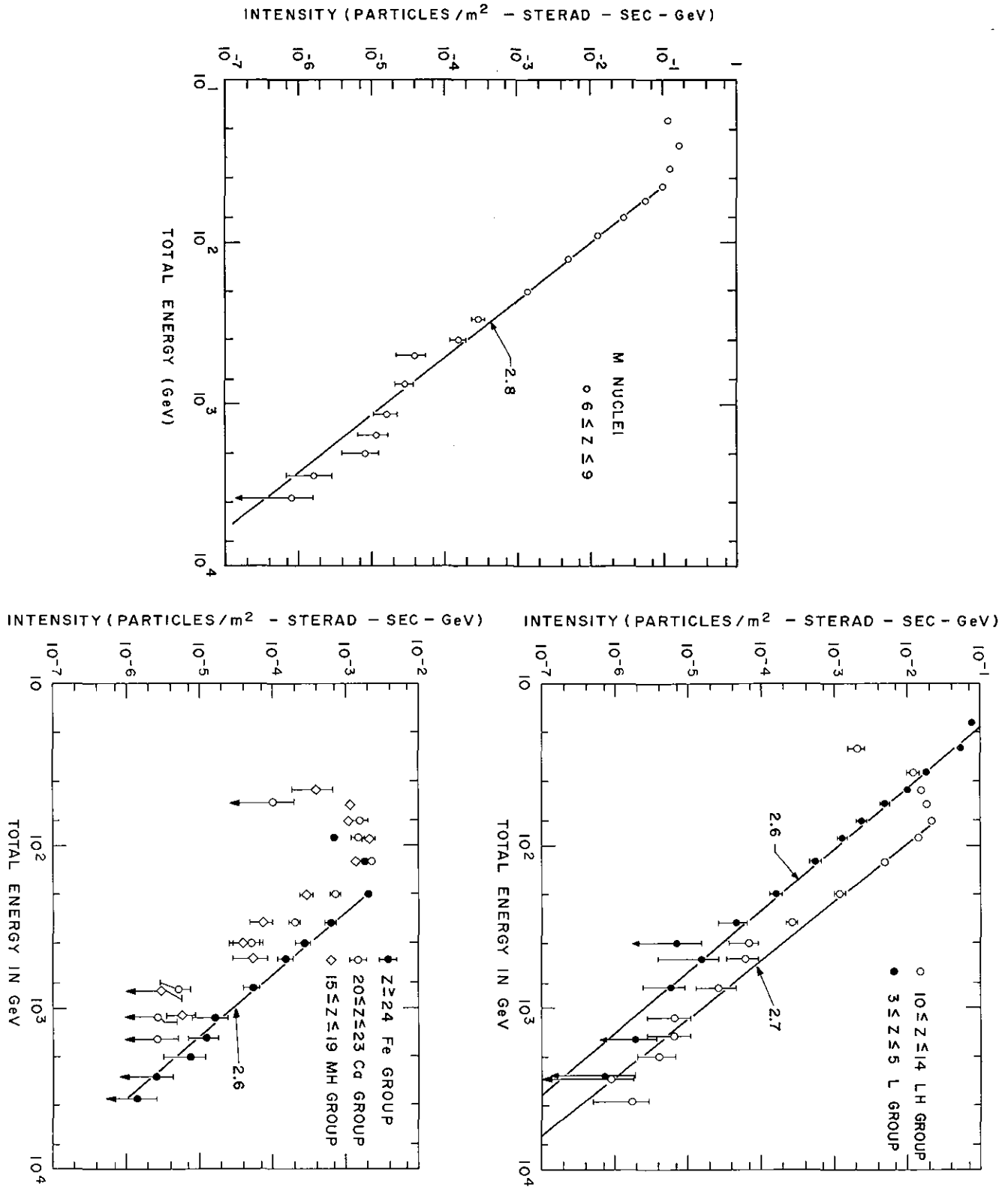
INTENSITY (PARTICLES/m² – STERAD – SEC – GeV)
TOTAL ENERGY (GeV)
M NUCLEI
○ 6 ≤ Z ≤ 9
2.8
INTENSITY (PARTICLES/m² – STERAD – SEC – GeV)
TOTAL ENERGY IN GeV
○ 10 ≤ Z ≤ 14 LH GROUP
● 3 ≤ Z ≤ 5 L GROUP
2.6
2.7
INTENSITY (PARTICLES/m² – STERAD – SEC – GeV)
TOTAL ENERGY IN GeV
● Z ≥ 24 Fe GROUP
○ 20 ≤ Z ≤ 23 Ca GROUP
◇ 15 ≤ Z ≤ 19 MH GROUP
2.6

FIGURE 6

ENERGY DEPENDENCE OF CROSS SECTIONS OF COSMIC RAY NUCLEI IN TUNGSTEN

V. K. Balasubrahmanyan, C. J. Crannell[†], F. A. Hagen*
J. F. Ormes, and M. J. Ryan[‡]
NASA/Goddard Space Flight Center
Greenbelt, Maryland, USA 20771

Abstract

An ionization spectrometer consisting of 12 layers of tungsten each 6.13 gm cm^{-2} thick and 7 iron modules each 70 gm cm^{-2} thick was flown in a balloon on November 14, 1970 at an altitude of 6 gm cm^{-2} for 16 hours. The distributions of the first interaction points are used to determine the mean free path of the incident particles. At energies of 20 GeV the proton m.f.p. of 140 gm cm^{-2} is in agreement with that of other workers. The m.f.p.'s of heavynuclei have been determined as a function of energy up to a total energy of 1,000 GeV. These results are compared with the overlap model of nucleus-nucleus collisions of Brandt and Peters. For C nuclei interacting with W the overlap parameter is -2.6×10^{-13} cms. The energy dependence of this parameter will be discussed.

1. Introduction

Nucleus-nucleus collisions at relativistic energies have been studied using the cosmic ray beam. This is the only available source of these particles because machines for accelerating heavy nuclei to high energies are not yet available. In this paper, the dependence of the collision mean free path of carbon and oxygen nuclei incident on alternate layers of tungsten and plastic scintillator are studied in the energy range 2 GeV/nuc. to 15 GeV/nucleon.

2. Experimental Details

The results were obtained from a balloon-borne ionization spectrometer used to determine the charge spectrum of cosmic rays in the energy range 10^{10} to 10^{13} eV (Ormes, et al. 1970). The instrument had a geometric factor of $\sim$ 450 cm^2 ster and collected data at 6.0 gm/cm^2 for 14 hours. Energy measurements were performed on a total of $\sim$ 1800 carbon and $\sim$ 1700 oxygen nuclei. The identity of the incident particles was determined in a charge module consisting of two plastic scintillators, a lucite Cerenkov counter, a CsI scintillator mosaic, and a four module wire spark chamber. All the detectors had a sensitive area of 50 cm x 50 cm.

[†]Federal City College *University of Maryland [‡]NAS/NRC Research Assoc

The charge module was followed by an electron cascade section with 12 tungsten plates, each followed by a plastic scintillator. The tungsten plates were 6.13 gm/cm^2 thick (0.03 proton mean free paths) and the plastic scintillators were .63 gm/cm^2 thick (0.01 m.f.p.). The purpose of this section was to discriminate electrons from protons utilizing the rapid development of electromagnetic cascades in tungsten. This section was followed by a nuclear cascade section with 7 iron modules each 1/2 m.f.p. thick and was used to determine the energy of protons and other nuclear particles in cosmic rays. Using the electron cascade section, it was possible to study the passage of carbon and oxygen nuclei and to detect when they suffered nuclear interactions.

The C and O nuclei studied in this paper were selected using their consistent signatures in the multi-element charge module and in Figure (1) the charge resolution attained in the experiment is shown for the medium group of nuclei. The peak to valley ratio and charge resolution is quite good so that C and O nuclei could be selected unambiguously.

Figure (2) shows the pulse height resolution for the oxygen nuclei (as selected by the charge module) in some of the tungsten modules. Of the 12 detectors, all except the 5th module (called T-5) had resolution $\approx$ 15% FWHM with a pronounced peak due to the oxygen nuclei. Note that the peak of oxygen is becoming less abundant relative to the background with increasing depth in the tungsten. Results with carbon nuclei had similar resolution. The energy measurement is described in detail in an accompanying paper and will be published elsewhere (Ormes, et al., 1971). An incident nucleus is said to have interacted according to the following criteria: A_i is the mean pulse height for a given charge and W_i the full width at half maximum, where i represents the tungsten module. If a particle in the (i + 1), (i + 2), and (i + 3) detectors has its pulse heights such that $\frac{Pi}{A_i} > (1 + W_i)$ or $< (1 - W_i)$ in all the three successive detectors, then it is supposed to have interacted in the i detector. The probability of this occurring by a chance fluctuation was < .1%. Reducing the criteria for nuclear interactions to two successive detectors instead did not affect the results.

Figure (3) and Figure (4) show the exponential absorption of carbon and oxygen nuclei in the tungsten and plastic scintillators. It can be seen from the figures that as the energy increases from 1.5 GeV to 9 GeV/nuc., the particles are absorbed more quickly.

Figure (5) shows the mean free paths for carbon and oxygen nuclei as a function of energy. The mean free paths were calculated using the relation

$$\lambda_i = {}^{X}/(\Delta N_i/N_i)$$

where X is the absorber in gm/cm^2, N_i is the number of incident nuclei in a module and ΔN_i the number of interactions in the i^{th} module. (For the purposes of this calculation, data from detector T5 and all the other detectors which depended on T5 for definition of nuclear interaction were ignored.) The implied increase in cross section can be related on Bradt & Peter's (1950) phenomenological model for nucleus-nucleus collisions to the changes in the overlap parameter b in the formula

$$\sigma = \pi r_o^2 \quad (A_1^{1/3} + A_2^{1/3} - b)^2$$ where A_1 and A_2 are the mass numbers of the incident and target nuclei, $r_o = 1.1 \times 10^{-13}$ cms. The value b from these measurements varies from $-(2.6 \pm 0.5) \times 10^{-13}$ cms at 2 GeV/nuc. and $-(11.9 \pm 2.4) \times 10^{-13}$ cm at 15 GeV/nucleon. (From figure (5), one can see that the mean free path decreases as a function of energy for both carbon and oxygen nuclei.)

3. Discussion

The mean free paths of both carbon and oxygen nuclei are approximately equal and decrease by roughly a factor of 2.5 over the energy range 2 to 15 GeV/nucleon.

Aizu et al. (1960), for collisions with nuclei of nuclear emulsions, observed that the mean free path decreased from 16.2 ± 1.3 cm to 13.2 ± 0.7 cm when energy changes from 0.7 GeV/nuc. to 3 GeV/nuc. Data at higher energies are not available for comparison.

The change in b could be due to the relativistic deformation of the incident nucleus. At higher velocities, as seen from the reference frame of the target nucleus, the projectile will be disc shaped. This distortion might result in a higher effective b in the Bradt and Peters' model or alternatively, the distorted nucleus may be more prone to break-up resulting in a decreased mean free path at higher energies.

4. References

Aizu, H., et al. 1960, Prog. Theo. Phys., Suppl. No. 6, 54.

Bradt, H. L., and Peters, B., 1950, Phys. Rev. 77, 54.

Ormes, J. F., Balasubrahmanyan, V. K., McDonald, F. B., and Price, R. D., IEEE Trans. on Nuc. Sci., Vol. NS-15, 3, 566, 1968.

Ormes, J. F., Balasubrahmanyan, V. K., and Ryan, M. J. (paper presented at this conference in the O.G. session, to be published).

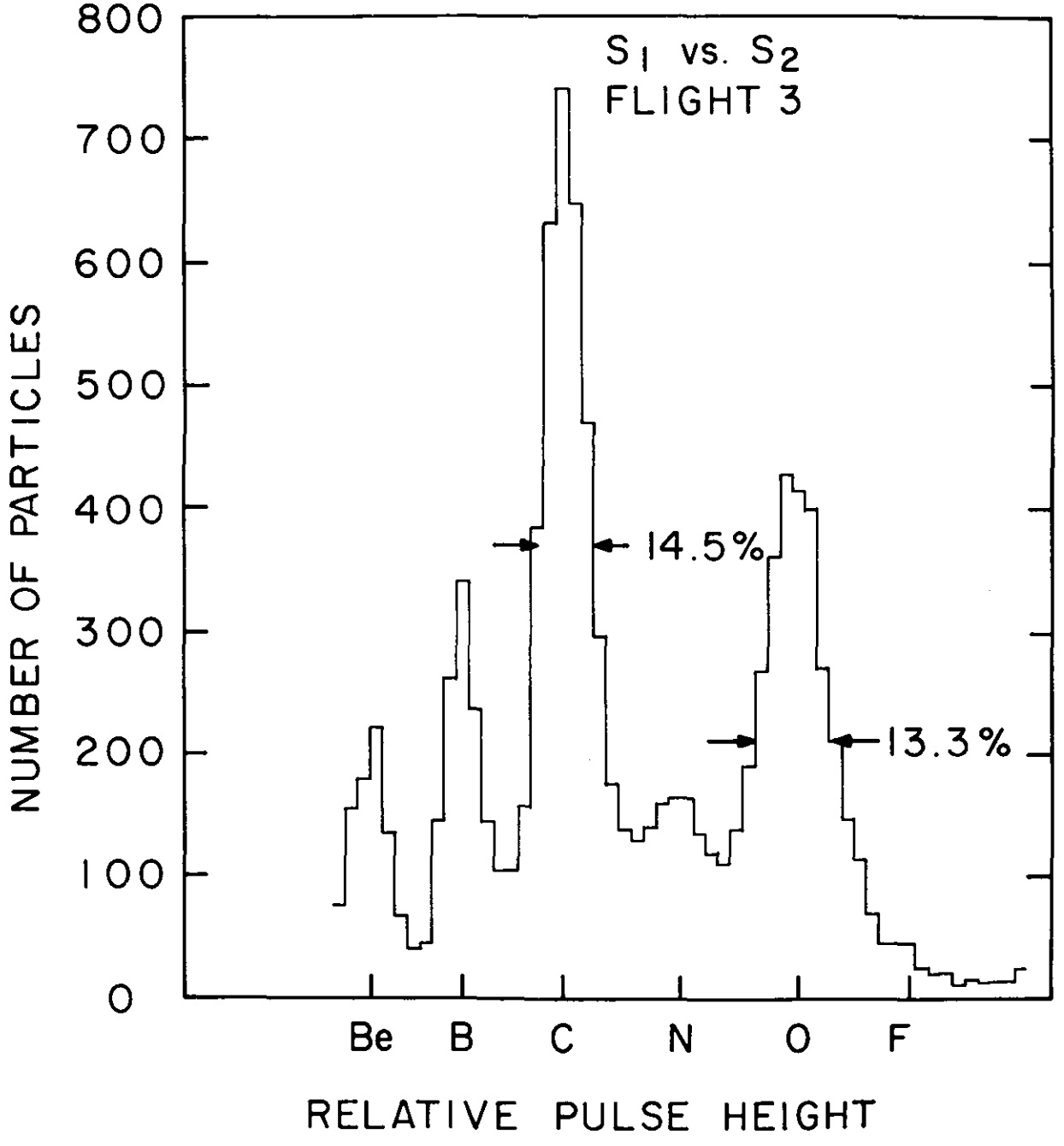
800
700
600
500
400
300
200
100
0
NUMBER OF PARTICLES
S1 vs. S2
FLIGHT 3
14.5%
13.3%
Be
B
C
N
O
F
RELATIVE PULSE HEIGHT

FIGURE 1

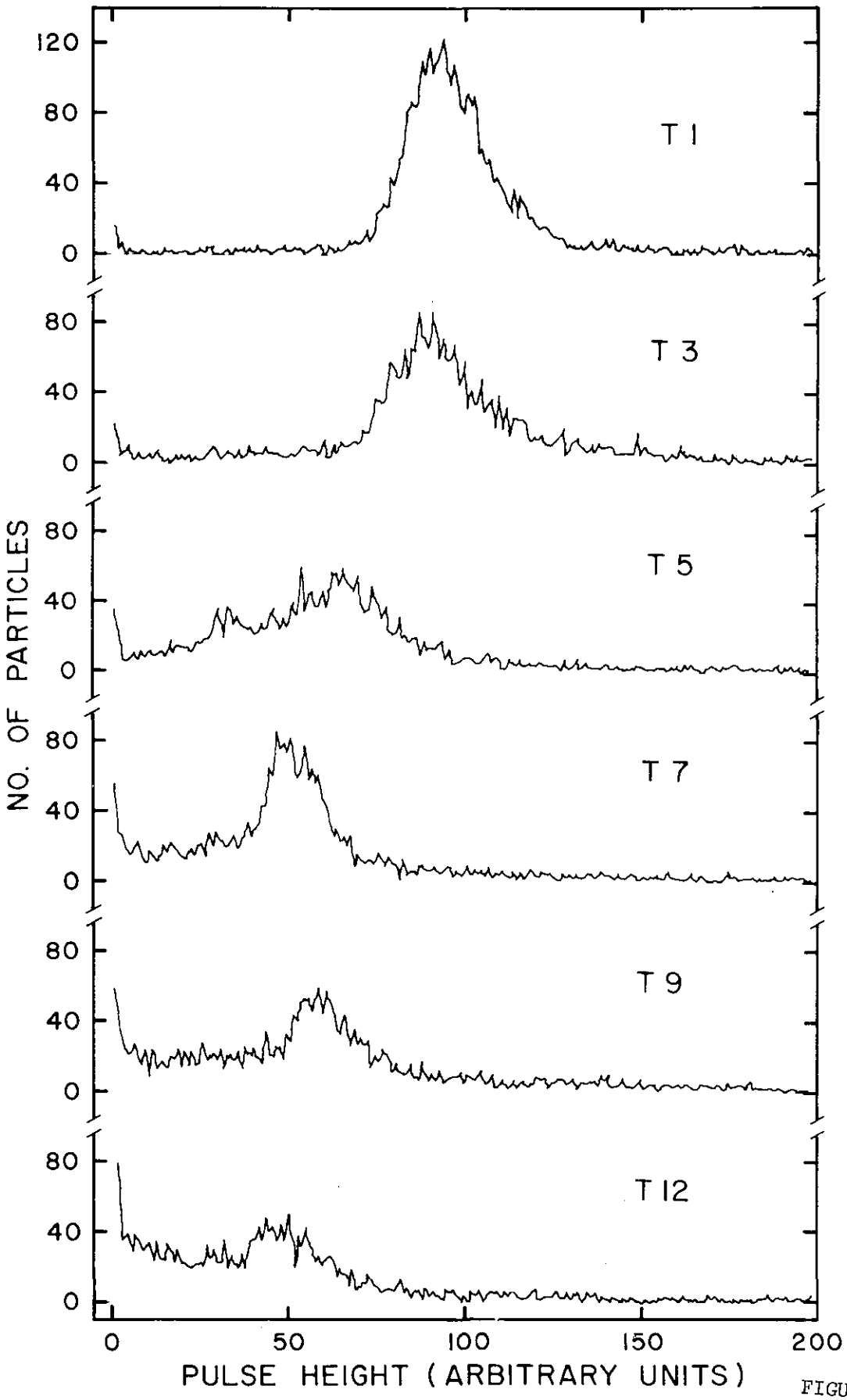
120
80
40
0
T 1
80
40
0
T 3
80
40
0
T 5
80
40
0
T 7
80
40
0
T 9
80
40
0
T 12
NO. OF PARTICLES
0
50
100
150
200
PULSE HEIGHT (ARBITRARY UNITS)

FIGURE 2

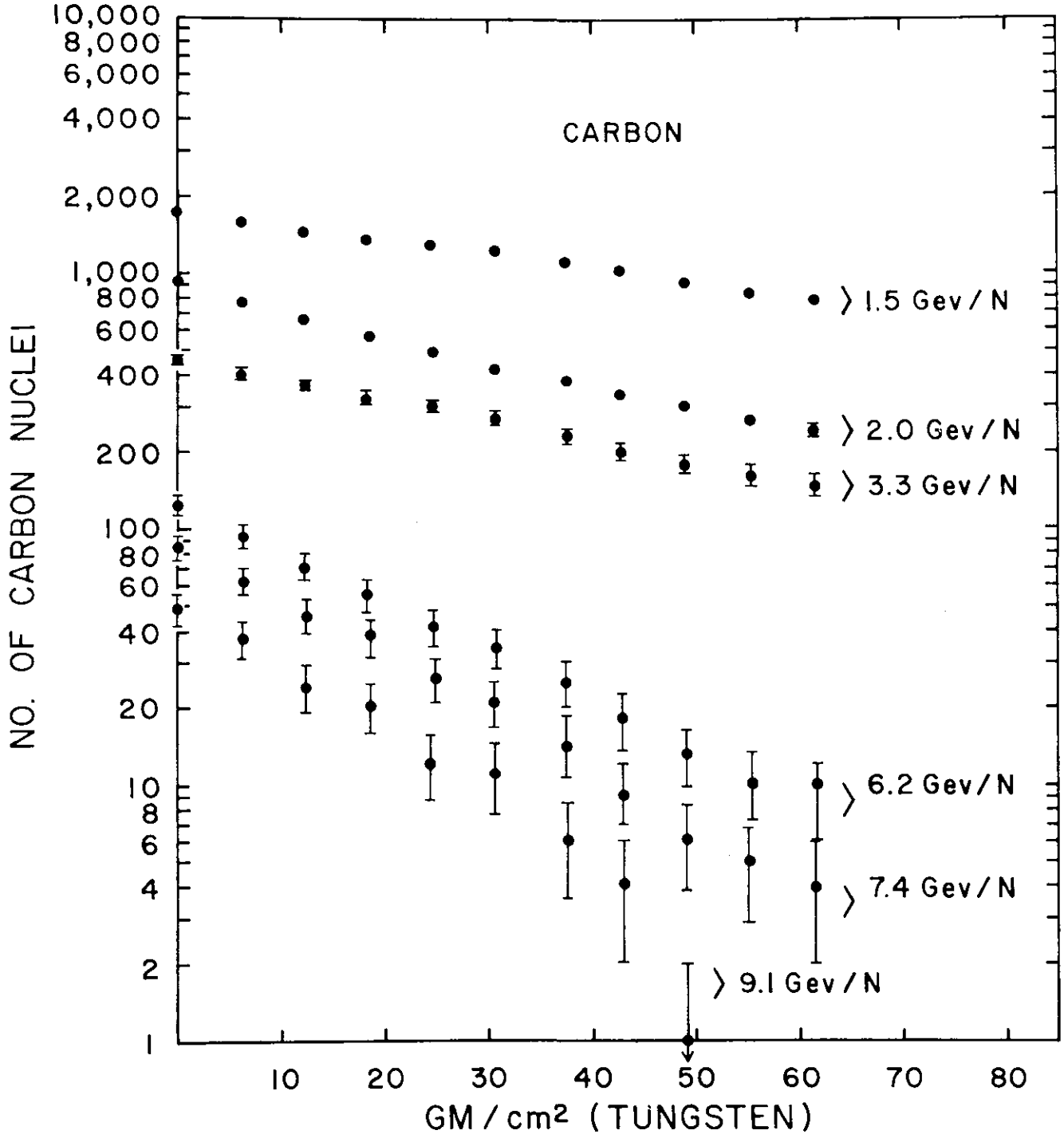
CARBON
NO. OF CARBON NUCLEI
10,000
8,000
6,000
4,000
2,000
1,000
800
600
400
200
100
80
60
40
20
10
8
6
4
2
1
10
20
30
40
50
60
70
80
GM / cm² (TUNGSTEN)
〉 1.5 Gev / N
〉 2.0 Gev / N
〉 3.3 Gev / N
〉 6.2 Gev / N
〉 7.4 Gev / N
〉 9.1 Gev / N

FIGURE 3

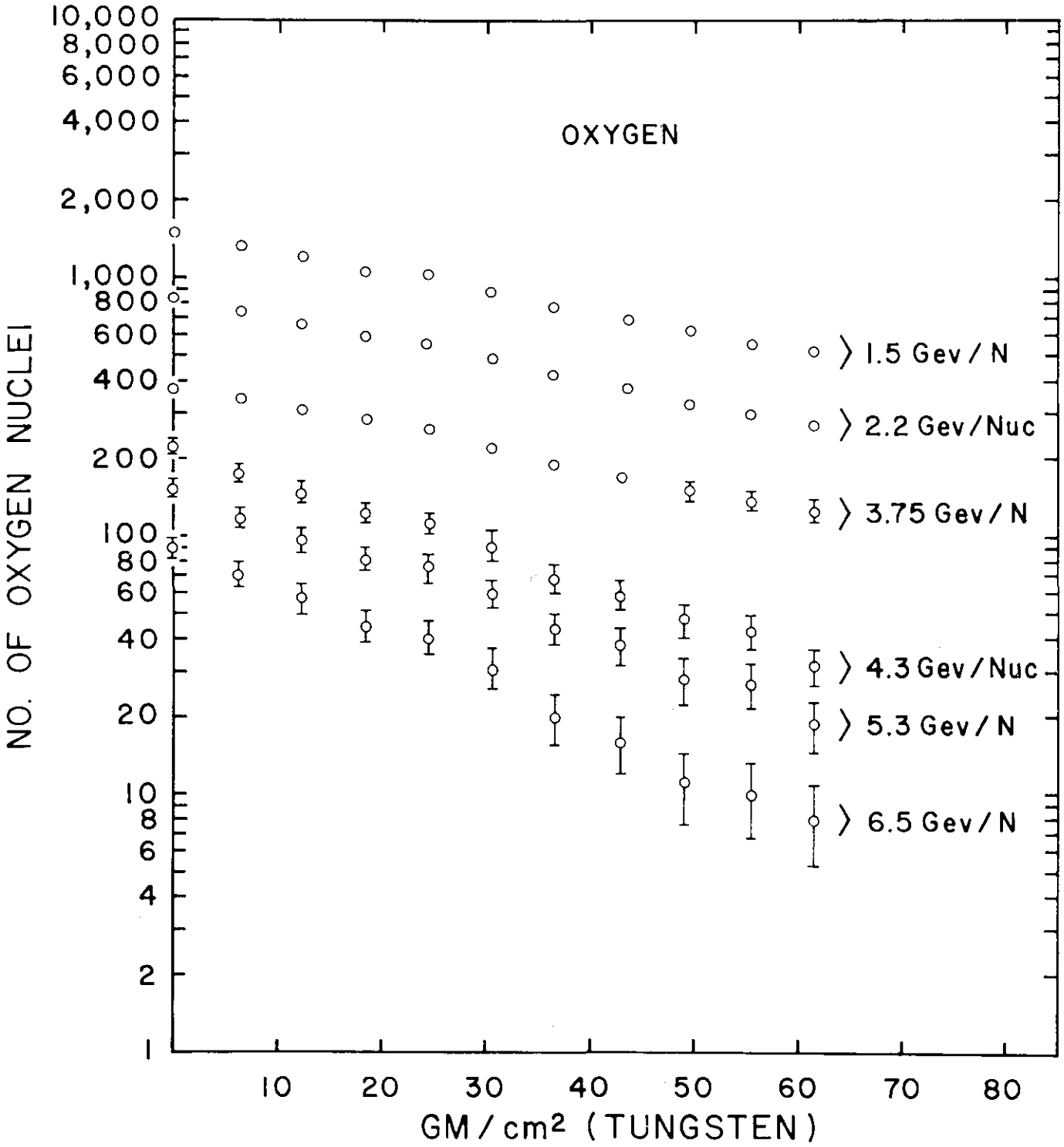
OXYGEN
NO. OF OXYGEN NUCLEI
10,000
8,000
6,000
4,000
2,000
1,000
800
600
400
200
100
80
60
40
20
10
8
6
4
2
1
10
20
30
40
50
60
70
80
GM / cm² (TUNGSTEN)
〉 1.5 Gev / N
〉 2.2 Gev/Nuc
〉 3.75 Gev / N
〉 4.3 Gev/Nuc
〉 5.3 Gev / N
〉 6.5 Gev / N

FIGURE 4

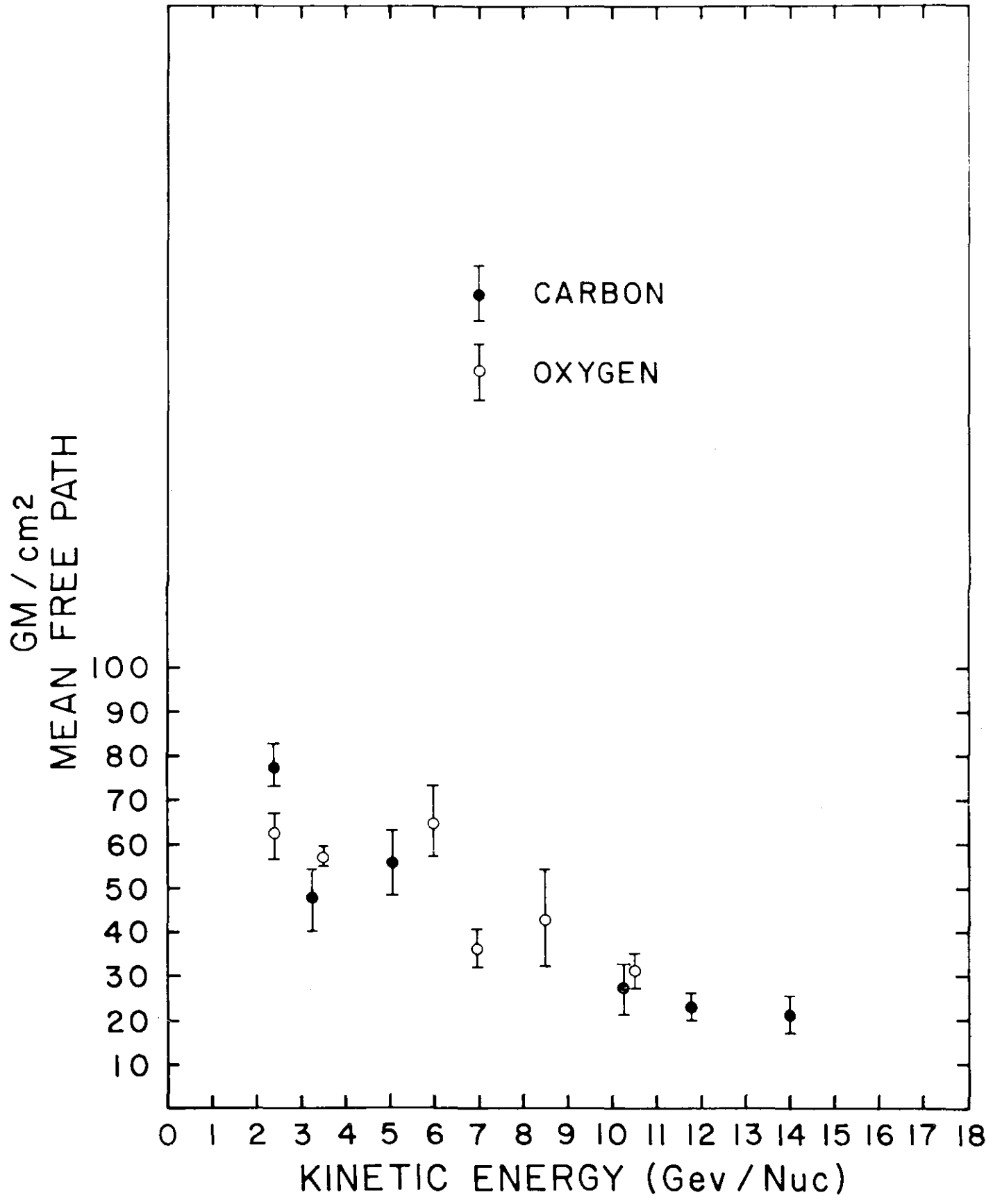
CARBON
OXYGEN
GM / cm²
MEAN FREE PATH
100
90
80
70
60
50
40
30
20
10
0 1 2 3 4 5 6 7 8 9 10 11 12 13 14 15 16 17 18
KINETIC ENERGY (Gev / Nuc)

FIGURE 5

THE PRIMARY COSMIC RAY ELECTRON SPECTRUM FROM 10 GeV TO ABOUT 200 GeV

R. F. Silverberg*, J.F. Ormes, V.K. Balasubrahmanyan,
M. J. Ryan+
Goddard Space Flight Center,
Greenbelt, Md.

Abstract

An ionization spectrometer consisting of 10.8 radiation lengths of tungsten and 35 radiation lengths of iron has been used to determine the energy spectrum of cosmic ray electrons above 10 GeV. The spectrometer was calibrated with electrons from 5.4 to 18 GeV at the Stanford Linear Accelerator and then flown at an altitude of 6 gm-cm^{-2} for 16 hours. Separation of electron initiated events from proton events was achieved by utilizing starting point distributions, the shower development in tungsten, and the energy deposited in the large thickness of iron absorber. The exponent of the differential energy spectrum of the electrons is -3.1 ± 0.2 while the exponent of the background is consistent with the proton exponent of $-2.7 \pm .2$.

1. Introduction

The energy spectrum of cosmic ray electrons has been given much attention in recent years because of its astrophysical significance. While results up to a few hundred GeV have been obtained in balloon flights (Nishimura et al. 1969; Anand et al. 1968; Anand et al. 1969; Scheepmaker, 1971) serious discrepancies in the spectral shape and absolute intensity are apparent.

In the hope of clarifying the high energy electron spectrum, a large area electron detector was flown from Alamogordo, New Mexico in April of 1969 at a depth of 7.9 g/cm^2 residual atmosphere and again in November 1970 at 6.0 g/cm^2 for a total exposure factor of 4800 M^2-ster-sec.

2. Description of the Detector

The experiment consists of three main sections. These are: (a) the charge module consisting of three scintillators and a Cerenkov counter. A digitized spark chamber is used to determine the trajectory of particles so that geometrical corrections can be made to the pulse heights from the detectors. The spark chamber is also useful in eliminating particles entering the sides of the detector and other background; (b) the electron cascade section of the detector consists of 12 modules each containing a 1/8" thick tungsten sheet and a 1/4" plastic scintillator. Each module is 0.9 radiation lengths thick; (c) the nuclear cascade section consists of 7 iron modules each of which is 4.5 radiation lengths thick. (Its primary use is for nucleons; see Ryan et al. this conference.) This section of the detector was not flown on the 1969 flight.

A diagram of the experiment as flown in 1970 is shown in Figure 1.

*University of Maryland
+NAS-NRC Research Associate

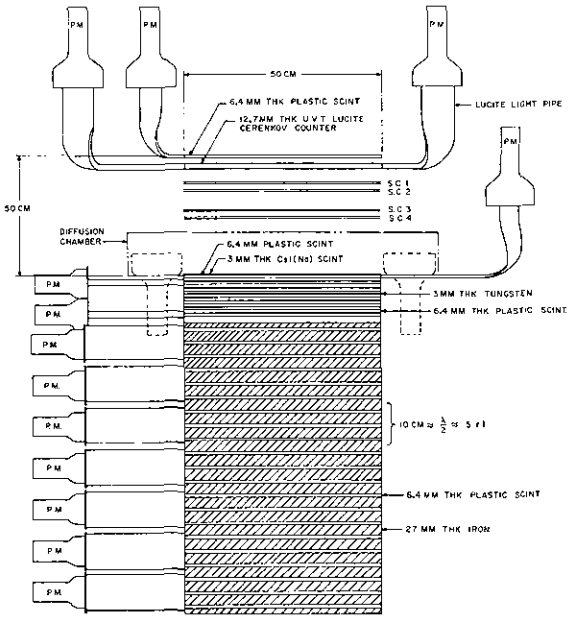

IONIZATION SPECTROMETER

3. Triggering Modes of the Experiment

In order to reduce background and the dead time in the experiment, the electron trigger criteria were set to demand the equivalent of a 7 GeV electron in the tungsten modules by requiring a minimum pulse height in each of the 12 scintillators. This not only discrminated against low energy particles, but also eliminated triggers from most of the high energy protons interacting deep in the tungsten. The only protons which triggered the electron mode were those which interacted early in the tungsten stack. In the proton trigger mode, particles were selected which deposited 40 GeV or more in the iron modules. These particles were used to determine the background proton correction to the electron intensity.

4. Energy Determination

The detector was calibrated on positrons from 5.4 to 18 GeV at the Stanford Linear Accelerator (SLAC) in 1969, and on protons up to 18 GeV at the Brookhaven National Laboratory in 1970.

The energy of an incident electron is determined by the minimization of the parameter $\chi^2 = \sum_i \frac{(N(E_o, t_o, t_i) - N_{\text{observed}}(t_i))^2}{\sigma^2(E_o, t_o, t_i)}$ (1)

where $N(E_o, t_o, t_i)$ is the number of particles that an electromagnetic cascade initiated by an electron of energy E_o will produce at depth t_i if it started to cascade at depth t_o. $\sigma^2(E_o, t_o, t_i)$ is the variance of $N(E_o, t_o, t_i)$. At SLAC energies, we observed $\sigma^2(E_o, t_o, t_i) \approx 4\, N(E_o, t_o, t_i)$ except at small depths where the deviations were larger.

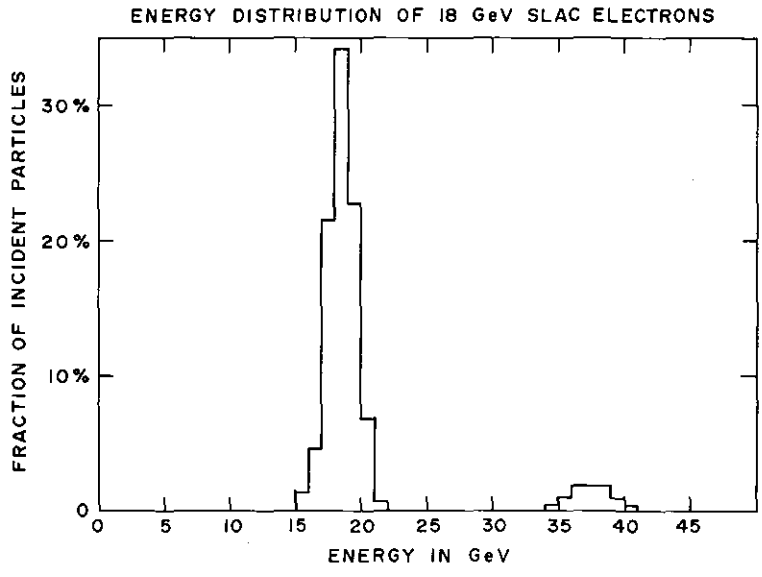

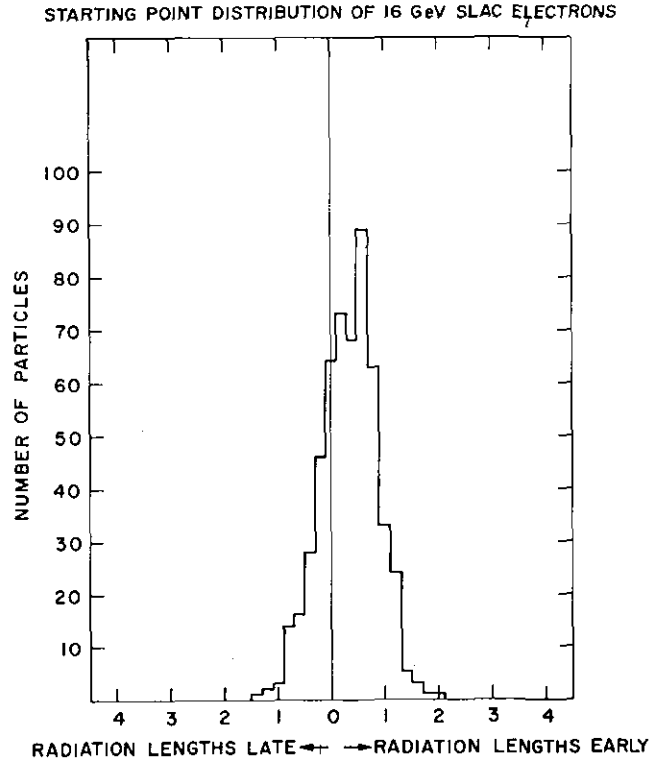

A two parameter fit to the data (E_o and t_o) is used to minimize χ^2. This determines E_o, the best estimate to the energy of the electron and t_o, the best estimate of its starting point. By using our data from SLAC, a χ^2 distribution for electrons was determined.

The energy distribution observed by applying the procedure outlined above to a run with 18 GeV electrons from SLAC is shown in Figure 2. The FWHM of the distribution is ~ 17%. The small peak below 40 GeV is due to two 18 GeV electrons incident on the experiment within the resolving time.

5. Discrimination against Protons

Due to the fact that the electron component of cosmic rays is at best only a few percent of the proton component, any measurement of electrons is usually plagued with a large component of protons which may masquerade as electrons. Any interaction which produces a π° meson may produce a cascade that is, in practice, indistinguishable from a cascade produced by an electron.

Our study of accelerator electrons and in-flight high energy protons has revealed that the method of fitting the cascades to the equation described above provides a sensitive means

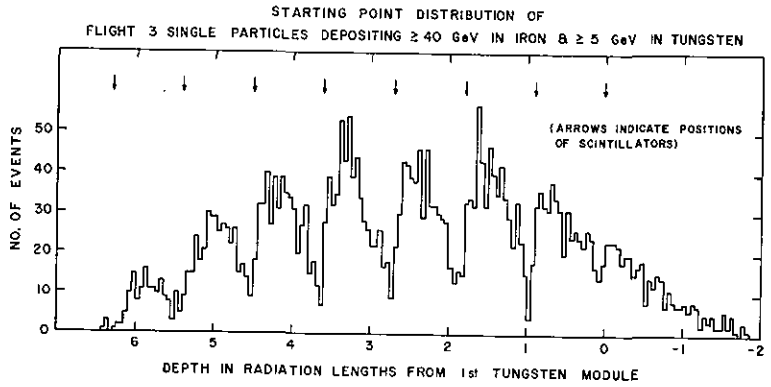

of discrimination against the proton background. In Figure 3 is presented the distribution of "apparent starting points" of a sample of 16 GeV electrons at SLAC. This curve is representative as we have noted no energy dependence from 5.4 to 18 GeV. Note that although there is only about 0.2 radiation lengths of material before the tungsten stack (0 radiation lengths on the graph), the "apparent starting point" distribution peaks at about 0.5 radiation lengths. In contrast to the electrons, a group of singly charged particles was selected from the 1970 flight which deposited $\geq$ 40 GeV in the iron and $\geq$ 5 GeV in the tungsten. Furthermore E (iron)/E (tungsten) > 1, implying that this class of particles is dominated by protons. Their "apparent starting point" distribution is shown in Figure 4.

The distribution in figure 4 exhibits marked structure. The source of the structure is not well understood at this time. One quarter of the interactions take place in the plastic scintillators which are invisible on this radiation length scale. The structure is the result of a competition between the process of fitting electromagnetic shower curves to nuclear interactions, the transport of γ-rays from π^0 decay into subsequent tungsten slabs and the shift of the "apparent starting point" by a few tenths of a radiation length. At any rate, the structure is real, is present for both protons and especially for background events and says that the shower fitting procedure is defining an "apparent starting point" with an accuracy of at least $\pm$.2 radiation lengths.

6. Data Analysis

Each possible electron event is examined to be sure that it is caused by a singly charged particle as determined by the top plastic scintillator and the Cerenkov detector. Both of these detectors are 30 cm above the tungsten stack. If the particle is singly charged, the spark chamber data is used to extrapolate the path of the particle to the twelfth tungsten module. Only particles whose trajectories pass inside of one inch of the edge of the 12th tungsten module are

analyzed.

Each possible electron event is then fitted to determine its energy and apparent starting point. The value of the minimum χ^2 is examined to see if the probability of it being an electron is greater than .05. If the apparent starting point is outside the limits observed at SLAC, the particle is discarded as it is likely to be caused by a proton interaction. Particles passing all of the above tests are estimated to be 85% electrons, the remaining 15% being background that is indistinguishable from electrons. It is important to note that the spectral index of rejected particles is -2.7 in agreement with the proton spectrum. We have also looked for energy dependent effects such as backscatter and find no effect large enough to cause the observed 0.5 change in spectral index. The resultant electron spectrum at the top of the atmosphere is presented in Figure 5.

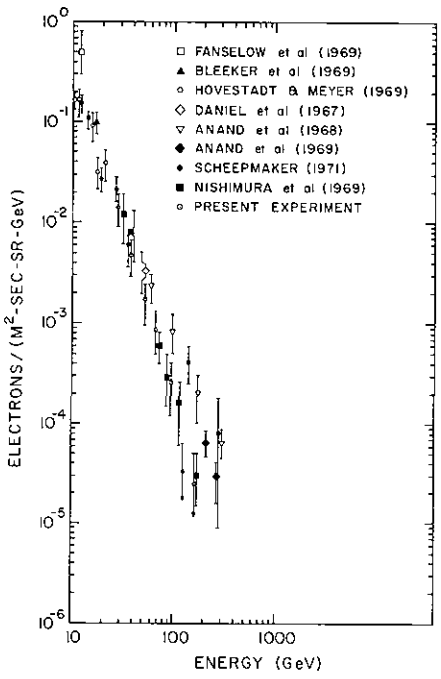

7. Conclusions

While the intensity in figure 5 agrees with the results of others at about 10 GeV, the spectrum is significantly steeper. The data can be fitted to a power law with a spectral index of -3.1 $\pm$0.2.

Our measured spectrum shows no sharp break but a consistent dropoff of the intensity of primary cosmic ray electrons. The spectral index of -3.1 may indicate a spectrum steepened by 0.5 power from -2.6. If the spectrum at lower energies has an index of -2.6, then steepening by half a power may occur in range of 10 GeV or below. This would be consistent with the model suggested by Jokipii and Meyer (1968) in which cosmic ray electrons diffuse in an isotropic medium.

8. References

Anand, K.C., Daniel, R.R., Stephens, S.A., 1968, Phys. Rev. Letters 20, 764.

Anand, K.C., Daniel, R.R., Stephens, S.A., 1969, Paper OG-11, 11th Int. Conf. on Cosmic Rays, Budapest.

Bleeker, J.A.M., Burger, J.J., Deerenberg, A.J.M., Hulst, H.C., Scheepmaker, A., Swanenburg, B.N., Tanaka, Y., 1969, paper OG-34, 11th Int. Conf. on Cosmic Rays, Budapest.

Daniel, R.R., Stephens, S.A., 1969, Proc. Ind. Acad. Sci., 65, 319.

Fanselow, J.L., Hartman, R.C., Hildebrand, R.H., Meyer, P., 1969, Ap. J. 158, 771.

Hovestadt, D., Meyer, P., 1969, paper MO-118, 11th Int. Conf. on Cosmic Rays, Budapest.

Jokipii, J.R. and Meyer, P., 1968, Phys. Rev. Letters 20, 752.
Nishimura, J., Mikumo, E., Mito, I., Niu, K., Ohta, I., Tiara, T., 1969, paper OG-43, 11th Int. Conf. on Cosmic Rays, Budapest.
Ryan, M.J., Ormes, J.F., Balasubrahmanyan, V.K., 1971, "The Cosmic Ray Proton and Helium Spectra above 50 GeV", this conference.
Scheepmaker, A., "Primary Cosmic Ray Electron Spectrum between 5 and $\simeq$ 300 GeV", unpublished, University of Leiden, 1971.

ACCELERATION AND PROPAGATION OF HIGH Z COSMIC RAYS IN A PULSAR ENVIRONMENT

V. K. Balasubrahmanyan, J. F. Ormes, and M. J. Ryan*
Goddard Space Flight Center, Greenbelt, Md. 20771

ABSTRACT

The survival of high Z nuclei in the X-ray photon field of a pulsar is investigated. For heavy nuclei with energies $\geq$ 100 GeV/nucleon, 100 keV X-ray photons have sufficient energy to cause photodisintegration with cross sections of $\approx 10^{-25}$ cm^2. Using the observed properties of the Crab pulsar, extrapolation back to epochs when the pulsar was more active indicates that the photon field is sufficiently dense to prevent the acceleration of heavy nuclei within the velocity of light cylinder. On this model, the upper limit on the energy of the escaping nuclei varies with time. The models for cosmic ray acceleration in supernova explosions or by pulsars will be related to experimental observations.

1. Introduction

The discovery of pulsars associated with supernova remnants in the Crab Nebula (NP0532) and the Gum Nebula (PSR0833-45) have led to a detailed description of the radiation processes in the pulsar environment (Goldreich, 1969) and also to an extremely efficient acceleration model for energetic cosmic rays (Gunn and Ostriker, 1969).

The possibility of photodisintegration of heavy nuclei by the blue shifted photon flux in the radial shock wave of Colgate's model has been considered by Kinsey (1969) and Colgate (1969). In this paper, we will discuss the more general problem of photodisintegration of heavy nuclei (pointed out by Appa Rao and Rengarajan, 1970) by the recently detected flux of high energy X-rays emitted by pulsars (Kurfess, 1971). We shall consider the implications of the latest cosmic ray observations on the various acceleration models.

2. Experimental Observations and Calculations

Results of the direct observation of charged cosmic rays with energies less than 10^{12} eV/nucleon are shown in Figure 1. The experimental method and detailed results will be published elsewhere. These results are in reasonable quantitative agreement with the spectra of all charged particles as presented by Grigorov et al. (1969) who also used ionization calorimeter techniques and of Koshiba et al. (1967) using a limited sample of events from emulsion stacks. Indirect observations at extensive air shower energies suggest that the composition remains unchanged up to energies of 10^{15} eV (Brandt and Rappaport, 1969; Bray et al., 1965), but above these energies, it is likely that there is a change in composition (Peters, 1960). The total spectrum from 10^9 to 10^{15} eV is shown in Figure 2.

*NAS-NRC Resident Research Associate

The X-ray flux from the most popular (and hopefully, most typical) pulsar NP0532 has now been measured by several groups. Figure 3 is taken from the paper for Kurfess (1971) and shows the observed flux from 1 keV up to several MeV. The total energy emitted above 100 keV is comparable with that from all energies below 100 keV and in this energy region the pulsed flux accounts for nearly half the emission of the nebula. X-rays of these energies can cause photodisintegration of heavy nuclei whose energies exceed 100 GeV/nuc., with a cross-section $\approx 10^{-25}$ cm^2.

Taking NP0532 to be at a distance of 2 kpc and assuming isotropic emission, the number density of 100 keV photons at a distance R(cm) from the pulsar is

$$n = 4.0 \times 10^{31} R^{-2} \text{ photons/cm}^3 \qquad (1)$$

We shall first consider the region within the velocity of light circle of the pulsar. The energy loss of the pulsar as a function of time is given by Bachall et al. (1970)

$$I(t) = I(o)\left[1 + \frac{2t}{t_o}\right]^{-2} \qquad (2)$$

where I(o) is the intensity at t = 0 and $t_o \approx 1$ year.

This expression assumes that the main source of loss is by magnetic dipole radiation. We assume that the X-ray emission has a similar time dependence, since the observed X-ray emission of $\sim 2.5 \times 10^{36}$ ergs sec^{-1} (Kurfess, 1971) is a large fraction of the total electromagnetic radiation.

Consequently the photon density within the light circle was much higher in the past, because of the increased emission and the smaller radius. The probability of survival of a heavy nucleus propagating radially through this flux within the light circle

$$P = \exp(-R\, n\, \sigma) \qquad (3)$$

If the energy loss is by magnetic dipole radiation, then

$$R \propto I^{-1/4} \qquad (4)$$

and

$$P = \exp\left[-1.7 \times 10^{8}(1 + 2t)^{-2.5}\right] \qquad (5)$$

This expression is shown by the 100 GeV/nucleon curve in Fig. 4. Also shown are the curves for 10 GeV/nucleon and 1 GeV/nucleon particles which have been calculated assuming the photon flux spectrum continues with a constant exponent =-1.2 up to 10 MeV.

The intense fields of the pulsar and its emitted radiation will not allow straight line motion of the heavy nuclei, as assumed here, and this will result in an increased probability of disintegration.

Outside the light circle in the nebula itself, the X-ray flux is assumed to have a similar radial and time dependence to that given by equations (1) and (2), but in this case the radius will be that of the supernova shell. If we assume the parameters quoted by Shklovsky (1968) then,

$$R = 789\ t + 1.2 \times 10^{-8} \times t^2 \text{ km} \qquad (6).$$

The probabilities of photodisintegration using these parameters is $< 10^{-2}$ for 100 GeV/nucleon particles except for times $t \approx 1$ year. During this time the pulsar parameters are uncertain because of the possibility of large energy loss by gravitational radiation (Ostriker, 1969).

3. Discussion and Conclusions

If all the charged cosmic rays are accelerated in the supernova shock wave process, then the observed spectra shown in Figure 1 definitely refute Kinsey's original suggestion that there would be a sharp cut-off at 15 GeV/nucleon for a field acceleration process or about 32 GeV/nucleon for a plasma wave process. However, if as pointed out by Colgate (1967) the final energy of the stellar matter is proportional to γ^2 shock the cut-off energies become 225 and 1000 GeV/nucleon respectively (Kinsey, 1969). More recent calculations by Colgate (1969) predict for small mass supernovae an attenuation of heavy nuclei at $\approx$ 400 GeV/nuc. These energies are beyond the limits of the detailed measurements of Figure 1. The lack of a bend in the all particle spectrum of Grigorov (1969) suggests that this is not the dominant cosmic ray acceleration mechanism. If resynthesis of the heavy nuclei should occur behind the shock wave, it is unlikely that the resulting composition would be energy independent.

The Gunn and Ostriker mechanism of acceleration by the E x B fields of low frequency, large amplitude electromagnetic waves is so efficient, that for a pulsar with properties similar to NP0532, all particles will be accelerated to an energy of at least 2×10^{12} eV/nucleon in the vicinity of the light circle. But as shown earlier, it is unlikely that the heavy nuclei can survive in this region, especially at earlier epochs. It is at these times that the major fraction of the pulsar's energy is lost and that most of the particle acceleration would occur.

Consequently if a pulsar acceleration process is responsible for the majority of the observed heavy cosmic rays then we should expect a steepening of the spectrum in the region of 10^{11} eV/nucleon. In this model, it is expected that the composition of cosmic rays would be that ejected by the neutron star (Ostriker 1970) but strongly modified by photodisintegration. The net result will be a complex composition enhanced in particles of lower charge.

However, photodisintegration in the nebula itself has a very small probability of occurrence so that the suggestion by Ostriker (1970) of acceleration in that region is tenable. This model makes use of the energy dissipated by the interaction of the magnetic dipole radiation with the expanding envelope. The composition of cosmic rays accelerated in this region is expected to be similar to that of supernova ejecta. On this model it is possible that the observed steepening of the all particle spectrum at $\approx 10^{16}$ eV is caused by photodisintegration in the nebula by intense ultraviolet fluxes near the acceleration regions of these cosmic rays.

If the constancy of the ratio of protons to heavy charged particles (directly observed up to 10^{11} eV) remains up to 10^{15} eV as suggested by the E.A.S. results, then the nebula acceleration process is the only likely mechanism for accelerating the charged particles within a discrete source.

Acknowledgements

We would like to thank Reuven Ramaty, Elihu Boldt, and Don Reames for useful criticism and discussion.

References

Appa Rao, Krishna, M.V., and Rengarajan, T.N., 1970, Ap. J. Letters, 6, 229.
Bachall, N.J., Rees, M.J., and Salpeter, E.E., 1970, Ap. J., 162, 737.
Barrett, P.H., Bollinger, L.M., Cocconi, G., Eisenberg, Y., and Greisen, J.K., 1952, Rev. Mod. Physics, 24, 133.
Bradt, H., and Rappaport, S.A., 1970, Phys. Rev. Letters, 22, 760.
Bray, A.D. et al., 1965, Proc. of 9th Int. Conf. on Cosmic Rays, 2, 668.
Colgate, S.A., 1969, Proc. 11th Int. Conf. on Cosmic Rays, 1, 359.
Colgate, S.A. and White, R.H., 1966, Ap. J., 143, 626.
Colgate, S.A. and White, R.H., 1963, Roc. Int. Conf. on Cosmic Rays, Jaipur, 3, 335.
Colgate, S.A., 1967, Ap. J., 150, 163.
Goldreich, P., and Julian, W., 1969, Ap. J., 157, 869.
Greisen, K., 1960, Ann. Rev. Nucl. Sci., 10, 63.
Grigorov, N.L. et al., 1969, Proc. 11th Int. Conf. on Cosmic Rays, 1, 518.
Gunn, J., and Ostriker, J., 1969, Phys. Rev. Letters, 22, 728.
Gunn, J., 1970, Ap. J., 160, 979.
Kinsey, J. H., 1969, Ap. J., 158, 295.
Koshiba, N., Suda, E., and Takasaki, F., 1968, Can. J. Phys., 49, 651.
Kurfess, J.D., 1970, preprint submitted to Ap. J., May.
McCusker, C.B.A., and Peak, L.S., 1964, Il Nuovo Cimento, 31, 526.
Nikolsky, S.J., 1962, Usp. Fiz. Nauk. 78(5), 365.
Ormes, J.F., Balasubrahmanyan, V.K., and Ryan, M.J., 1971, to be published.
Ostriker, J. and Gunn, J., 1969, Ap. J., 157, 1395.
Ostriker, J., 1969, Proc. 11th Int. Conf. on Cosmic Rays, 1, 69.
Peters, B., 1960, Proc. of Moscow Cosmic Ray Conf., Vo. 1, 157.
Shklovsky, I.S., 1968, "Supernovae", 206, John Wiley & Sons publishers.

Figure Captions

Fig. 1 - Total energy spectra of L, M, LH, MH, Ca and Fe group of nuclei observed with an ionization spectrometer flown on a balloon on 14 Nov. 1970. The intensities have been corrected for spallation in the atmosphere and in the detector. The turnover at low energies is due to the geomagnetic cut-off. The straight lines are the best power law fit to the observed points.

Fig. 2 - Cosmic ray energy spectra from 10^{10} to 10^{16} eV. The Goddard Space Flight Center results and the results of Grigorov et al. are in close agreement but at higher energies there is a discrepancy between Grigorov et al. and the air shower results. There is a change in the spectral exponent from -1.7 to -2.2 at 2×10^{15} eV.

Fig. 3 - Observed X-ray flux from the Crab Nebula and its associated pulsar NP0532. Taken from Kurfess (1971).

Fig. 4 - Survival probability of an iron nucleus near the velocity of light cylinder of a pulsar similar to NP0532 at different epochs. Particles with energies greater than 100 GeV/nucleon will not survive for ages less than 1,000 years.

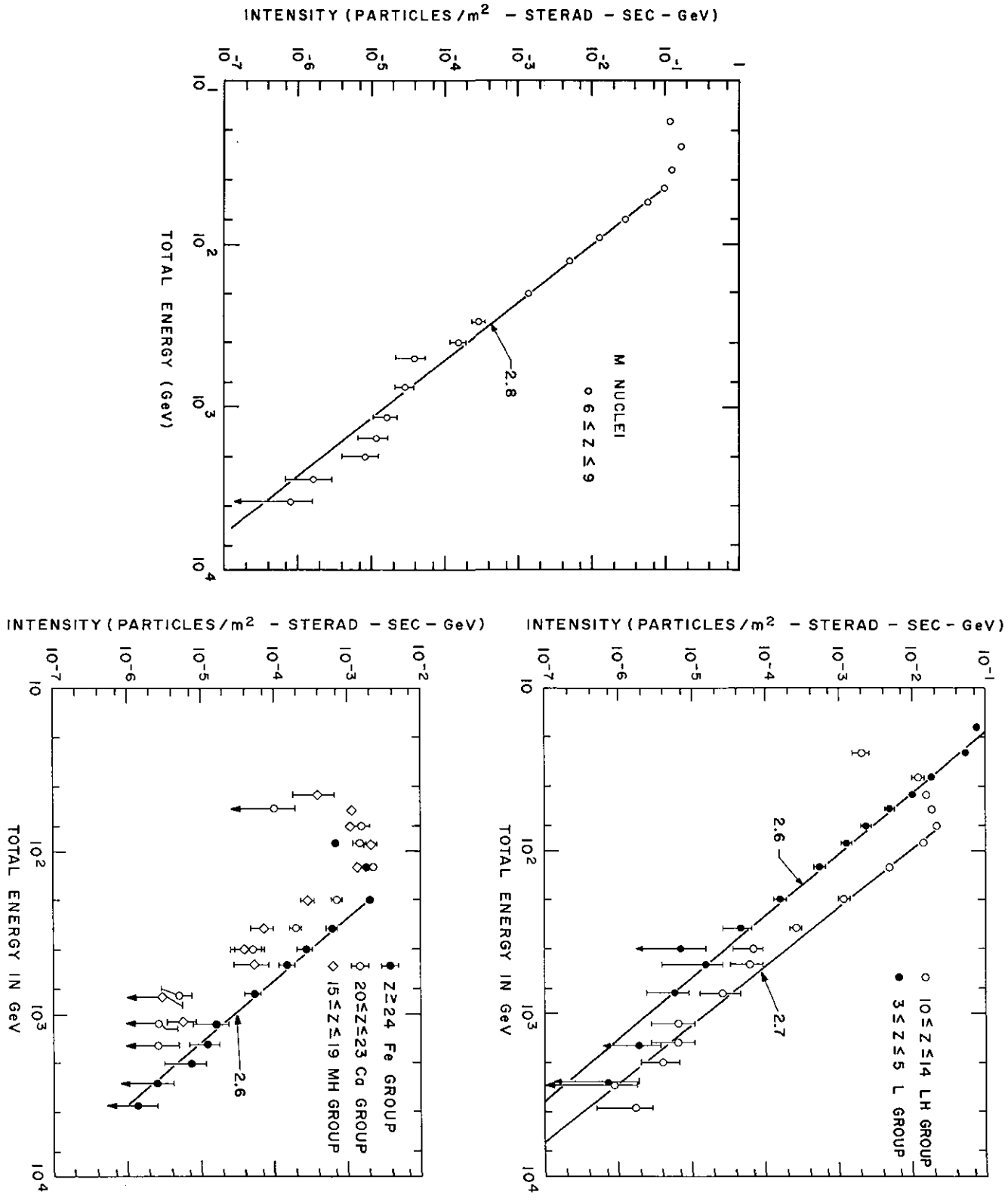
INTENSITY (PARTICLES/m² - STERAD - SEC - GeV)
TOTAL ENERGY (GeV)
M NUCLEI
○ 6 ≤ Z ≤ 9
2.8
INTENSITY (PARTICLES/m² - STERAD - SEC - GeV)
TOTAL ENERGY IN GeV
○ 10 ≤ Z ≤ 14 LH GROUP
● 3 ≤ Z ≤ 5 L GROUP
2.6
2.7
INTENSITY (PARTICLES/m² - STERAD - SEC - GeV)
TOTAL ENERGY IN GeV
● Z ≥ 24 Fe GROUP
◇ 20 ≤ Z ≤ 23 Ca GROUP
◇ 15 ≤ Z ≤ 19 MH GROUP
2.6

FIGURE 1

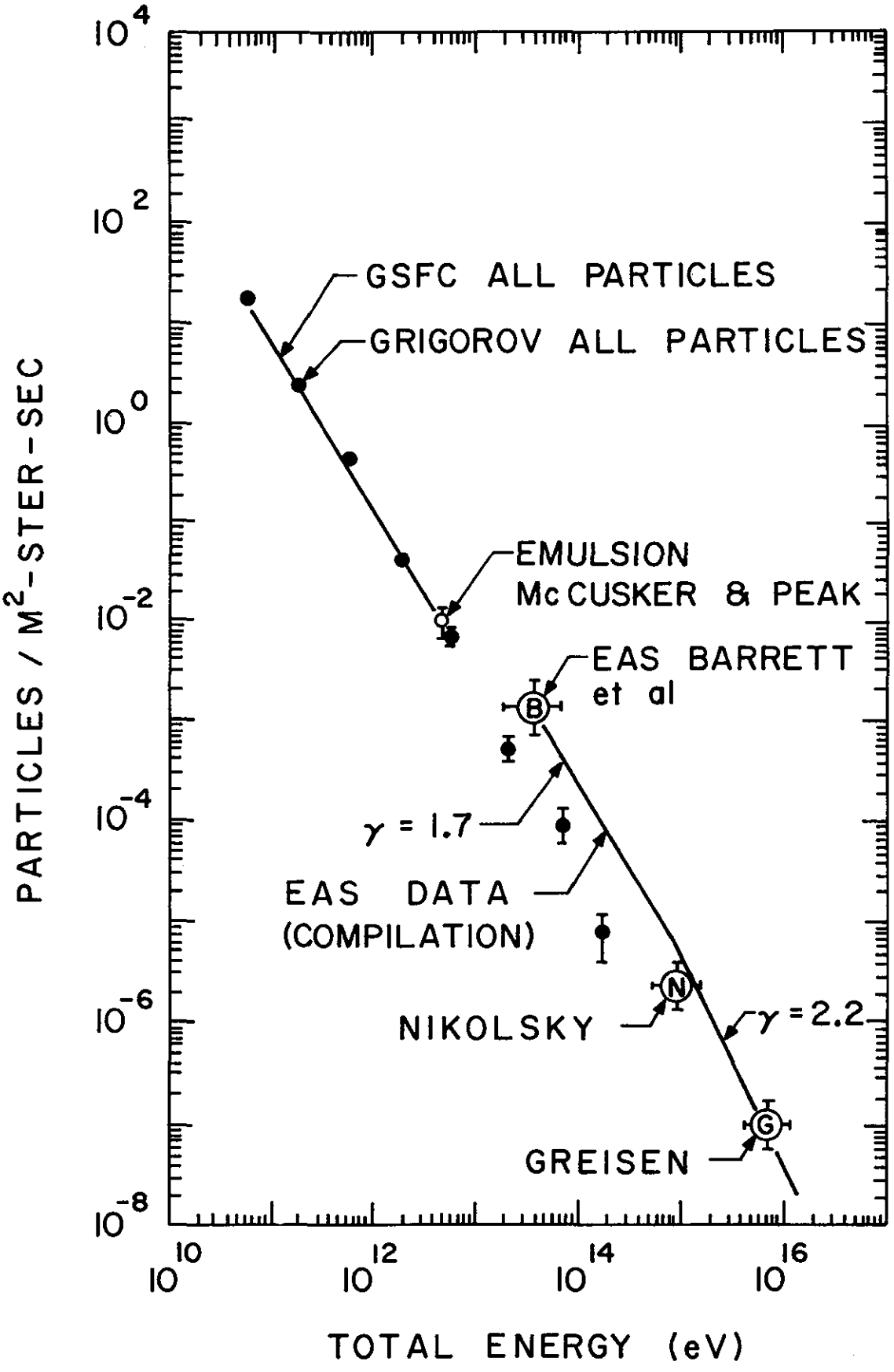
GSFC ALL PARTICLES
GRIGOROV ALL PARTICLES
EMULSION
McCUSKER & PEAK
EAS BARRETT
et al
γ = 1.7
EAS DATA
(COMPILATION)
NIKOLSKY
γ = 2.2
GREISEN
PARTICLES / M²-STER-SEC
TOTAL ENERGY (eV)
10⁴
10²
10⁰
10⁻²
10⁻⁴
10⁻⁶
10⁻⁸
10¹⁰
10¹²
10¹⁴
10¹⁶

FIGURE 2

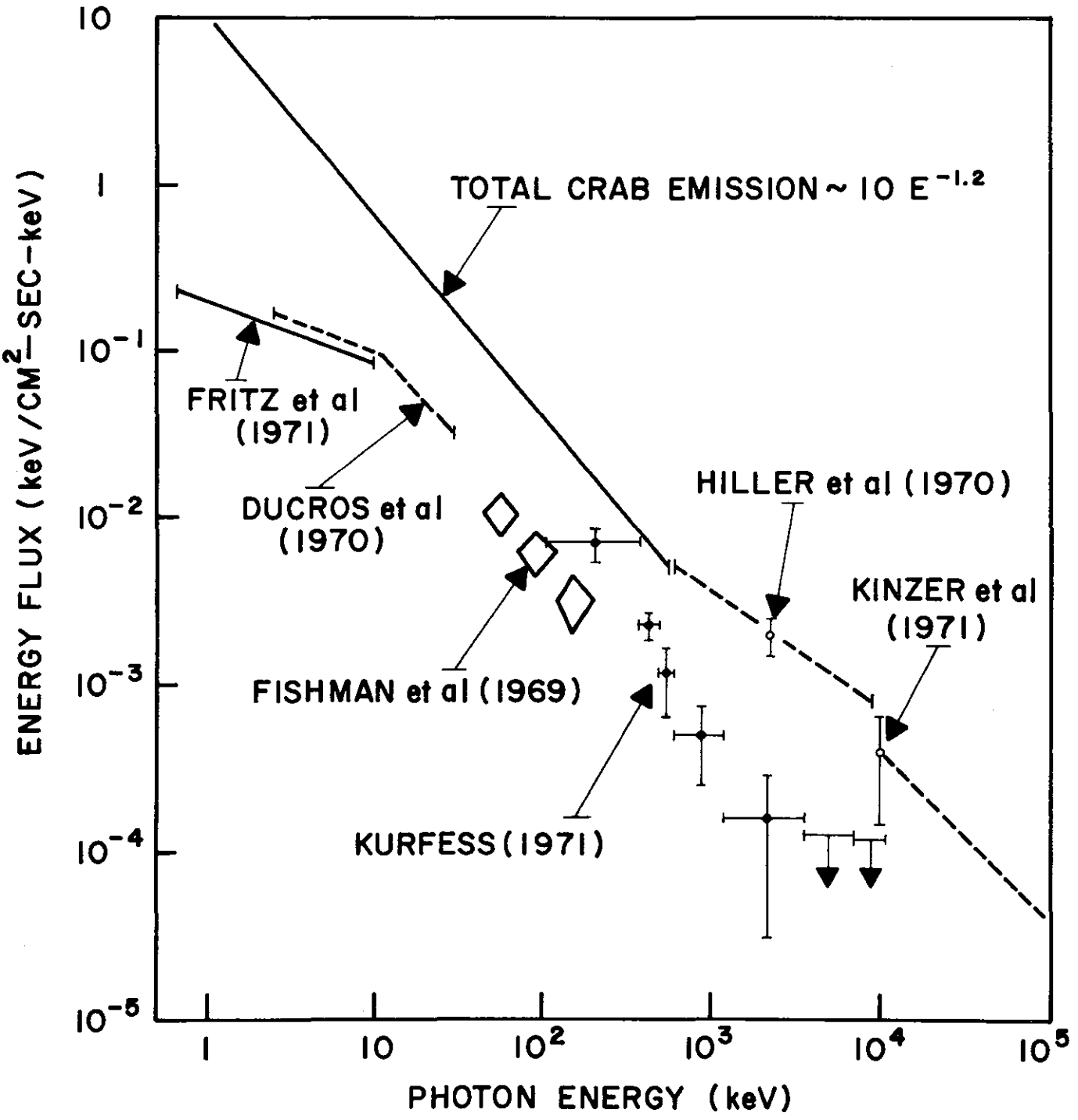
10
1
10^{-1}
10^{-2}
10^{-3}
10^{-4}
10^{-5}
ENERGY FLUX (keV/CM^2-SEC-keV)
TOTAL CRAB EMISSION ~ 10 $E^{-1.2}$
FRITZ et al (1971)
DUCROS et al (1970)
HILLER et al (1970)
KINZER et al (1971)
FISHMAN et al (1969)
KURFESS (1971)
1
10
10^2
10^3
10^4
10^5
PHOTON ENERGY (keV)

FIGURE 3

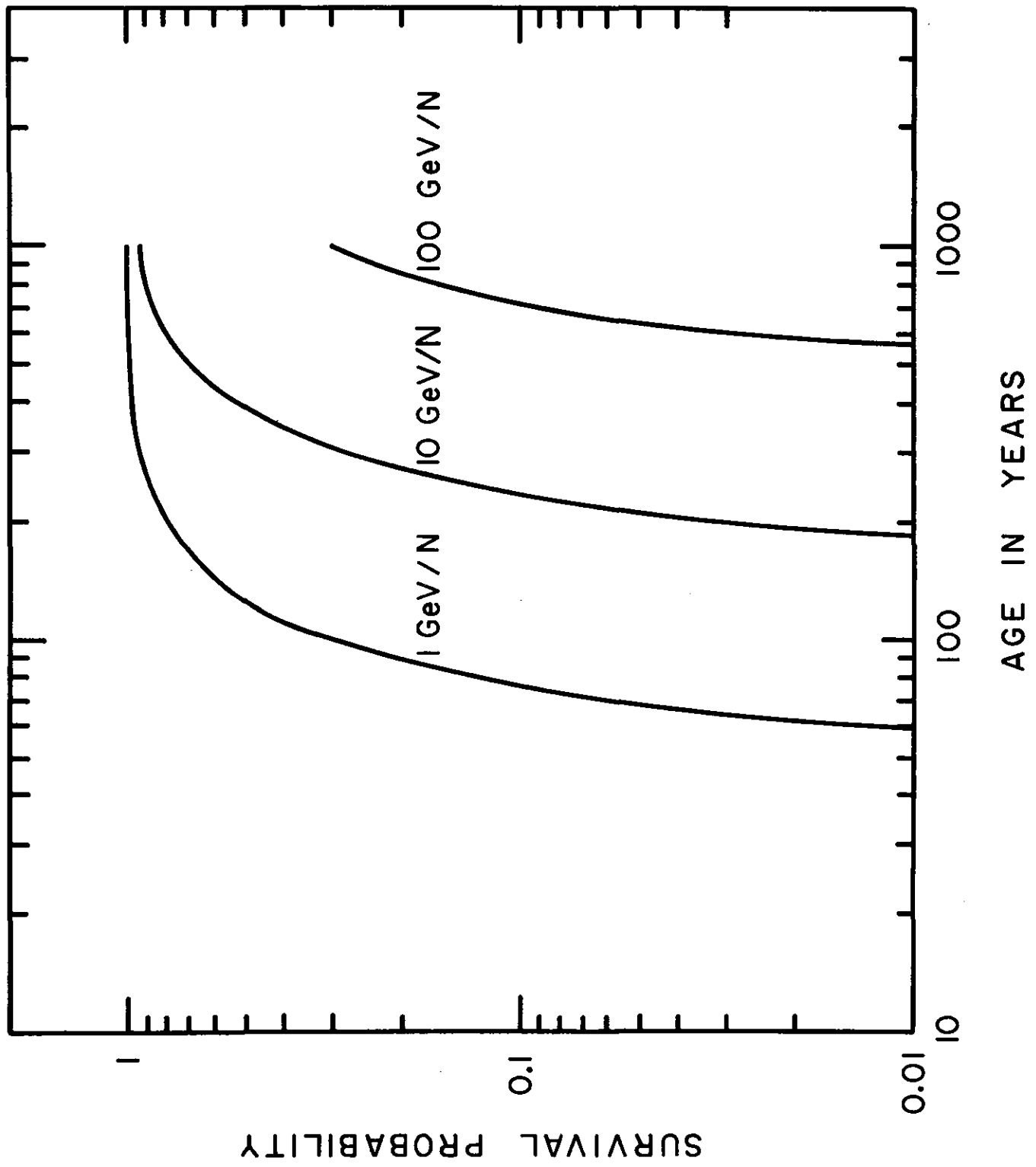
SURVIVAL PROBABILITY
1
0.1
0.01
10
100
1000
AGE IN YEARS
1 GeV/N
10 GeV/N
100 GeV/N

FIGURE 4

THE GAMMA RAY EXPERIMENT FOR THE SMALL ASTRONOMY SATELLITE B (SAS-B)

C. E. Fichtel, C. H. Ehrmann, R. C. Hartman,
D. A. Kniffen, H. B. Ögelman*, and R. W. Ross

Goddard Space Flight Center, Greenbelt, Md. 20771

Abstract

A magnetic core digitized spark chamber gamma ray telescope has been developed for satellite use and will be flown on SAS-B in less than one year. The SAS-B detector will have the following characteristics: Effective area = 500 cm^2, solid angle = $\frac{1}{4}$ SR; Efficiency (high energy) = 0.29; and time resolution of better than two milliseconds. A detailed picture of the galactic plane in gamma rays should be obtained with this experiment, and a study of point sources, including short bursts of gamma rays from supernovae explosions, will also be possible.

1. Introduction

The SAS-B gamma ray telescope represents the first satellite version of a planned evolution of a gamma ray digitized spark chamber telescope which began with the development of a balloon borne instrument. The telescope is aimed at the study of gamma rays whose energy exceeds about 20 MeV.

In the early 1960's, it was realized that the celestial gamma ray intensity was very low compared to the high background of cosmic ray particles and earth albedo. For this reason, a picture type detector seemed to be needed to identify unambiguously the electron pair produced by the gamma ray and to study its properties - particularly to obtain a measure of the energy and arrival direction of the gamma ray. In addition, the secondary gamma ray flux produced by cosmic rays in the atmosphere, even at the altitudes of the present large balloons, severely limits the gamma ray astronomy which can be accomplished with balloons and dictates that gamma ray astronomy must ultimately be accomplished with detector systems on satellites. The combination of the need to develop a satellite instrument together with the requirement of handling a large amount of data led us in 1963 to begin development of a rugged magnetic core digitized spark chamber which could also be used for many other experiments.

---

*Present address:
Middle East Technical University
Ankara, Turkey

D. L. Bertsch will present the paper at the meeting.

2. General description of the Instrument

A schematic diagram of the gamma ray telescope to be flown on the SAS-B satellite is shown in Fig. 1.

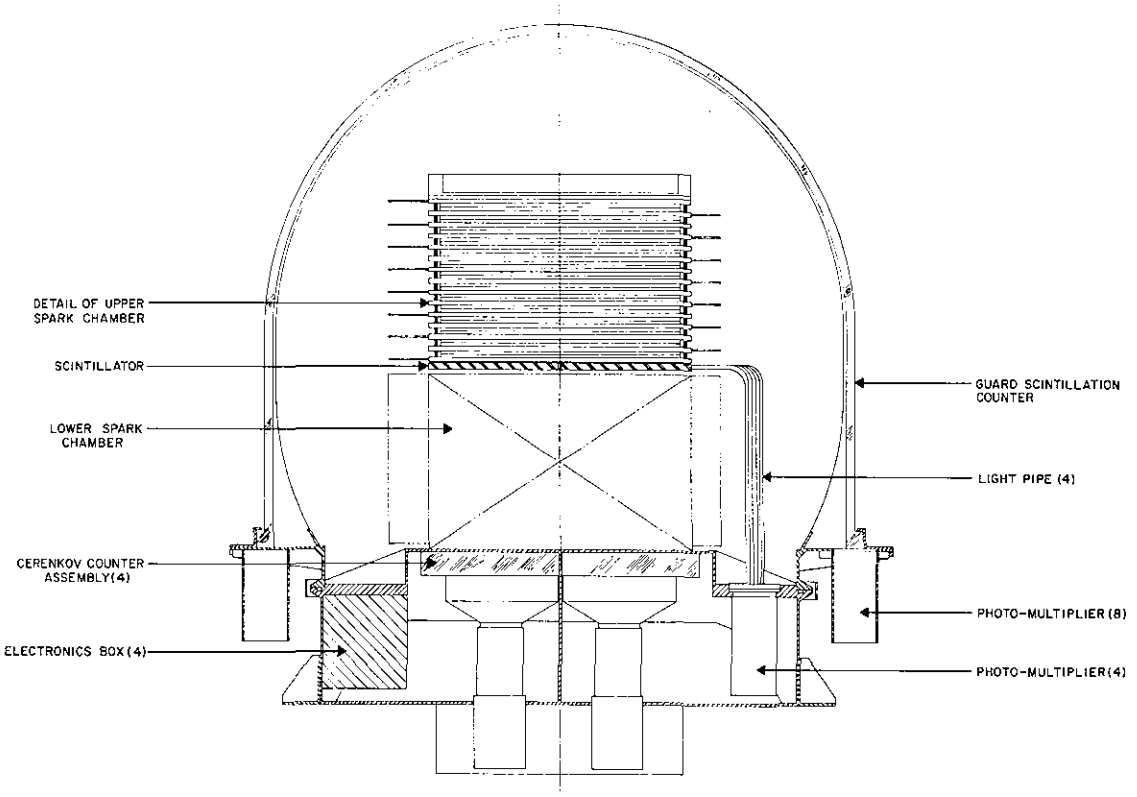

SAS-B GAMMA RAY EXPERIMENT
FIG. 1

The spark chamber assembly consists of 16 spark chamber modules above a set of four central plastic scintillators and another 16 modules below these scintillators. Thin tungsten plates, averaging 0.010 cm thick -- corresponding to 0.03 radiation lengths -- are interleaved between the spark chamber modules. In the upper half of the spark chamber assembly these plates serve a dual purpose, first to provide material for the gamma ray to be converted into an electron pair and secondly to provide a means of determining the energy of the electrons in the pair. An estimate of the energy of each electron is obtained by measuring the average Coulomb scattering as they pass through the plates in the upper and lower spark chamber assemblies. The plates in the lower half of the spark chamber assembly are there primarily for this latter purpose.

The spark chamber assembly is triggered if a charged particle passes through one of the four equal plastic scintillator tiles and the corresponding directional lucite Cerenkov counter immediately below, and, at the same time, there is no pulse in the surrounding plastic scintillator anticoincidence dome. Each of the four scintillator Cerenkov counter telescopes acts independently of the others and has a full-width-half-maximum opening angle of about 30^{o}. The anticoincidence dome prevents the spark chamber system from being triggered by charged particles, and the directional feature of the Cerenkov counter prevents the telescope from being triggered by upcoming neutral events or charged particles which might stop above the central scintillator before reaching the anticoincidence dome. Absolute time of each gamma ray event will be known to about 1 millisecond; thereby, permitting a careful analysis of pulsars and other time varying objects.

Another spark chamber trigger mode is the hodescope trigger, which is included to detect bursts of gamma rays predicted to be associated with supernovae explosions. In this mode, the anticoincidence dome is not used since some of the gamma rays in the postulated short ($<$ 1 microsecond) pulse would probably convert in the dome giving rise to a pulse which would be detected by the phototubes viewing the anticoincidence dome. Instead all four scintillator counters and all four Cerenkov counters are required to have a coincidence within 0.4 microseconds, so that an electron shower produced in the telescope by several gamma rays interacting in the thin plates between the spark chambers will trigger the system. Some complex cosmic ray induced events may also trigger this mode, but they can be rejected by an analysis of the spark chamber data for the particular event.

Turning to the spark chambers, each module consists of two parallel planes of 200 wires with a gap between the planes of 0.4 cm. The wires in each plane are parallel and orthogonal to the wires of the opposite plane. Each of the grid wires threads a magnetic core which is activated when current flows along the wires intercepted by the spark. Thus reading out and recording the location of the set cores provides two orthogonal coordinates for the intersection of the charged particle trajectory with each modular or z-level.

The data obtained in orbit are stored at a one kilobit per second rate on magnetic tape. Once per orbit, the tape recorder will be commanded into a playback mode to telemeter the information accumulated for that orbit to a ground receiving station. The spark chamber information will be analyzed using advanced versions of automatic computer techniques developed over the last several years to analyze balloon experiment data (Fichtel et al., 1971). The computer programs will examine all spark chamber telescope events. Events which cannot be analyzed automatically will be transferred to a Graphics Display Unit where a data analyst will examine the event and make necessary decisions to allow the automatic analysis to proceed. The display will also be used to analyze a selected number of "good" events to check the performance of the automatic procedure.

The effective area, which is limited by the size of the Cerenkov scintillators, is 540 cm^2. The opening angle for detection of gamma rays is approximately $\frac{1}{4}$ Sr. The efficiency for detection of gamma rays of very high energy is 0.29, and for detection of 100 MeV gamma rays is about 0.21.

The efficiency and solid angle will be determined precisely as a function of energy before launch by calibration at the synchrotron facility of the National Bureau of Standards.

By combining the energy and directional information for each electron in accordance with procedures described previously (Fichtel, Kniffen and Ogelman, 1969), the direction and energy of the primary gamma ray can be obtained. The uncertainty in the arrival direction for a gamma ray is about 1 $\frac{1}{2}^{o}$ at 100 MeV and varies with energy approximately as $E^{-2/3}$. The threshold is not sharp, but is about 20 to 25 MeV. The energy of the γ-ray can be measured up to about 200 MeV, with an accuracy of about 30 to 40%.

It is planned that SAS-B will be launched from San Marco off the coast of Kenya into an approximately circular equatorial orbit with a 3^{o} inclination and a 550 kilometer apogee. The satellite is capable of being pointed in any direction, but the time to change the direction of pointing is relatively long so that normally for the period of one orbit the satellite will point in essentially the same direction. Hence, for approximately 0.38 of the orbit the detector will point at the earth, and for another approximately 0.08 of the orbit the earth albedo gamma ray flux will be quite high leaving about 0.54 of the orbit for collection of celestial gamma ray data. Combined with an expected percentage live time (the period when cores are not being read out and the gamma ray telescope is ready to accept another event) of about 90%, the portion of an orbit during which celestial data is collected is estimated to be just under 0.5. The net exposure for a one week viewing period directed at some point on the celestial sphere will be about 3.3×10^{7} cm^{2} sec for 100 MeV gamma rays from a point source and about 10^{7} cm^{2} sr sec for diffuse radiation.

3. Possible Scientific Studies

SAS-B should be able to explore the galaxy with fine spatial and energy resolution. The latter will separate gamma rays of π^{o} origin from other processes, and the former will permit a better understanding of the dynamic processes occurring in our galaxy, as well as a search for point sources. Our galactic disk is believed to be in a state of dynamic equilibrium. The expansive pressures of the hot cosmic ray gas, the magnetic fields, and the kinetic motion of matter in the galactic disk are counter-balanced by the gravitational attraction of galactic matter (Parker, 1966). Of the three expansive pressures mentioned, that due to the cosmic rays is the only one which seems likely to have the capability of changing markedly over short periods (less than 10^{4} years in this context), if some of the more accepted current concepts of the origin of cosmic rays are correct. Therefore, a study of the cosmic ray distribution in the galaxy will permit an analysis of the expansive pressures of cosmic rays after their release and also aid in locating the origin of recent cosmic ray sources, as suggested by Pinkau (1970). The cosmic ray distribution can be determined with the aid of high energy gamma ray astronomy, since cosmic rays reveal their presence through interactions with interstellar matter which lead to π^{o} mesons which in turn decay into high energy gamma rays with a characteristic energy spectrum.

SAS-B may also be able to speak even more directly to the origin of cosmic rays. To associate the cosmic ray particles directly with a source experimentally, a neutral and long-lived component must be used, since the charged cosmic ray particles themselves suffer an unknown number of deflections and spirals in the complicated magnetic fields of the intervening space. With this in mind, Colgate (1968) predicted that a very short, highly energetic photon pulse should occur if the hydromagnetic supernova cosmic ray origin theory is correct. Following the calculations of Fichtel and Ogelman (1968), several such pulses should be seen by SAS-B in a year if the theory is correct.

Finally, the search for point sources can be pursued unencumbered by atmospheric background to the sensitivity levels indicated in the previous section. Pulsars can be examined to see if the source mechanism is such that radiation extends into the gamma ray region. Of particular interest will be the Crab pulsar. If the present estimates of the Crab x-ray pulsar flux are extended to the gamma ray region, 10^3 gamma rays could be seen in a week's observation. Thus, quite significant information will be obtained about the origin of the Crab pulsed radiation - even if there should be a null result. A positive result with an energy spectrum would, of course, provide very exciting information on the highest energy region of the source mechanism.

4. References

Colgate, S. A. 1968. Canad. J. Phy. 46, 5476.

Fichtel, C. E., Hartman, R. C., Kniffen, D. A., and Sommer, M. 1971. "Gamma Ray Observations of the Galactic Center and Some Possible Point Sources", submitted for publication in the Astrophysical Journal.

Fichtel, C. E., Kniffen, D. A., and Ogelman, H. B. 1969. Ap. J. 158, 193.

Fichtel, C. E., and Ogelman, H. B. 1968. NASA Technical Note TN D-4732.

Parker, E. N. 1966. Astrophys. J. 145, 811.

Pinkau, K. 1970. Phys. Rev. Letters 25, 603.

SHORT TIME-SCALE OPTICAL PULSATIONS IN THE NIGHT SKY BACKGROUND

D. L. Bertsch

Goddard Space Flight Center, Greenbelt, Md. 20771

A. Fisher and H. Ogelman, Middle East Technical University, Ankara, Turkey

ABSTRACT

A network of monitoring stations designed to detect large scale fluorescence emission in the atmosphere has been in operation for over two years. The motivation for the search arises from the prediction by Colgate that an energetic photon burst would be produced in a supernova and this burst, when absorbed in the atmosphere, would produce fluorescence. This paper reports on observations up to February 1971. No supernova-like events have been found, although 4.4 were expected. One class of non-fluorescence events is described that evidence suggests is related to electrical discharge in the atmosphere. Another type of non-fluorescence pulse appears to be related to particle precipitation in the atmosphere.

1. Introduction

One of the most significant advances in astrophysics has been the development of a detailed theory describing a supernovae explosion and subsequent neutron star formation (Colgate and Johnson, 1960; Colgate and White, 1966; Arnett, 1967). Among the several important implications of this theory, a plausible mechanism for the production of cosmic rays is furnished. On the basis of a rather general argument, Colgate (1968) predicted energetic photons also will be produced during the relativistic shock expansion when the outer mantle of the star is accelerated to cosmic ray velocities. Basically these energetic photons result from optical photons that are Doppler shifted during the shock expansion. Colgate predicted that the photon pulse would contain a total energy $\sim 5 \times 10^{49}$ ergs with individual energies up to $\sim$ 2 GeV and with a pulse duration of $\sim$ tens of microseconds.

In an effort to detect the photon wave fronts predicted by Colgate, a monitoring program has been operated for more than two years. Details of the experiment have been presented previously (Fichtel and Ogelman, 1968; Ogelman and Bertsch, 1970). This paper reviews the experimental apparatus and summarizes the observations up to February 1, 1971. In searching for extraterrestrial events, local station records reveal two categories of events that apparently are related to geophysical effects and these are described.

2. Experimental Approach

The mode of operation of the experiment is to use a wide-angle, ground-based photomultiplier system designed to detect fluorescence emission that is expected to be produced by the absorption of the primary photon pulse in the atmosphere. It has long been known that the upper atmosphere fluoresces in the UV, visible, and infra-red spectral regions as a result of stimulation from a

wide energy band of X-rays, γ-rays, and charged particles. Considerable work on the fluorescence phenomenon has been done by workers at Cornell (Greisen, 1965; Bunner, 1966) with the aim of utilizing fluorescence in air shower detection. Hartman (1963) made extensive laboratory studies of fluorescence phenomena. These studies show that for ground-based photomultiplier detectors, the only significant fluorescence emission is from the N_2^+ first negative band system of molecular nitrogen in the wavelength region from 3200 Å to 4500 Å with the principal contribution at 3914 Å. Absorption occurs in the atmosphere at altitudes that depend on the photon energy. Above 100 keV, Compton and pair production processes dominate and this occurs at 20 to 30 km with an efficiency of $\sim 5 \times 10^{-4}$. Below 10 keV, the photo-electric process is the most important. Here absorption occurs at $\sim$ 100 km, near the zero-pressure efficiency of 5×10^{-3}. The time-scale for the conversion is $\sim$ 1 μsec for absorption and $\sim$ 100 nsec. for the fluorescence emission. A large-scale primary pulse, however, is broadened by propagation delays from different regions of the sky to a width of 100 to 300 μsec.

In a given event, the number of fluorescence photons per unit area, N, of energy, E_ν that enter a photomultiplier tube as a result of a supernovae of energy, W, at distance, R and direction θ from the zenith can be written as

$$N = \frac{W\epsilon\lambda}{8\pi R^2 E_\nu} \cos\theta \quad \text{, photons/unit tube area}$$

where ϵ is the fluorescence efficiency and λ is the atmospheric absorption. If the triggering threshold of the detector is set at some level above background noise, say T, the requirement that $N > T$ in the equation given above defines a sensitive radius for the detector. Then by assuming that galaxies are uniformly distributed at a density of ρ and that supernova occur with frequency f, the predicted observation rate, integrated over θ in one hemisphere is

$$r = 0.0145\ \rho f \left(\frac{W\epsilon\lambda}{TE_\nu}\right)^{3/2} \quad \text{per unit time}$$

Using the following values for the parameters: $\rho = 5\times10^{-75}$ galaxies/cm^3, f = 1 supernova/100 years, $\epsilon = 10^{-3}$, $\lambda = 0.5$, $E_\nu = 5.1 \times 10^{-12}$ ergs and $W = 5\times10^{47}$ ergs gives for the rate:

$$r = \frac{28.5}{T^{3/2}} \quad \text{per hour}$$

where the threshold T is to be expressed in photons per cm^2 of tube area, that enter the tube during the integration time of the detector. Typically T varies from 50 to 200 photons/cm^2 in a 50 μsec sample time.

In order to determine that the fluorescence event is due to a large-scale, extraterrestrial source and is not locally produced, the stations are operated at well separated locations, and each event is accurately timed. Coincidence at different locations can then be required as a signature of a supernovae event.

3. Detector System

A detailed description of the detector system has been reported previously (Ogelman and Bertsch, 1969) and since no significant changes have been made, only the key features will be reviewed here. Figure 1 shows a block diagram of the system.

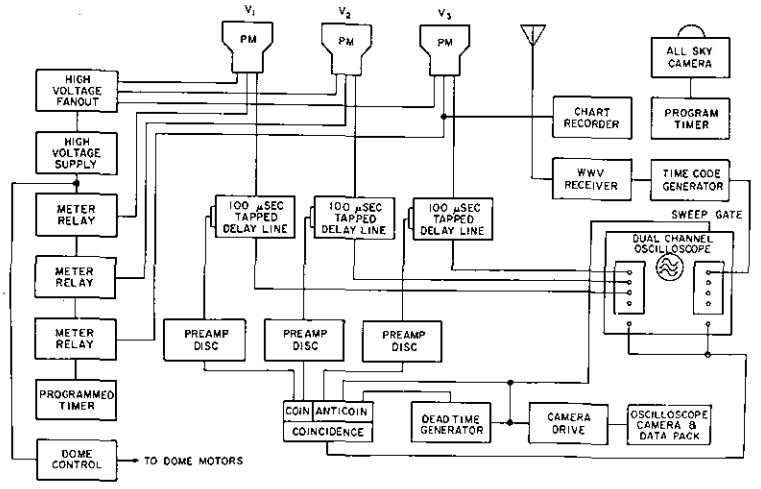

Figure 1. Block Diagram of the detector for a single station.

Three 12-inch photomultiplier tubes are employed. Two of these, V1 and V2 have transmission filters whose spectral response is between 3100 Å and 4300 Å, and hence are sensitive to the expected fluorescence bands near 3914 Å. The third tube Y3 has a filter whose lower wavelength cutoff is 4300 Å and consequently should not respond to fluorescence events. The output from each tube is connected through a 100 microsecond delay line to the chopped beam inputs of an oscilloscope. Each delay line has 5 μsec taps, ten of which are added to give a 50 μsec integrated signal that is tested by discriminator and logic circuits. If triggering levels are exceeded and coincidence requirements are met, the oscilloscope is triggered so that the beam is sweeping before the leading edge of the signal comes from the delay line. An open-shutter camera records the traces on film and at the end of the sweep, automatically moves a new frame into position. In order to time each event, the code from a time code generator is displayed in a one-second sweep on the second beam of the oscilloscope. Because V1 and V2 are sensitive to the same signals coincidence of signals is usually demanded to reduce noise.

4. Results

Two essentially identical systems of the design described in the preceding section have been operated at various locations since late 1968. Table 1

summarizes the supernova event monitoring up to February 1, 1971 at each location.

TABLE 1 SUMMARY OF SUPERNOVA RUNNING TIMES

Station Location	Operation Interval	Threshold (Photons/ cm^2 in 50 μsec	Expected Supernova Rate (Events/hr)	Running Time (hrs.)	2-Sta. Coinc. Time (hrs.)	Expected Number Coinc.
Goddard, Maryland	Sept 1968 -Sept 1969	200	1/96	450	170	1.7
Fan Mtn., Virginia	June 1969 -Dec 1969	70	1/21	350		
Mount Hopkins, Arizona	Nov 1969	50	1/13	60	60	2.7
Middle East Tech. Univ., Turkey	June 1970 -Jan 1971	100	1/36	376		
No. of Events Expected in Single Station Runs ~36 Possible No. ~10 No. of Events Expected in Coincidence ~ 4.4 Observed No. = 0						

The triggering threshold values in this table are determined from calibration measurements and the level of threshold is set according to local background light conditions. The expected supernova rate is determined using the rate expression given in Section 2 along with the tabulated thresholds. During each time period, only the moon-free running times, totally clear of cloud cover were accepted in the analysis. Coincidence measurements were possible during two intervals: one from June to September 1969 between Goddard and Fan Mountain, Virginia where the baseline is 175 km, and the other during November 1969 between Fan Mountain and Mt. Hopkins, Arizona where the baseline is 3300 km. In the coincidence mode of operation, absolute time of each event to within ~ 10 millisec is recorded and the records from the two stations are compared later. The expected rate for coincidence is determined by the site with the lesser sensitivity. As shown in Table 1, no events that could be classified as supernova events on the basis of time scale and the absence of wavelengths above 4300 Å were observed in coincidence, although 4.4 were expected. The records of single station runs show a possible total of 10 while 36 were predicted. This result, however, must be viewed as an upper limit in view of the ambiguity with many background noise events.

Several distinct types of non-fluorescence events are apparent from the records. Two predominant ones are shown in Figures 2a and 2 b.

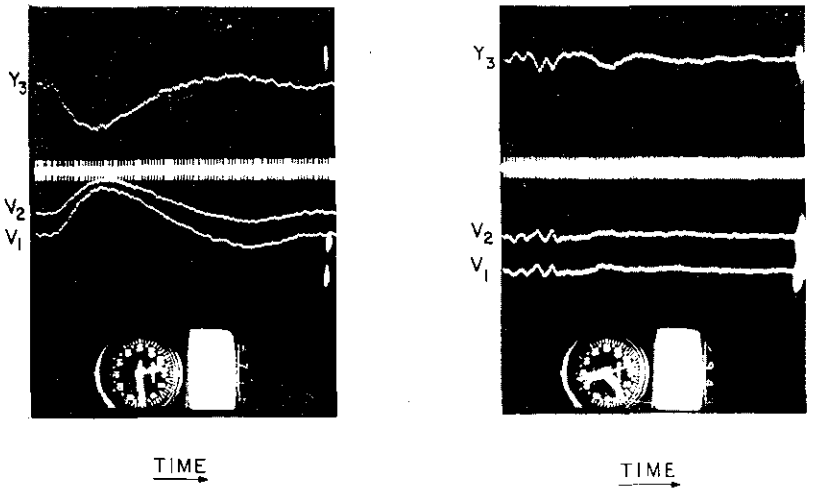

Fig. 2. Examples of non-fluorescence events. Y3 unit response is inverted for identification ease. Full scale time is 900 microseconds. A one second time frame of the NASA 36-bit code is displayed for timing. Fig. 2a on the left is an A-type of event, probably due to electrical discharge. Fig. 2b is an X-type of event, characterized by the high frequency components. See text for discussion.

The first, called an A-event, has the feature of a supernova event, except for the signal in Y3. Events like this have been seen in coincidence over the 175 km baseline, with events that have the characteristics of lightning. In the records of the Turkey station these events have a strong correlation with universal time, peaking at 1800 UT. It is known that the Earth's electric field also correlates with UT and reaches a maximum at 1800 UT. It is therefore probable that these events are due to electrical discharge in the atmosphere. It should be pointed out, however, that 1800 UT is near the turn-on time in Turkey when conditions may not be completely stabilized. An observation at another location would be useful to establish if these signals do in fact correlate with the electric field. Unforunately stations in the United States cannot operate at 1800 UT due to sunlight conditions.

The second type of event (called X-events) shown in Fig. 2 b is characterized by the high frequency structure with negative excursions. These events have also been observed over ~ 175 baselines, but not over 3300 km baselines. However, for the large baseline, a night with a high rate in one location is accompanied by a high rate in the second station. This suggests a rather large-scale phenomenon with localized structure. It has been observed that on two occasions on November 10, 1969 and Jan. 25, 1971, during large magnetic storms, that the rate of X-events was unusually high. For moderate or small magnetic events, however, the correlation is not good. Other indicators of solar activity have also

been examined for correlation, including solar wind velocity, proton intensity > 10 MeV, and neutron monitor activity. None of these correlate particularly well with X-event rates. It is known (O'Brien and Taylor, 1964) that electron precipitation in the atmosphere is a strong source of 3914 Å emission. Electrons ~ 100 keV have a fluorescence conversion efficiency of $\sim 10^{-3}$ (Dalgarno, 1964), similar to the value for ~10 keV photons. O'Brien and Taylor (1964) have shown that the amplitude of 3914 Å light correlates strongly with low energy trapped electron intensities. So far no low energy-trapped particle data has been available to correlate with our observed X-event rates, but based on O'Brien and Taylor's observation it is quite likely that these events are due to particle precipitation in the atmosphere. If so, the observed high frequency (~20 kHZ) components indicate a modulation effect is present and the nature of this mechanism might have important implications.

5. Conclusion

At the present time no positive detection of supernova events has been made. It must be recognized, however, that many of the parameters needed to estimate an expected rate are only crudely known. Nonetheless, the negative result given here implies that the combined quantity of $\rho f W^{3/2}$ is less than 2.6×10^{-13} $erg^{3/2}/cm^3$-sec, to within an 85% confidence limit, provided it is still assumed that galaxies are uniformly distributed.

The non-fluorescence results presented here suggest a relationship with the Earth's electric field in the case of one category of event, and to particle precipitation in the other. More definite statements on these phenomena will be clear when more observations are made and when comparisons with other types of data can be made.

References

Arnett, W. D. 1967. Canad. J. Phys. 45, 1962.

Bunner, A. N. 1966. "Cosmic Ray Detection by Atmospheric Fluorescence," Ph.D. Thesis, Cornell Univ.

Colgate, S. A. and H. J. Johnson. 1960. Phys. Rev. Letters 5, 235.

Colgate, S. A. and R. H. White. 1966. Ap. J. 143, 626.

Colgate, S. A. 1968. Canad. J. Phys. 46, S476.

Dalgarno, D. 1964. Ann. de Geophysique 20, 65.

Fichtel, C. E. and H. Ogelman. 1968. "Experimental Tests of the Supernovae Origin of Cosmic Rays," NASA TN D-4732.

Greisen, K. 1965. "Proceedings Ninth International Conference on Cosmic Rays," London.

Hartman, P. 1963. "Luminescence Efficiency of Air on Electron Bombardment," Los Alamos Report.

O'Brien, B. J. and H. Taylor. 1964. J.G.R. 69, 45.

Ogelman, H. and D. Bertsch. 1970. Acta Physica 29, Suppl. 1, 35

CHARGE COMPOSITION OF SOLAR COSMIC RAYS

D. L. Bertsch, C. E. Fichtel, and D. V Reames

Goddard Space Flight Center, Greenbelt, Md. 20771

ABSTRACT

The composition of energetic solar particles is reviewed for all solar events in which measurements on helium and heavier nuclei have been made simultaneously in the same detector during a given particle event. For nuclei of equal charge-to-mass ratio, the relative abundances have been the same within uncertainties in every measurement, and consistent with spectroscopic photospheric estimates. Iron has a slightly different charge-to-mass ratio but is still of considerable interest. An observation of the Fe/O in the January 24, 1971 solar event has provided a second determination of this value.

1. Introduction

The existence of heavy nuclei among the energetic solar particles has been known for about a decade, and they have now been seen by many observers in several different solar particle events. However, because of the low abundances of nuclei with charges greater than two, only the most intense solar particle events have intensity levels sufficiently high to study details of the particle composition. Before the most recent event to be reported here, namely that on Jan. 24, 1971 there were only six events in which such measurements were made. The Jan. 24, 1971 event is also only the second event in which Fe group nuclei have not only been detected, but in which the flux of Fe nuclei can be compared directly to the abundance of medium nuclei (C,N,O, & F). The first was the September 2, 1966 event (Bertsch, et al., 1969). In the other events when detectors capable of distinguishing Fe group nuclei were flown, either the intensity of the event was too small to expect to see Fe group nuclei at the energy/nucleon threshold for the detector (Fichtel and Guss, 1961; Biswas et al., 1962; Biswas et al., 1963; Biswas et al., 1966; Bertsch et al., 1971) or it was not possible to compare directly the Fe group flux to medium or helium nuclei measured in the same instrument because of the nature of the detector (Fleischer et al., 1970; Crozaz and Walker, 1971; Price et al., 1971).

One outstanding feature of the energetic solar particle composition, which has been seen in an examination of the experimental results, is the constancy of the relative abundances of particles with the same charge-to-mass ratio within experimental errors in all events where a comparison could be made at energies where the nuclei are fully ionized. Moreover, the observed abundances show a strong similarity to photospheric and coronal values measured by spectroscopic techniques.

2. Experimental Technique

The most recent data presented here were obtained from nuclear emulsion stacks flown on sounding rockets during the solar particle event which began at about 2309Z on January 24, 1971. The payloads and their Nike-Apache vehicles were kept on standby at the Fort Churchill Research Range in Manitoba, Canada prior to the event as part of a continuing SPICE (Solar Particle Intensity and Composition Experiment) Program. There were two sounding rockets flights which reached apogee at about 0819Z and 1512Z on January 25, 1971, i.e. about nine and 16 hours respectively after the event began.

Each payload had two nuclear emulsions stacks consisting of 24 pellicles with lateral dimensions 2.5 in. x 2.8 in. A thin cover of stainless steel and lexan, having a total thickness equivalent to 72 microns of emulsion, separated the outermost pellicle from the particle radiation. This first pellicle was 200 microns thick. It was followed by three 300-micron and twenty 600-micron pellicles. Experience has shown that this arrangement of thicknesses is advantageous since the high density of solar proton tracks in the outer pellicles of the stack makes it difficult to analyze tracks in a 600-micron plate. The two stacks had different sensitivites: one was made from Ilford K.5 material sensitive to minimum ionizing events, and the other was made from Ilford K.2 emulsion sensitive to protons of energy less than 40 MeV.

During the flight, the nosecone of the payload was opened while the payload was above about sixty kilometers yielding an exposure time of 245 sec. By means of spin stabilization, the emulsion plates were held in a vertical plane. The zenith angle of arrival of each particle in the stacks can therefore be determined during the analysis. Those events that entered the stacks from directions below the horizon are excluded from the analysis because of their unknown energy loss and possible interactions in the atmosphere.

An area scan is made in the top plate of the K.5 emulsion stack to locate nuclei heavier than helium, and heavy nuclei tracks with entrance angles from 10° to 60° with respect to the surface are accepted. In addition, a minimum projected length of 78 microns is demanded to ensure a sufficient track length for analysis. Identification of multiply-charged particles is accomplished by measuring the total obscuration as a function of range using the Goddard digitized T.V. microscope system. Helium nuclei are resolved from protons in the less sensitive K.2 emulsion stack by measuring the grain density of each track near the point where the particle enters the emulsion plate. More details on the general type of data analysis used in the SPICE program including figures are given by Bertsch et al. (1971).

3. Results and Discussion

As mentioned in the Introduction, composition measurements on energetic solar particles have now been reported for six solar particle events. These include ten independent measurements at different times during the events ranging from a few hours to several days after the onset of the flare associated with an event. In all but one case (18 July 1961), the time associated

with a measurement is approximately 4 min. so that one would expect temporal variations in the flux or spectral shapes to be small during each measurement period. All particle species are, of course, recorded during the same time interval.

One striking feature of the results obtained has been the constancy of the composition of the multiply-charged nuclei (as measured by the helium-to-medium-nuclei ratio) with energy, with time during an event, and from one event to the next. This constancy prevails within the 15 to 20% statistical uncertainty of the individual measurements despite large variations in the intensity, changes in the spectral shape, and large differences in the proton-to-helium ratio. The weighted average of the He/M ratio is 58 ± 5. The energy region spanned by the measurements is from 10 to 200 MeV/nucleon.

The spectra of helium and medium nuclei from the most recent event (12 April 1969) in which the measurements for both have been completed are shown in Fig. 1.

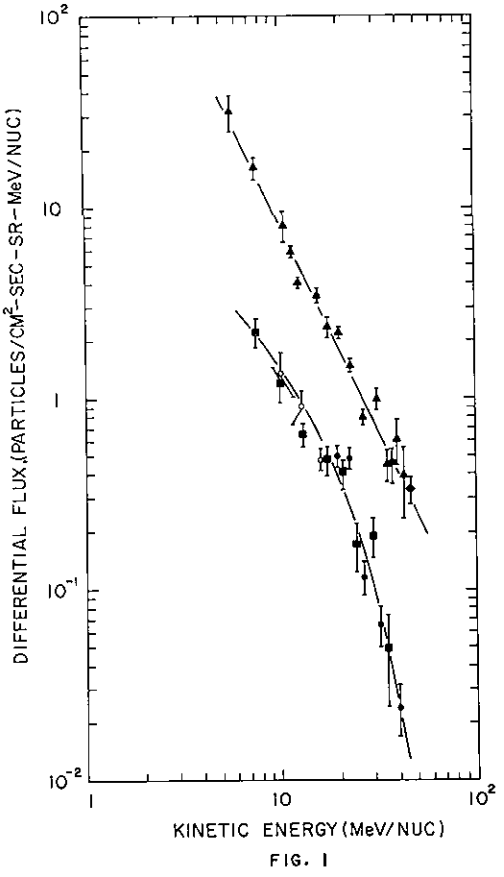

FIG. 1

Fig. 1. Differential energy spectra for protons, helium, and medium group nuclei ($6 \leq Z \leq 9$). Proton fluxes shown here are divided by 10 for ease of representation. Proton fluxes determined from ionization and range measurements on individual events are shown by triangles whereas fluxes determined by taking the difference of integral particle counts at different depths in the stack are labeled by diamonds, Helium nuclei are represented by squares. Medium nuclei are multiplied by 58 the best estimate of the helium-to-medium ratio, and are shown by circles. Solid circles are used for energy regions where charges could be assigned to individual members of the medium group. Open circles refer to medium nuclei which are resolved from helium, but are not individually identified. (Bertsch et al., 1971).

The fluxes of the medium nuclei shown in the figure have been multipled by 58 to allow direct comparison with the helium fluxes. Proton fluxes multiplied by 0.1 for convenience in plotting are also shown in Fig. 1.

In several events it has been possible to observe more detailed abundances of individual elements. Where comparisons are possible, these abundances also appear to be independent of time and energy. The average abundances relative to that of oxygen are shown in Fig. 2 together with the corresponding photospheric and coronal abundances that have been obtained from spectroscopic measurements. Error bars on the points corresponding to spectroscopic measurements in Fig. 2 indicate the range of values quoted in the literature and not statistical errors.

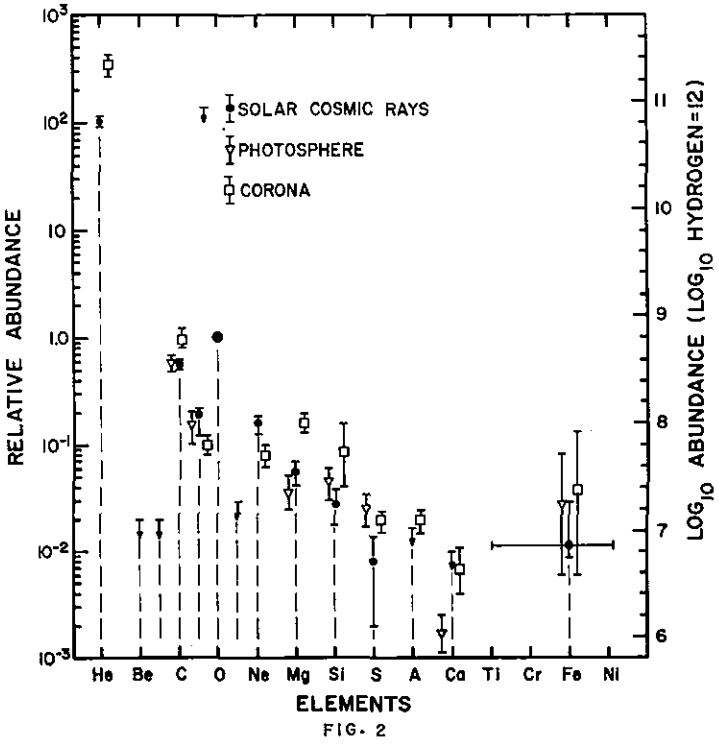

FIG. 2

Fig. 2. Solar abundances relative to oxygen determined from solar cosmic ray measurements and from spectroscopic measurements of the solar corona and photosphere. The uncertainties in the results from solar cosmic ray abundances represent experimental uncertainties in abundance ratios relative to oxygen. For both spectroscopic studies, the error bar symbol is used to denote a range of values quoted by different authors. The horizontal bars on the iron point denote a group of charges for both cosmic ray and spectroscopic data. For the general coronal abundances, see Dupree and Goldberg (1967) and Pottash (1964a and 1964b). For the iron abundance in the corona see Jordan (1966), Nikolsky (1969), Pottash (1967), and Wilding and Sandlin (1968). General photospheric abundances are from Goldberg, Muller, and Aller (1960); and Lambert and Warner (1968). For the iron abundance in the photosphere see Garz and Koch (1969), Garz et al. (1969), Goldberg, Kopp, and Dupree (1964), Grevesse and Swings (1969), Rogerson (1969), and Warner (1968). The energetic solar particle abundances are compiled from Fichtel and Guss (1961), Biswas et al. (1962), Biswas, et al. (1963), Biswas et al. (1966), Durgaprasad et al. (1968), Bertsch et al. (1969), and Bertsch et al. (1971).

From Fig. 2, the solar-particle composition is seen to be in better agreement with the spectroscopic photospheric abundance estimates than with those of the corona. This is seen particularly in the C and Mg abundances. If the solar-particle abundances do reflect those of the photosphere, then we may use the particle measurements to obtain abundances of elements such as

He and Ne for which no measurements exist in the photosphere. These abundances relative to that of oxygen are shown in Fig. 2. Combining the photospheric H/O ratio and the solar-particle He/O ratio, we find H/He = 16 $\pm$ 2 for the sun.

The relative constancy of the abundances of the multiply-charged solar particles presumably arises from the constancy of their charge-to-mass ratio. Stripped of all orbital electrons (at the energies of observation), two nuclear species of the same velocity will have the same magnetic rigidity and will behave similarly in electromagnetic fields during their acceleration and propagation. In this connection, special attention must be paid to the measured abundance of Fe whose charge-to-mass ratio differs by 7% (for Fe^{56}) from that of the lighter nuclei measured. Owing to this difference, a larger error has been assigned to the solar-particle Fe-group abundance shown in Fig. 2 (see Bertsch et al., 1969 and 1971). The determination of the solar Fe abundance from measurements in solar-particle events requires that any time or energy dependent effects resulting from the different charge-to-mass ratio must be understood. The Fe abundance shown in Fig. 2 comes from a single measurement on 2 Sept. 1966, the only measurement prior to the one to be reported here for which there is a direct comparison to the medium nuclei intensity determined at the same time in the same detector.

Preliminary data are now available from the sounding rocket flights on 25 Jan. 1971. Particle fluxes were sufficiently great on both flights into this event to allow measurements on Fe-group nuclei. These were located by scanning the entire outermost plate of each stack, selecting only very heavy events ($Z \geq 18$). Preliminary identification of the iron-group nuclei has been made in these scans. More detailed scans of $\sim$ 10% of the outer plate in each flight have also been completed in order to locate all medium and heavier events. While measurements have not been made to resolve each of the species in this sample, previously observed abundances can be used to correct for tracks formed by nuclei above the medium group ($\sim$ 8% correction). Then by assuming the oxygen-to-medium ratio that has been observed in all the earlier measurements, the Fe/O ratio given in Table I is determined for the second flight in the Jan. 1971 event.

TABLE I
SUMMARY OF SOLAR IRON-GROUP MEASUREMENTS

$(Log)_{10}$ Solar Cosmic Rays		$(Log)_{10}$ Spectroscopic Values	
		Photosphere	Corona
Nov. 12, 1960	$< 7.2^*$	6.6 - 7.7	6.6 - 7.9
Sept. 2, 1966	$6.89\text{-}7.26^*$		
April 12, 1969	$< 7.0^*$		
Jan. 24, 1971	$6.91\text{-}7.54^*$		

*Values are relative to oxygen assumed to be $(Log)_{10}(Oxygen) = 8.8$

The range of uncertainty in the most recent measurement is in part due to the still uncertain medium flux in the energy region where iron is detected (> 22 MeV/nucleon). Iron has been observed in the first flight as well, but

7 00

the medium nuclei flux measurements have not progressed to the point where an Fe/O ratio can be quoted.

In conclusion, the Fe/O ratio observed in Jan. 1971 at the present time appears to be similar to the previous measurement, and consistent with the 85% confidence upper limits set in the two other events given in Table I. It should be pointed out, however, that the possibility for a higher abundance exists here, perhaps reflecting a propagation effect. More detailed measurements are being made.

4. References

Bertsch, D. L., Fichtel, C E , and Reames, D. V , 1969. Ap. J. (Letters), 157, L53.

Bertsch, D. L., Fichtel, C. E., and Reames, D. V., 1971. NASA X-662-71-210, submitted to the Astrophysical Journal.

Biswas, S., Fichtel, C. E., and Guss, D. E., 1962, Phys. Rev., 128, 2756.

Biswas, S , Fichtel, C. E., and Guss, D E , 1966. J. Geophys. Res. 71, 4071.

Biswas, S., Fichtel, C E , Guss, D. E., and Waddington, C J., 1963. J. Geophys. Res., 68, 3109.

Crozaz, G., and Walker, R. M., 1971. Science 171, 1237.

Dupree, A., and Goldberg, L , 1967. Solar Physics, 1, 229.

Durgaprasad, N., Fichtel, C E., Guss, D E., and Reames, D. V., 1968. Ap. J., 154, 307.

Fichtel, C. E., and Guss, D. E , 1961. Phys. Rev. Letters, 6, 495.

Fleischer, R. L., Hart, H. R., and Cómstock, G. M., 1970. G.E. Report No. 71-C-021.

Garz, T , and Koch, M., 1969. Astron. Astrophysics, 2, 274.

Garz, T., Koch, M., Richter, J., Bascheck, B., Holiweger, H., and Unsold, J , 1969. Nature, 223, 1254.

Goldberg, L., Muller, E. A., and Aller, L. H., 1960. Ap. J. Suppl., 5, 1.

Goldberg, L., Kopp, R. A., and Dupree, A. U., 1964. Ap. J., 140, 707.

Grevesse, N., and Swings, J. P., 1969. Astron. and Astrophys., 2, 28.

Jordan, C , 1966. M.N.R.A.S., 132, 463.

Lambert, D., and Warner, B., 1968. M.N.R.A.S., 138, 2.

Nikolsky, 1969. Solar Physics, 6, 309.

Pottash, S. R., 1967. Bull. Astr. Inst. Netherl., 19, 113.

Pottash, S , 1964a. M.N.R.A.S., 128, 73.

Pottash, S , 1964b. Space Sci. Rev., 3, 816.

Price, P. B., Hutcheon, I., Cowsik, R., and Barber, D. J., 1971. Phys. Rev. Letters, 26, 916.

Rogerson, Jr., J., 1969. Ap. J., 158, 797.

Warner, B., 1968. M.N.R.A.S., 138, 229.

Wilding, K. G., and Sandlin, G P., 1968. Ap. J., 152, 545.

SOLAR PROTON, HELIUM, AND MEDIUM NUCLEI ($6 \leq Z \leq 9$) OBSERVED FROM THE IMP-VI SATELLITE

T. T. von Rosenvinge*, F. B. McDonald, B. J. Teegarden

Goddard Space Flight Center, Greenbelt, Md.

Abstract

Proton, helium, and medium nuclei energy spectra have been measured from the IMP-VI satellite for a recent solar flare. Above 2 MeV/nucleon these spectra are based upon single and dual parameter pulse height analysis in addition to threshold rate counting. Pulse height analysis of medium nuclei is assigned a high priority for telemetry readout so that telemetry does not become saturated by the high proton intensity. In this manner the number of pulse height analyzed medium nuclei has been increased by a factor of ~ 200. Individual medium nuclei have been resolved in the energy interval 8 - 23 MeV/nucleon.

1. Introduction

Fichtel and coworkers (for example, Bertsch, et al., this conference [1]) have emphasized the point of view that the relative abundances of solar flare particles with charge $Z \geq 2$ are constant as a function of velocity from flare to flare and represent the relative abundances before acceleration. In this view, the relative abundances of various elements in the sun which cannot be obtained from spectroscopic data alone can be obtained by the addition of flare particle data. An important example of this is the abundance ratio of solar hydrogen and helium which cannot be determined at the flare location by either technique alone. Also, spectroscopic determinations are often difficult for other elements [2] so it is desirable to have an independent measure of relative abundances from flare particles.

Possible deviations from the above picture have been the subject of theoretical speculation in the past (e.g. [3]) and have been recently reported as having been observed at low energies ($\lesssim$ 10 MeV/Nucleon) by Price, et al. [4] for iron nuclei and by Armstrong and Krimigis [5], Krimigis [6], and Beedle, Van Allen, and Webber [7] for the helium to $Z \geq 3$ ratio. Whether or not these latter measurements are inconsistent with the results of Fichtel and coworkers above ~ 20 MeV/nucleon is currently a matter of dispute [8] and will be discussed later. Price, et al. [4] found that the Fe spectrum becomes considerably steeper below ~ 10 MeV/nucleon. Fleischer, et al. [9] however, found a constant spectral exponent down to ~ 1 MeV/nucleon. These two experiments were nearly identical, both involving the study of tracks etched in glass from the Surveyor 3 spacecraft (exposed on the moon for over two and one half years).

It is interesting to note that only five solar events since 1960 have been intense enough for a detailed study of flare particle composition to be made using rocket-borne emulsion techniques. No comparable measurement (i.e. individual charges resolved above charge 2) has been previously reported from satellite-borne detectors. This paper will report the first such measurement.

*NAS/NRC Research Associate

2. Description of the Experiment

The present experiment utilizes the low energy detector (LED) illustrated in Fig. 1. This telescope consists of a thin (146μ x 300 m^2) silicon surface barrier detector (detector A) and a thick (3mm x 500 mm^2) Li drifted detector (detector B) surrounded by an active anti-coincidence shield (detector C). Detector A acts as a total energy detector for particles stopping in A and as the dE/dx element of a dE/dx by E telescope for particles stopping in detector B. The response matrix for this telescope is also illustrated in Fig. 1. The dashed line on this matrix separates protons and helium nuclei from nuclei with charge greater than two. Below the dashed line the signals are analyzed in a high gain mode, while above the dashed line the signals are attenuated by a factor of 10 before being analyzed. The pulse height analyzers are linear over more than 400 channels, giving a total dynamic range of ~ 4000.

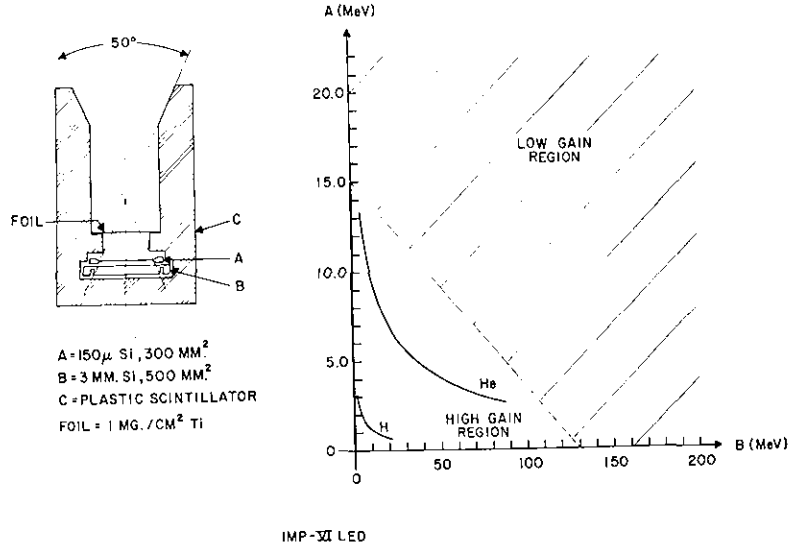

Fig. 1 - The IMP-VI Low Energy Detector and its response matrix.

The unique feature of this experiment is its priority system. Because of a limited telemetry data rate, only one analyzed event may be read out every 0.64 seconds whereas many particles will enter the telescope in this sample time. To prevent the telemetry from being saturated by protons, rare events are given a higher priority for readout. In this manner the number of pulse height analyzed medium nuclei above 1.5 MeV/nucleon has been increased by a factor of ~200 over conventional systems.

Four different event types are identified: 1. Particles with charge greater than 2 stopping in detector B; 2. Particles with charge less than or equal to 2 stopping in detector B; 3. Particles with charge greater than 2

stopping in detector A; and 4. Particles with charge less than or equal to 2 stopping in detector A. Thus the gain change boundary described earlier also separates event types 1. and 3. from event types 2. and 4.. During any given sample time the priority system then works as follows. The first event to occur is always accepted and its event type recorded. Subsequent events of the same type or types having lower priority are then rejected, while a higher priority event will be analyzed and the corresponding pulse heights replace those measured for the earlier (lower priority) event. Rates counters keep count of each particle detected for each event type irrespective of whether the particle is pulse height analyzed and read out. These counters thus provide the information for renormalization to actual intensities. In practice, the priority for each event type is changed cyclically to prevent any one event type from saturating telemetry read-out.

Prior to launch of IMP-VI on March 13, 1971, the LED telescope and its associated electronics were calibrated at the Naval Research Laboratory Cyclotron using protons from 2.5 to 30 MeV. No observable gain changes have taken place.

3. Experimental Results

The particles reported upon here originated in a class M5 flare of importance 1B. This flare occurred at S18W80 on the sixth of April at 0935 UT. Particle onset was observed at IMP-VI 1.5 hours later as illustrated in Fig. 2, which shows particle counting rates versus time. Velocity dispersion is clearly evident in this figure. The curve labeled .6-4 MeV shows an irregular rise to maximum owing to the contribution of electrons which peaked early in the event.

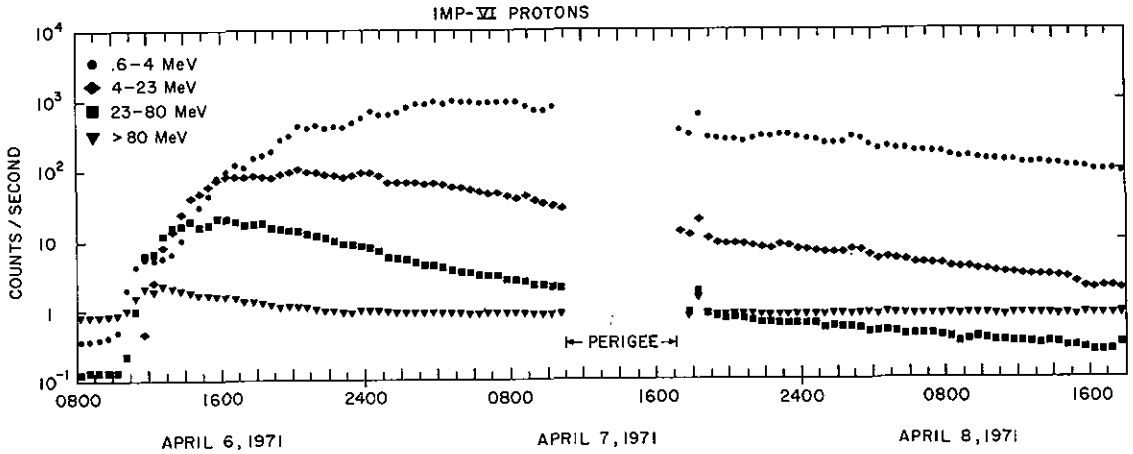

Fig. 2 - Particle counting rates versus time for various energy intervals.

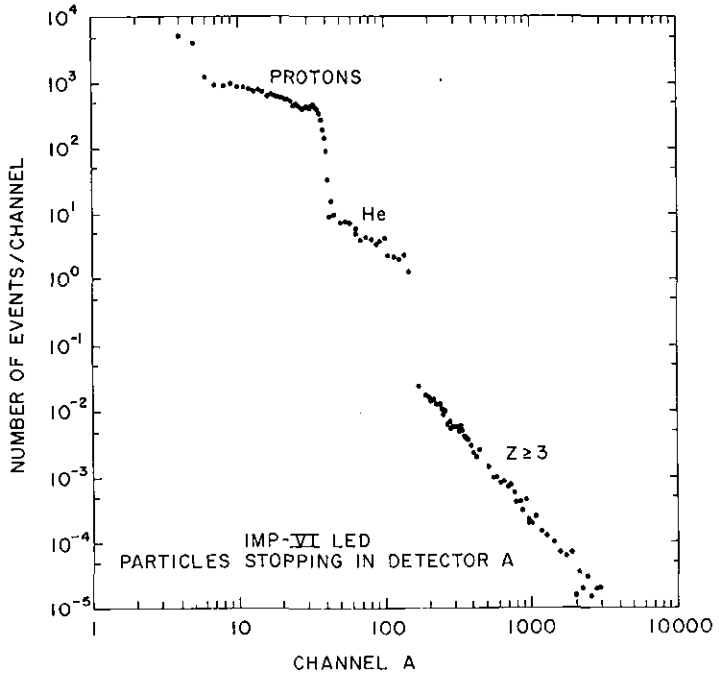

Fig. 3 - Example of a one-dimensional pulse height distribution in channel A for particles stopping in detector A.

The one dimensional pulse height distribution in Channel A for particles stopping in detector A (B pulse height = 0) is a composite response to all particles. Some measure of charge resolution is possible, however, as is illustrated in Fig. 3. The sharp transitions in the distribution are due to protons and helium nuclei above 4 MeV/nucleon entering the B detector. They provide a useful internal calibration. This distribution was accumulated over ~ 21 hours from the start of the flare and spans some nine decades in intensity. The active anti-coincidence detector (detector C) is a critical element for making measurements of intensity over such a broad range.

It may be noted that a fixed band of pulse heights in the $Z \geq 3$ region of Fig. 3 corresponds to different energy bands for particles with differing charges. For example, the band of pulse heights which corresponds to oxygen nuclei between 1.56 and 4 MeV/nucleon corresponds to Fe nuclei between .61 and 1.45 MeV/nucleon [10].

If the spectra are steep then clearly Fe nuclei will be present in this band of pulse heights disproportionately to their relative abundance. It may, in fact, be possible for them to contribute a non-negligible amount to the total $Z \geq 3$ intensity. An attempt to estimate the contribution of $Z > 9$ particles to this pulse height band will be mentioned later.

Two dimensional pulse height matrices for the same 21 hour period are illustrated in Fig. 4. From the high gain matrix we can qualitatively observe the absence of background events. Over one hundred thousand events are represented on this matrix. The low gain matrix illustrates clearly the distinct separation of C, N, and O nuclei. Some 101 particles appear here, all in the approximate energy interval of 8 - 23 MeV/nucleon. This matrix represents the first two dimensional measurement by an electronic counter of flare particles with charge greater than two.

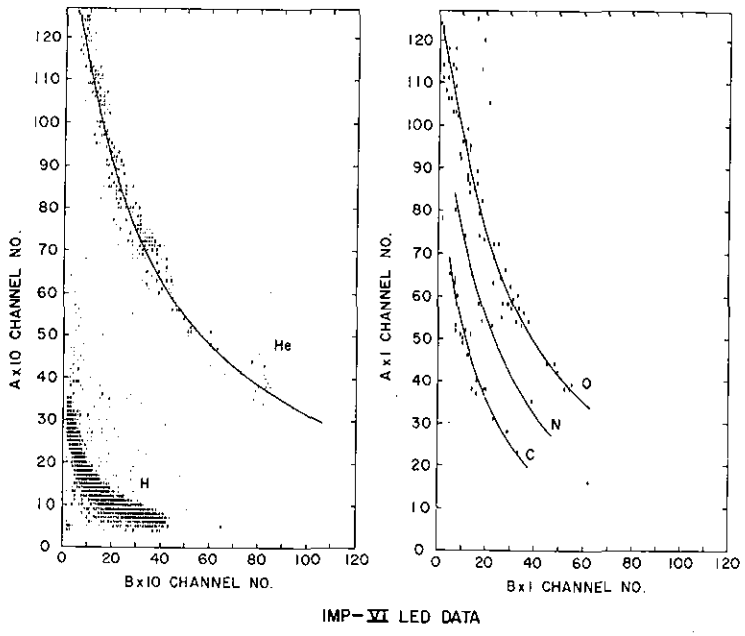

Fig. 4 - Examples of the high gain and the low gain two-dimensional pulse height distributions.

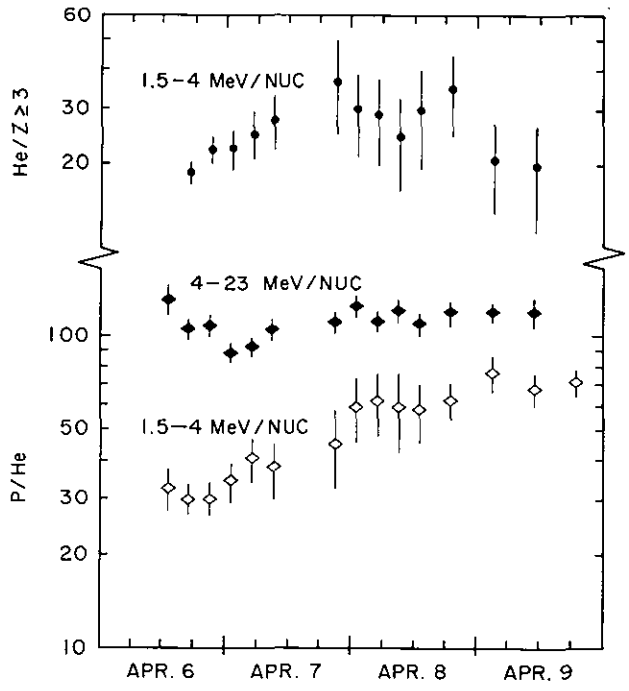

Fig. 5 - The P/He ratio and the He/Z ≥ 3 are illustrated as a function of time for the energy interval 1.5-4 MeV/nuc., as well as the P/He ratio for the interval 4-23 MeV/nucleon.

In Fig. 5 we illustrate the behavior of the proton to helium ratio with time for the energy ranges 1.5-4 MeV/nucleon and 4-23 MeV/nucleon. For the first of these energy ranges the proton to helium ratio increases with time, while for the second it is essentially constant at a rather higher value.

Also shown in Fig. 5 is the He to Z ≥ 3 ratio versus time measured using particles stopping in detector A. The resulting values are similar to those obtained in other events by Armstrong and Krimigis [5] using a single detector, a passive collimator, and two threshold levels. The bands of pulse heights used for the present measurement correspond to equal intervals in energy/nucleon for He and oxygen nuclei (1.56-4 MeV/nucleon). There is some indication that the resulting ratio increases slightly early in the event, but it is sensibly constant. On this basis we will assume that the He to medium nuclei ratio is also constant in the 8-23 MeV/nuc. region (large statistical fluctuations in the measured values mask possible time variations). Using this assumption, we present in Table 1 values for various ratios integrated over the event.

The measured He to medium nuclei ratio of 46 $\pm$ 9 in the interval 8-23 MeV/nuc. is lower than (but consistent with) the value 58 $\pm$ 5 obtained by Fichtel and co-workers above about 20 MeV/nucleon. It

	1.5–4 MeV/NUC	8-23 MeV/NUC	FICHTEL, et al ≥ 20 MeV/NUC
He/M	37±5	46±9	58±5
C/O	—	.42±.11	.56±.06
N/O	—	.20±.08	$.19^{+.03}_{-.07}$

Table 1 - Summary of various ratios obtained by integrating over most of the event.

should be realized that the value 58 ±5 is an average over ten separate measurements for 5 different solar events. The value 46 ±9 is very typical of these 10 separate measurements. The C/O and N/O ratios measured in the 8-23 MeV/nuc. interval are in excellent agreement with those of Fichtel and co-workers.

The He to medium nuclei ratio (He/M) of 37 ±5 quoted in Table 1 for the energy interval 1.5-4 MeV/nuc. has been estimated from He to Z ≥ 3 ratio of Fig.5. It has been assumed that the spectral index for each charge above charge 3 is the same and independent of energy. Under these assumptions a spectral index has been derived and the abundances of nuclei above charge 9 measured by Fichtel and co-workers have been used to deduce the quoted He/M ratio. We find that the He to Z ≥ 3 ratio must be multiplied by ~ 1.35 to obtain the He/M ratio. The quoted error of ±5 does not include an estimate for the error in this factor. The final result of 37 ±5 is decidedly lower than the result 58 ±5 of Fichtel and co-workers. Possible interpretations are (1) the He/M ratio is truly different at low energies than it is at high energies; (2) the correction factor of 1.35 is incorrect, either because the abundances used for nuclei with charge > 9 are incorrect or because the spectra of these nuclei become steeper at low energies in accordance with the results of Price, et al. [4]. We hope to be able to select between these alternatives after further study of this and subsequent events.

4. References

[1] Bertsch, D.L., Fichtel, C.E., and Reames, D.V., 1971, Nuclear Composition and Energy Spectra in the April 12, 1969 Solar Particle Event, this conference.

[2] Garz, T., Koch, M., Richter, J., Baschek, B., Holiweger, H., and Unsold, J., 1969, Nature, 223, 1254.

[3] Korchak, A.A., and Syrovatskii, S.I., 1958, Dokl. Navk. SSSR, 122, 792 [Sov. Phys. Dokl., 3, 983].

[4] Price, P.B., Hutcheon, I., Cowsik, R., and Barber, D.J., 1971, Phys. Rev. Letters, 26, 916.

[5] Armstrong, T.P., and Krimigis, S.M., 1971, A Statistical Study of Solar Protons, Alphas and Z ≥ 3 nuclei in 1967-68, to be published in J. Geophys. Rev.

[6] Krimigis, S.M., 1971, Transactions American Geophysical Union, 52, Paper SC4, page 311.

[7] Beedle, R.E., Webber, W.R., and Van Allen, J.A., 1971, Transactions American Geophysical Union, 52, Paper SC3, page 311.

[8] Fichtel, C.E., Reames, D.V., 1971, Constancy of the He to Medium Nuclei Ratio in the Solar Cosmic Rays, to be published J. Geophys. Res. together with a reply from Armstrong, T.P., and Krimigis, S.M.

[9] Fleischer, R.L., Hart, Jr., H.R., and Comstock, G.M., 1971, Science 171, 1240.

[10] Northcliffe, L.C., and Schilling, R.F., "Range and Stopping Power Tables for Heavy Ions", Nuclear Data, Vol. A7, 233, Academic Press, N.Y., 1970.

OBSERVATIONS OF THE SCATTER-FREE SOLAR-FLARE ELECTRONS IN THE ENERGY RANGE 20-1000 keV

J. R. Wang* and L. A. Fisk
Goddard Space Flight Center, Greenbelt, Md.

R. P. Lin
Space Science Laboratory
University of California, Berkeley, Ca.

Abstract

Observations of the scatter-free electron events from solar active region McMath No. 8905 are presented. The measurements were made from Univ. of California Solar Particle Experiment and Goddard Space Flight Center Cosmic-Ray Experiment on IMP-IV satellite. The data show that more than 80% of the electrons from these events undergo no or little scattering and that these electrons travel only ~ 1.5 a.u. between the sun and the earth. The duration of these events cannot be accounted fully by velocity dispersion alone. It is suggested that these electrons could be continuously injected into interplanetary medium for a time interval of ~ 2 - 3 minutes. Energy spectra of these electrons which should represent the spectra near the flare site will be discussed.

1. Introduction

Solar flare particles observed near the Earth generally display an intensity-time profile which suggests a diffusion-dominant process. There are, however, some solar flare electrons which undergo very little or no scattering at all in the interplanetary medium between the sun and the earth. In this paper, we report two such events occurring in July 30, 1967. The observations were made with University of California solar electron experiment, the University of Chicago charged particle experiment (J. A. Simpson, private communication) and the GSFC galactic cosmic-ray experiment aboard the IMP-IV satellite. These experiments cover electron energy ranges of 22-45 keV (Lin, 1970a), of 170-1000 keV and 750-1600 keV (Sullivan, 1971), and of 100-400 keV and 500-1100 keV (Wang et al., 1972).

2. Observations

Figure 1 shows two typical scatter-free electron events observed on July 30, 1967 when IMP-IV was near apogee (~ 34 earth's radii). Observation of these events at low energies (> 22 kev and > 45 kev) was first reported by Lin (1970b). However, better understanding of these events could be achieved by addition of higher-energy observations. The electron intensity at both ~ 500-1100 Kev and ~ 170-1000 Kev energy windows started to increase around 1633 U.T., following the observed onset of a 1N flare at ~ 1615 U.T. In contrast to the normal classical electron events (Simnett 1971; Cline and McDonald 1968) in which the decay time was generally about one order of magnitude

*NAS-NRC Research Associate

longer than the rise time (~ 30-60 min), the electron intensity rose rapidly and reached maximum within 3-5 minutes. The intensity then dropped to background level within another 5 minutes or so. On the other hand, the intensity onset for three lower-energy channels did not begin until the intensity at two higher-energy channels reached maximum. By the time when > 22 kev and > 45 kev electron intensities reached their peak values, the 500-1100 Kev and 170-1000 Kev electron intensities were already in the background level. The duration of the event varied with energy. For 500-1100 Kev, 170-1000 Kev and 100-400 Kev energy intervals, the event lasted approximately 7,10 and 12 minutes respectively; while for two lower channels at > 22 Kev and > 45 Kev, it lasted more than 20 minutes. Most of the event duration time could be accounted for by the velocity dispersion of the electrons at various energies. However, more careful analysis revealed that the duration time was consistently ~ 3-5 minutes longer than that expected from velocity dispersion alone for all energy intervals. Following the peak, there was a small fraction of the electrons which displayed a long exponentially decaying intensity-time profile similar to a classical event. We shall call the initial peak which is dominated by velocity dispersion, the scatter-free component and the long tail portion, the scattered component.

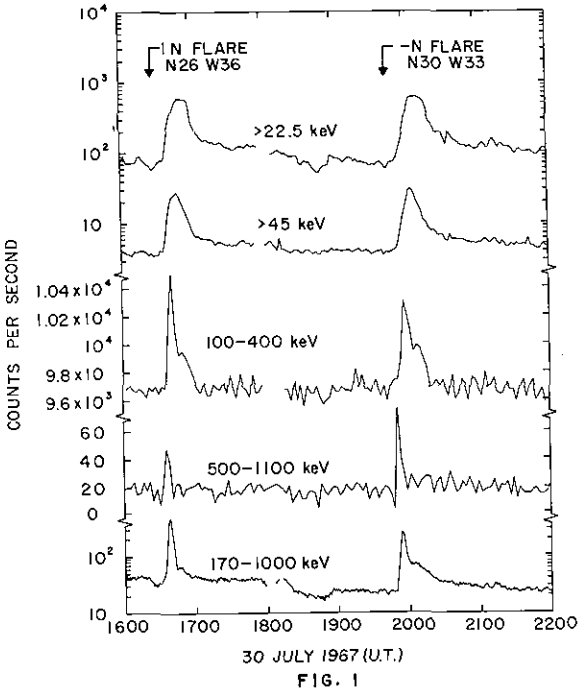

FIG. 1

Another event occurred around 2000 U.T. after a -N flare at ~ 1945 U.T. This event more or less followed the same pattern as the first one, except that the duration time was ~ 2 minutes longer at all energies and that larger fraction of electrons was scattered. To illustrate the latter point about the scattered component, we call attention to the intensity-time profile of 170-1000 Kev electrons. The intensity at this energy interval reached a maximum value of ~ 270 counts/sec at ~ 1955 U.T. After a sharp drop in intensity, there was a barely observable second maximum at ~ 2006 U.T. which was followed by an exponential decay for ~ 20 minutes. The ratio of the first and second intensity maxima for this event was ~ 4. For the first event at ~ 1640 U.T., this same ratio was ~ 7. Furthermore, the decay time of the scattered component seemed to be longer for the second event than the first one. It appears that the duration time of the scatter-free component, the fraction of the electron scattered, and the decay time of the scattered component for a given event are inter-related.

It is clear from the above description that the distinct features of these events are their rapid rise and decline in intensity - the intensity-time profile is symmetric or nearly symmetric about the time of maximum. Only a small fraction of electrons undergoes diffusion-like decay similar to classical flare event. Velocity dispersion for these events is very pronounced which excludes the possibility of these electrons as being locally accelerated near the Earth's bow shock (Fan et al., 1966; Lin and Anderson, 1966).

3. Distance traveled by Scatter-Free Electrons

The observations described above suggest that the scatter-free electrons, once released into the interplanetary medium, simply follow the magnetic field lines. Therefore, if ejected at the same time, they should travel about the same distance between the sun and the Earth, and should obey the relation

$$S = c\beta\ (T - To) \qquad (1)$$

Here S is the distance traveled, c is the velocity of light, β is electron speed (in unit of c), T is the time of observation near Earth, and To is the time of electron injection at the sun. The velocity dispersion observed in Figure 3 reflects the relation between β and T, because S is a constant for a given event.

In Figure 2 we show the β vs. $S/c(T - To)$ plot for the event at $\sim$ 1640 U.T. For each data point plotted, we used β and T corresponding to average energy and time of peak intensity respectively. The upper and lower limits in β correspond to upper and lower bounds in energy derived from the detector responses, while those in T correspond to the times when electron intensity is half of its peak value.

It is clear from this figure that the electron transport between the sun and the earth obeys Eq. (1) quite well for this event. The time of electron injection near the sun and the distance travelled were found to be $\sim$ 1623 U.T. and $\sim$ 1.45 a.u. respectively. This distance was comparable to the length $\sim$ 1.2 a.u. of Archimedean magnetic field line between the sun and the earth assuming a solar wind velocity of $\sim$ 400 km/sec.

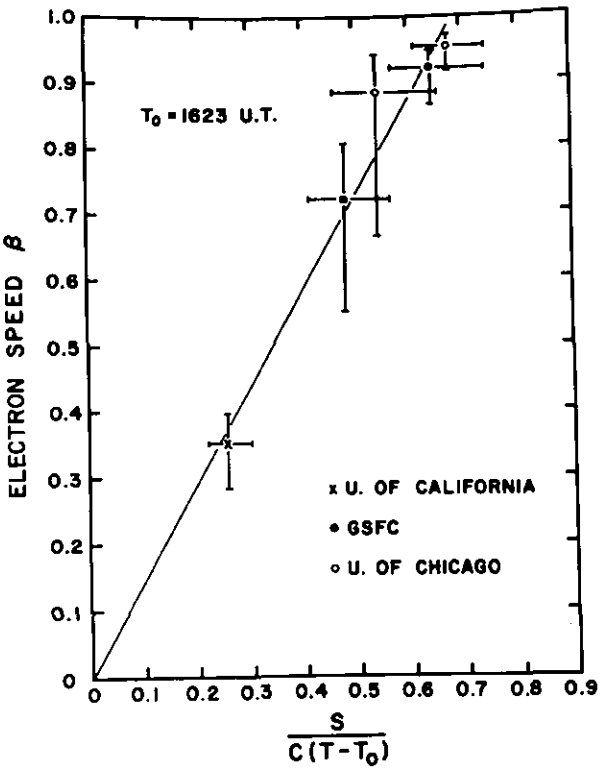

FIG. 2

When the same plot was made for the event at ~ 2000 U.T., essentially the same conclusion was reached. The time of electron injection and distance travelled were ~1938 U.T. and ~ 1.65 a.u. respectively.

The times of electron injection at the sun derived from this approach can be compared with the times of optical flares for both events. We find that the electron injection times for both events lie in between the onset times and the times of maximum phase of the associated optical flares. This suggests that these electrons were accelerated near the times of optical flares and that after acceleration, they were immediately released into the interplanetary medium. This is in contrast to the observation of some electron events (Simnett, 1971) in which the accelerated electrons were trapped near the sun over a long time period before being released into the interplanetary space.

4. Energy Spectrum

It is clear from the previous sections that the intensity-time profile of the scatter-free electrons is characterized by velocity dispersion. Therefore, the electron energy spectrum at the point of observation varies from time to time. In order to obtain a meaningful spectrum for these electrons, we must adopt a different method from the one usually employed. Instead of calculating the average electron intensities for all energies over a fixed time interval, we simply integrate the total number of scatter-free electrons for a given event and express the results in terms of electrons/(cm^2-ster-keV). By this approach, we eliminate the difficulty due to velocity dispersion and obtain the electron energy spectrum near the flare site.

Figure 3 shows the scatter-free electron energy spectra derived in this way for the event at ~ 1640 U.T. The observed electrons/(cm^2-ster-KeV) near the ecliptic plane and near the direction normal to the ecliptic plane are respectively represented by open and solid circles. Clearly, the electron intensities from both ecliptic plane and the direction normal to the ecliptic are comparable at high energies. It is also clear that the observed electron spectra near the ecliptic plane for both events is not well represented by the power law of the form $\sim E^{-\gamma}$; there appears to be a flattening in the energy spectra at energies < 600-700 KeV.

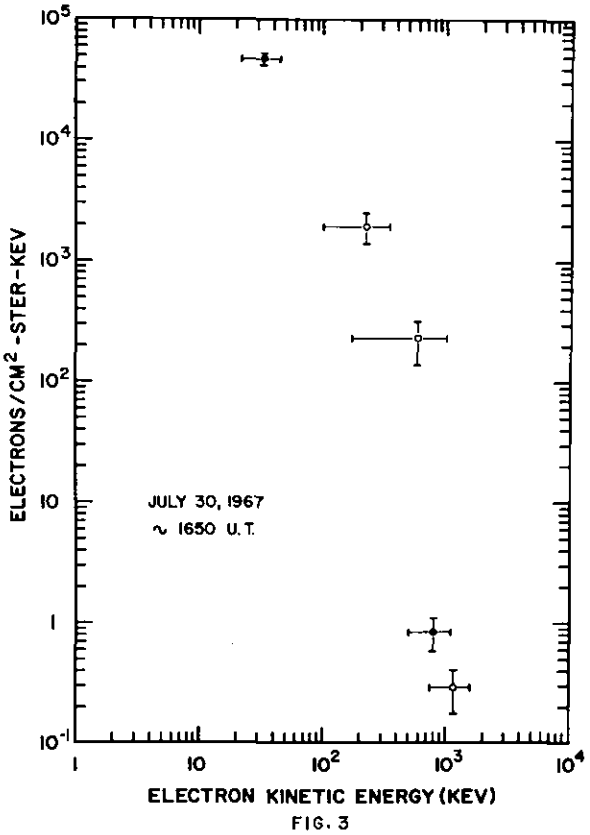

FIG. 3

This flattening in the electron energy spectra at low energies is also implied by the measurements of electrons from the direction normal to the ecliptic plane. For example, if we assume a spectrum of $\sim E^{-\gamma}$ as determined by the two solid data points in

Figure 3 and integrate the total number of electrons above $\sim$ 45 KeV, we obtain $\sim 3\times10^5$ electrons/cm^2-ster. This is $\sim$ 40% lower than the measured total $>$ 45 KeV electrons of $\sim 5.5\times10^5$ electrons/cm^2-ster. Since there are not many electrons with energies $>$ 1000 Kev, this electron excess must come from the energy range of $\sim$ 45-1000 Kev. Thus, it appears that the electron energy spectrum is harder at lower energies. At energies $\gtrsim$ 700-800 kev, γ is $\gtrsim$ 6 if power-law energy spectra are assumed. Both the hardening of electron energy spectrum at low energies and the electron cutoff at energy $\sim$ 700-800 kev is also observed for the event at $\sim$ 2000 U.T. and is probably a general characteristic of the scatter-free electron events.

The electrons of solar origin in the energy range of $\sim$ 0.5-12 MeV have been studied rather extensively by Simnett (1971) These electrons in general displayed a spectrum of the form $\sim E^{-\gamma}$ with $\gamma \simeq 3$; $\gamma > 4$ was observed only when the electrons were stored in solar neighborhood over a long time period or were originated from a backside flare. Datlowe et al. (1970) also reported measurements of solar flare electrons in the energy range of 10-200 Mev. They obtained $\gamma \simeq 3$ for two events on June 9, 1968 and February 25, 1969. The event on July 13, 1968 had a steep energy spectrum of $\sim E^{-6.7}$, but this might be attributed to long-term storage of particles in the corona (Simnett, 1971; Simnett and Holt, (1971). Clearly, all these observations suggest $\gamma \simeq 3$ for normal classical electron events, which is at least a factor of 2 smaller than that for the events we consider in this paper. Since the effect of velocity dispersion is negligible for electrons with energies $\geq$ 0.5 Mev, this difference in γ cannot be due to the different methods used in obtaining the electron energy spectra. Consequently, the electron cutoff at $\sim$ 700-1000 kev appears as a distinct feature of scatter-free electron events which is not shared by the normal classical electron events such as those discussed by Simnett (1971) and Datlowe et al. (1970).

5. Anisotropy

The anisotropy during the pulse-like phase of these events should be $\sim$ 100%. The electrons are all propagating in one direction, out from the Sun, undergoing little or no scattering. The diverging interplanetary magnetic fields will also collimate the pitch angles of the electrons. However, direct measurements of the anisotropy during the two events considered here, from the University of Texas experiment on IMP-IV (Allum, private communication) indicate that the anisotropy is only $\sim$ 30%. Rather than implying that there is a basic inconsistency between the scatter-free nature of these events and their observed anisotropy, we feel that these anisotropy measurements point out the inherent difficulties in making reliable anisotropy measurements from earth orbiting satellites. The bow shock was located quite close to the satellite when these measurements were made, even though the satellite was near apogee (Fairfield, private communication). There was also evidence for high frequency waves upstream from the bow shock of the type reported by Fairfield (1969), (Fairfield, private communication). Scattering of the electrons off the bow shock or by these waves could easily account for the reduced anisotropy.

6. Is Electron Emission Continuous Over a Finite Time Interval?

From a careful analysis of these events, we found that the observed duration times of the scatter-free electrons are $\sim$ 3 min longer than the ones expected from velocity dispersion and are independent of detector energy windows. This suggests that processes other than velocity dispersion must be taken into account. When we assumed a time dependence of continuous electron release near the sun like $\sim e^{-t/to}$ and an energy spectrum shown in Figure 3, we were able to reproduce the intensity-time profiles at the point of observation and compare with the observed profiles. We found excellent agreement between the calculated and the observed intensity-time profiles when the characteristic times, to, were $\sim$ 3 min and $\sim$ 4 min for the events at $\sim$ 1640 U.T. and $\sim$ 2000 U.T. respectively. Therefore, the electron emission near the sun may be continuous over a finite time interval of $\sim$ 3 min for these events.

7. Summary

We have reported a rare class of solar flare particle events in which the electrons were scattered near the earth's bow shock. These electrons travelled only $\sim$ 1.5 AU between the sun and the earth. The differential energy spectrum of these electrons cannot be represented by a power law of the form $\sim E^{-\gamma}$ over the energy range of 20-1600 kev. The durations of the scatter-free component could mostly be accounted for by velocity dispersion. More careful analysis, however, revealed that these electrons might be continuously injected into the interplanetary medium over a finite time interval of $\sim$ 3 min.

8. Acknowledgements

We are grateful to Drs. J. A. Simpson and F. B McDonald for the use of IMP-IV data. Also, we thank D . D. H. Fairfield for providing magnetic field data during the events considered.

9. References

Bryant, D. A., Cline, T. L., Desai, U. D., and McDonald, F. B. 1965. Astrophys. J. 141, 478.
Cline, T. L. and McDonald, F. B. 1968. Solar Phys. 5, 507.
Datlowe, D., L'Heureux, J., and Meyer, P. 1969. Proc. 11th Conf. on Cosmic Rays (Budapest) 2, 644.
Fairfield, D. H 1969. J Geophys. Res. 74, 3541.
Fan, C. Y., Gloeckler, G., and Simpson, J. A. 1966. J. Geophys. Res. 71, 1837.
Lin, R. P. 1970a. Solar Phys. 12, 266.
Lin, R P. 1970b. J. Geophys. Res. 75, 2583.
Lin, R. P. and Anderson, K. A 1966. J. Geophys. Res. 71, 1827.
Simnett, G. M. 1971. Preprint, University of California (Riverside).
Simnett, G. M. and Holt, S S 1971. Solar Phys. 16, 208.
Sullivan, J. D. 1970. Thesis, The University of Chicago.
Wang, J. R. Fisk, L A and Lin, R. P. 1972. to be published.

THE NATURE OF RELATIVISTIC ELECTRON INTENSITY CHANGES DURING SOLAR FLARE QUIET TIMES BETWEEN 1963 AND 1969

F. B. McDonald and T. L. Cline
Goddard Space Flight Center, Greenbelt, Md.

and

G. M. Simnett
Physics Department, University of California, Riverside, Ca.

Abstract

Time variations of the 3-12 MeV interplanetary electron intensity, observed by the IMP-1, -3 and -4 spacecraft between 1963 and 1969, have been studied in detail. Apart from solar flare effects, there are five distinct periods when the electron intensity has undergone a series of increases, and these are strongly correlated with solar rotation. For only one period, in 1966, there is evidence that the intensity changes are recurrent solar electron events. The other intensity increases are a separate phonomenon, and are strikingly anticorrelated with increases in the low energy solar proton intensity. The electron energy spectrum during those non-solar, or "quiet-time" increases is typically represented by $dJ/dE = k\ E^{-2.0 \pm 0.25}$, similar to the galactic electron spectrum. Correlations of the electron intensity with the Deep River neutron monitor show that typically the neutron monitor is increasing through the period of a quiet-time electron increase. The magnitudes of the quiet-time electron intensity increases do not have a large variation, but are between about two and about five times the galactic background intensity seen at the earth. There are, in addition, Forbush decreases in the electron intensity frequently coincident with those in the neutron monitor rate. We conclude that these characteristics all support the hypothesis of a galactic origin for the electrons observed during quiet-time increases.

1. Introduction

The study of the low energy galactic cosmic-ray electron component is of fundamental importance to a variety of topics. Unfortunately, the effects of solar modulation and the presence of solar electrons greatly distort the low-energy galactic electron spectrum. A detailed study of the temporal intensity variations may be one possible means of separating the galactic and solar components, and it should also thereby provide information on the modulation of MeV electrons. With the availability of sophisticated particle detectors on spacecraft operating beyond the magnetosphere, it has been possible to make detailed observations of low energy interplanetary particles over a significant portion of a solar cycle.

An examination of the nucleon and electron data over wide energy intervals reveals two spectra which appear to be similar, each

apparently composed of a two-component structure with a power law at high energies, a plateau or minimum at medium energies, and finally a sharp rise at the lowest energies. Thus, the structure observed in both spectra might appear to be produced by solar modulation. However, the low energy components observed in the two spectra cannot both be explained as of solar origin in such a straightforward manner. In fact, the data to be presented suggest that the origin of the electron intensity enhancement is quite different from that producing the proton increases.

2. Observations

The temporal changes of the 3-12 MeV electrons observed from November, 1963 to September, 1969 can be grouped into five categories:

1) Flare-associated solar electron events: In general, these display the same characteristics as the accompanying solar proton events.

2) Co-rotating Solar Electron Increases: These appear to occur infrequently in the MeV region. They coincide with geomagnetic effects and with roughly simulteneous low energy electron and proton increases.

3) Forbush decreases: These are generally similar to those observed with high-latitude neutron monitors, except that the recovery phase for electrons has a different time profile.

4) The long-term modulation of low energy electrons: The existence of this phenomenon appears likely, but is difficult to establish because of the varieties of large-amplitude short-term intensity variations.

5) Quiet time increases: This new phenomenon is unique to the electron population above 1 MeV. The increases last for periods from a few days to two weeks and can display a 27-day recurrence. The intensity may increase as much as a factor of five above the minimum quite-time level at 1 A. U. The energy spectra of the increases above background are similar to that determined for the galactic component. These events are strikingly anticorrelated with low energy (few-MeV) proton events.

The implication of this picture of interplanetary electron phenomena, including the quite-time increases, the Forbush decreases and the suggestion of an eleven-year modulation, is that the galactic component probably dominates most of the time.

3. Experimental Technique

Observations of the interplanetary 3 to 12 MeV electron intensity have been made with identical detectors on-board four eccentric-orbiting IMP satellites; data were used for analysis from the following time periods, and over the following altitude intervals:

IMP I:	November 27, 1963 - May 5, 1964,	125000 to 193000 km (apogee)
IMP III:	May 30, 1965 - May 4, 1967,	125000 to 250000 km "
IMP IV:	May 24, 1967 - March, 1969,	100000 to 216000 km "
IMP V:	June 21, 1969 - September 24, 1969	100000 to 177000 km "

The energy loss detector in each consists of a 0.1 cm thick x 5.08 cm diameter CsI (Tl) crystal which is operated in coincidence

with a 2 cm thick x 5.08 cm diameter CsI (Tl) crystal, used as a total energy detector for stopping particles. A plastic anticoincidence guard counter surrounds the total energy detector.

The problem of normalizing the data from four different satellites operating over lengthy periods of time with no overlap involves primarily corrections for gain and background changes. The minimum-ionizing line and the end point of the stopping proton distribution provided methods for measuring gain changes, and the background contamination was subtracted using the method described by Simnett and McDonald (1969). A normalization was thereby made possible between time periods covered by the different IMPs. A plot of the daily electron counting rate in a common energy region over the periods treated with this analysis is shown in Fig. 1. The errors on the points are approximately constant and are therefore not individually shown. (The IMP-IV and IMP-V satellites incorporated an additional solid state element, used to obtain daily averages of 3.3 - 5 MeV protons; these data do not reflect the quiet-time level, but the fluctuations are representative of the intensity changes. The degree of anticorrelation of the proton increases with the quiet-time electron increases is significant in the present analysis.)

4. Interpretation of Results

It is evident from Fig. 1 that the electron component shows many types of variations. The flare-associated and recurrence electron increases, the Forbush decreases and possible eleven-year variation are extensions of known particle phenomena. However, there are some 18 or 19 increases occurring during the several-year observing period that appear to represent a new phenomenon. These tend to occur during relatively undisturbed times, so we have labeled them "quiet-time increases". They have the following properties:

(1) They represent a factor of 2 to 5 increase in the 3-12 MeV electron intensity and last about 3 to 14 days. The time history is symmetrical and markedly different from those in flare events. (2) The energy spectra of the increases are in general of a form much closer to the $E^{-1.75}$ obtained when the intensity was relatively constant than to the E^{-3} to E^{-5} of solar events. (3) There is a remarkable anticorrelation with low energy co-rotating proton events. (4) The increases tend to occur during periods of rising neutron monitor intensity. (5) The available evidence suggests there is not a strong dependence on solar activity. (6) The increases frequently display a 27-day periodicity. (7) In general, the increases are contained within a single interplanetary magnetic sector.

Sixteen of the quiet time increases were observed in three groups: 4 in early 1964, 3 in 1965 and 9 during an 8 month period in 1967 to 1968; there was only a single increase in 1966. The Dec. 1968 - Jan. 1969 period also displays several increases of a somewhat different appearance, as discussed later.

The first series of quiet-time increases, observed with IMP-I in early 1964, occurred with peak intensities at 27 $\pm$ 1 day intervals on

February 12, March 11, April 7, and May 3, and possible another in mid-January. (These are the least well defined, due to a lower data rate on that satellite.) This behavior was pointed out originally by Cline et al. (1964), as evidence that the electrons were of galactic or solar origin and not secondaries generated locally in the vicinity of the detector. The University of Chicago experiment on IMP-I observed a series of 4 co-rotating streams of MeV protons. These were contained within a single, positive recurrent interplanetary magnetic sector (Ness and Wilcox, 1965), displaced almost 180° from the electrons.

The next series consists of three well-defined events extending from mid-August through late September, 1965. Two of the events are spaced 27 days apart and the third is interspaced between them. There were three low-energy proton events observed with the University of Chicago detectors, on August 16, September 3, and September 30, and a small flare-associated event on October 4, 1965. The co-rotating proton events are indicated by arrows in Figure 1. Again, the anti-correlation between quiet-time electron events and the low-energy proton increases is most striking. There is no strong correlation either with the neutron monitor data (except for a general increase in the neutrons during the events) or with the direction of the interplanetary magnetic field.

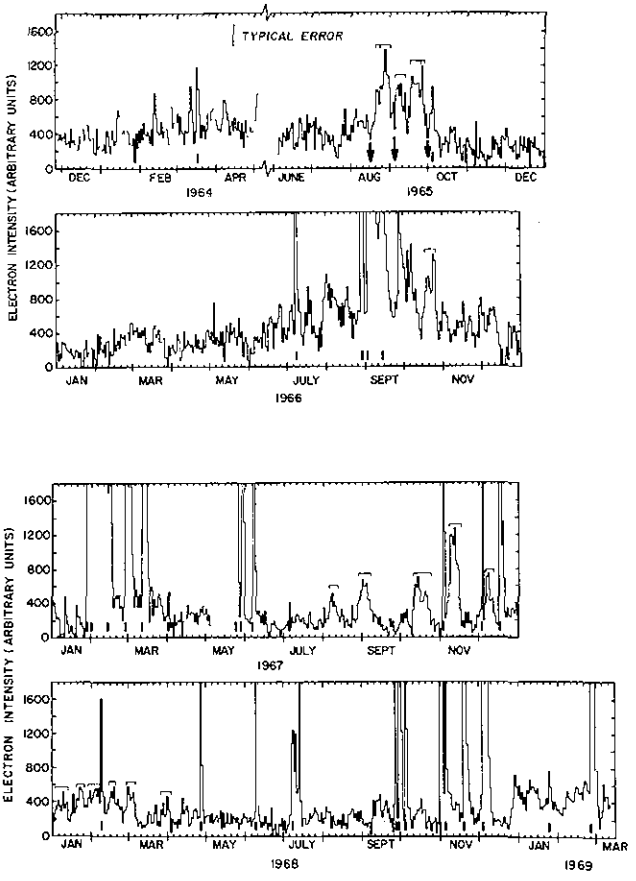

Some nine quiet time increases were observed with IMP-IV between August 1967 and March 1968; they are the most striking of all, and are shown in Figure 2. The first two events, in early August and September are approximately 27 days apart. The next event is centered on October 16, and lasts for some 12 days. The next event is centered on October 16, and lasts for some 12 days. From Nov. 5 to 15, there is a fourth event. (A moderate flare-associated event had occurred on November 2, but the electron intensity had returned to background by November 4.) This quiet time event occurs some 24 days after the October increase. Like the other events in this series the electron peak occurs at a minimum in the flux of low energy protons, although there is some overlap between the declining phase of the electron increase and a low energy proton event. Twenty seven days later the same pattern is reproduced. After a flare event early in December, there is another quiet time increase. Four more small increases occur during the first three months of 1968. Detailed examination shows that again for these nine events the low energy protons and

quiet time increases anticorrelate. In almost every case the centroid of the quiet time increases coincides with a minimum in the MeV proton distribution and most of the quiet time increases occur during periods when the neutron monitor rate is increasing. A comparison of the average profile of the five quiet time increases occurring between August and November with the averaged neutron monitor data, shows an essentially monotonic cosmic-ray increase throughout the electron increase with a later decrease 8 to 9 days after the electron maximum.

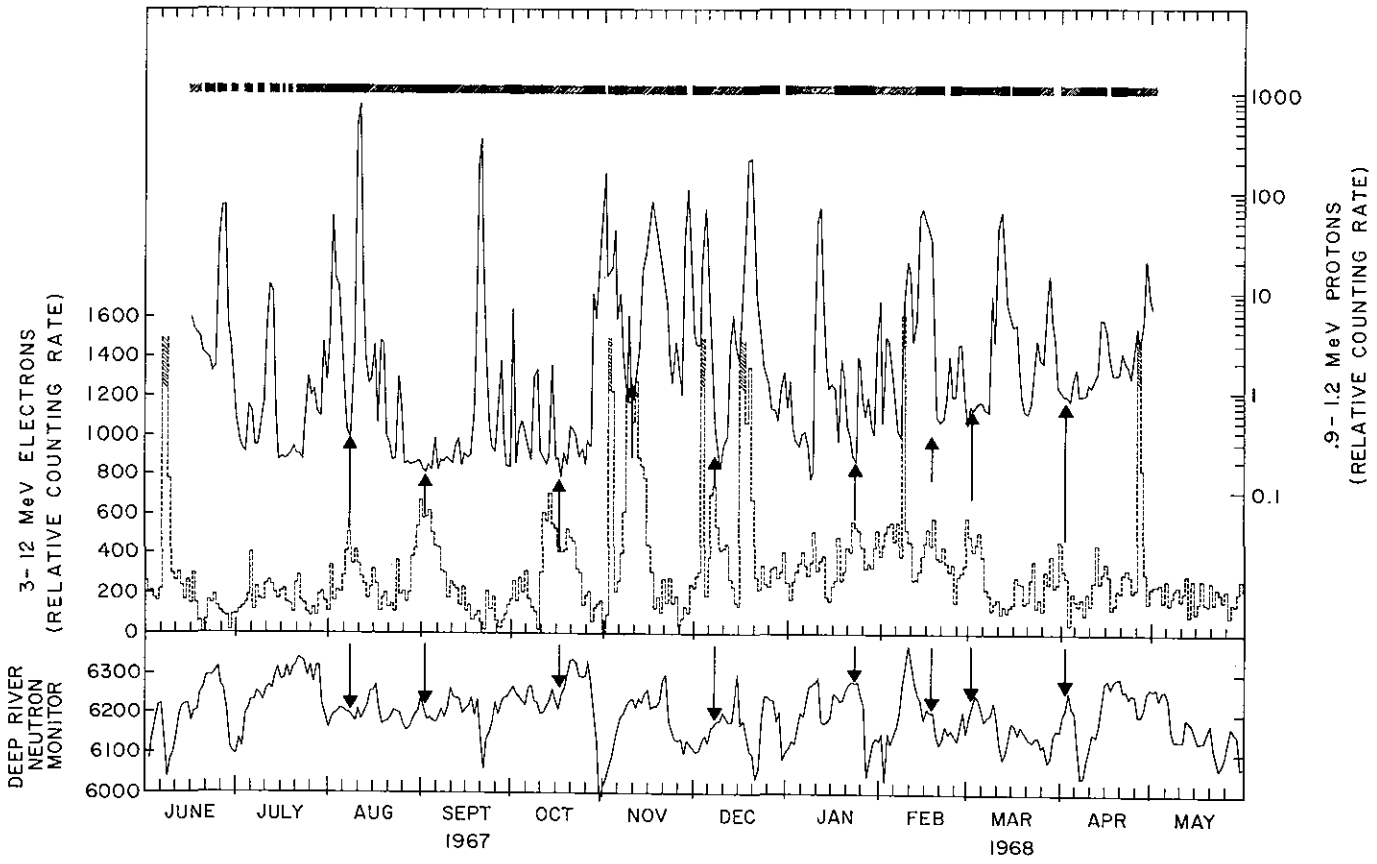

The large quiet time increases in 1965 show the same behavior. If the quiet time electron increases are galactic in origin and are visible because of a temporary change in the modulating mechanism, it might also be expected that the galactic protons also respond to the temporary change. It appears that there is a one week phase lag between the electron and nucleon components.

There are two additional periods which also may contain quiet time increases. A single increase takes place from October 15 to 27, 1966; it appears to be essentially identical to the November 1967 event discussed above. The second period of interest is the interval of December 1968 to February 1969. On December 27 there is a very small event, consistent with an origin on the non-visible disc of the sun.

There is a second increase extending from February 7-15, having an electron energy spectrum of the E^{-2} form, consistent with a quiet time increase. Starting on February 5 there is a steady increase, with some structure, that builds up to the large event of February 25. The energy spectrum suggest that the February 7 peak is a quiet time increase, it also follows some 27 days after the January event. However, the spectral data of the various structural details during this month are not conclusive.

5. Discussion

The low energy electron data suggest that two processes may be occurring in the modulation of galactic particles. The quiet-time increases suggest a sudden increase that takes place on the order of several days, while the 11-year modulation extends over a far larger time scale. Furthermore, during the quiet-time increases, there are no corresponding large increases in the low energy (20-80 MeV) galactic cosmic rays, and only a positive trend is evident in the neutron monitor. One possible resolution of this problem has been suggested by Fisk and Van Hollebeke (1971) who propose that the electron increases are not a result of the variation of electron modulation but rather an increase in the number of electrons that penetrate into a modulating region. One would expect a decrease in the peak intensity of quiet-time increases as solar activity increases if such a two-step process is involved, and this is qualitatively what is observed. In fact, not only is there a decrease in the peak amplitude as one goes from 1965 to 1969, but also the likelihood of occurrence seems to be less at solar maximum.

The question then arises as to whether the observed electrons are "interstellar secondaries" produced by the "knock-on" and $\pi \rightarrow \mu \rightarrow e$ processes or whether one is also observing primary electrons. During the quiet time increases, the observed peak intensity at 3 MeV was 5 times the calculated secondary interstellar intensity (see, e.g. Abraham et al., 1966). This suggests strongly that one must also have galactic "primary electrons" present in the MeV interplanetary electron component. It also makes difficult the determination of the energy dependence of the total modulation of galactic electrons in the inner solar system, or, conversely, of their intensity in the interstellar region.

6. References

Abraham, P.B., Brunstein, K. A. and Cline, T. L. 1966, Phys. Rev. 150, 1088.

Cline, T. L., Ludwig, G. H. and McDonald, F.B. 1964, Phys. Rev. Letters 13, 786.

Fisk, L. and Van Hollebeke, M. 1971, Hobart Conference, accompanying paper.

Ness, N. F. and Wilcox, J. M. 1965, J. Geophys. Res. 70, 5793.

Simnett, G. M. and McDonald, F. B. 1969, Astrophys. J. 157, 1435.

ELECTRONS IN QUIET-TIME INCREASES, SAMPLERS OF CONDITIONS IN THE OUTER SOLAR SYSTEM

L. A. Fisk and M. VanHollebeke*
NASA/Goddard Space Flight Center
Greenbelt, Maryland, USA. 20771

Abstract

An explanation for quiet-time electron increases is proposed which predicts the existence of a modulating region for cosmic ray particles lying at ~ 30 AU from the Sun.

1. Introduction

In the companion paper to this one, McDonald, Cline and Simnett report observations of increases in the intensity of 4-12 MeV interplanetary electrons, which they have labeled "quiet-time electron increases". The electron intensity is observed to increase by a factor ~ 5 over the background intensity of galactic electrons, with a more or less symmetric time profile. The intensity can remain enhanced for of order five days to two weeks, and the events have the curious feature of occurring in anti-coincidence with increases in the low energy solar proton intensity.

In this paper we discuss a possible explanation for quiet-time electron increases. In Section 2 we argue that the electrons in quiet-time increases are galactic in origin, but that the observed increases are not the result of any variation in the modulation of these particles in the inner solar system. We propose instead that quiet-time increases occur when more electrons than normal penetrate a modulating region that lies far beyond the orbit of earth. In Section 3 we discuss some observational evidence that supports this explanation, and in Section 4 we interpret this evidence as indicating, among other things, that the modulating region lies at ~ 30 AU from the Sun.

2. General Information and A Possible Explanation

In Figure 1 we have plotted the daily averages of the 4-12 Mev interplanetary electron intensity reported by McDonald et al. (1971) for the years 1967 through 1968. The quiet-time increases are marked in this figure with brackets. The events marked with dashed brackets are less clear-cut than the others since here it is not as readily established that the electron increase anti-correlates with an increase in the MeV proton intensity, and the increase over the local electron background is quite small.

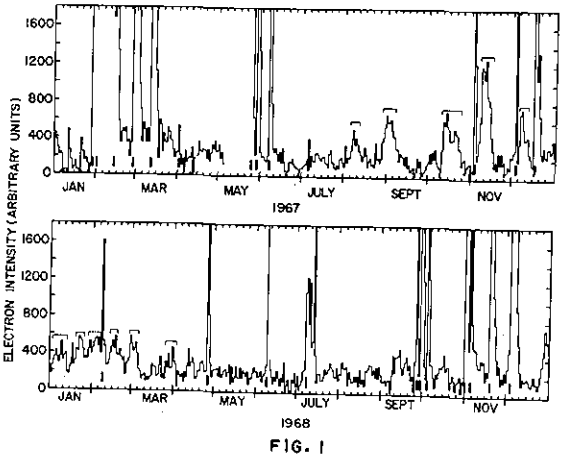

FIG. 1

*ESRO Postdoctoral Research Associate

We argue that the electrons in quiet-time increases are galactic in origin, these events representing localized increases in a general background flux of galactic electrons. Note in Figure 1 that during periods of limited solar activity there is present a relatively steady flux of electrons, which is of course real, detector background having been removed. Although it is hardly a conclusive argument, the steadiness of this background flux is a good indication that we are observing here mainly galactic electrons. A flux of solar electrons should exhibit the high variability characteristic of solar activity. More direct evidence for the galactic origin for the background flux has been obtained recently by Webber and Lezniak (1971) who observe that the radial gradient of the background electron intensity lies somewhere in the range 0-30%/AU. The gradient of a steady flux of solar electrons would be negative and perhaps $\sim$ -200%/AU. We can conclude that quiet-time increases are simply localized increases in this galactic background flux, because the spectral index for the intensity during a quiet-time increase is the same as it is for the background flux. McDonald, et al. (1971) report that this common spectral index is about -2, and thus it defines a flatter spectrum than is observed during flare events (a spectral index $\sim$ -3) or during recurrence events (a spectral index $\sim$ -4 or 5).

We argue also that quiet-time increases are not the result of any variation in the modulation, or scattering conditions, experienced by 4-12 MeV electrons in the inner solar system. Note in Figure 1 that the background flux of galactic electrons is relatively constant from year to year. McDonald et al. (1971) report that the background flux is reduced by a factor < 1.25 from 1965 to 1968, which covers solar minimum conditions to near solar maximum conditions. The evidence is, then, that 4-12 MeV electrons are relatively insensitive to changes in the scattering conditions in the inner solar system. We construe this to indicate that the electrons experience little scattering in the inner solar system, and consequently, we cannot alter these scattering conditions to account for the factor $\sim$ 5 increases observed during quiet-time increases. Evidently, the interplanetary magnetic field is not irregular to any significant degree with a scale-size comparable with the gyro-radius of a 4-12 MeV electron ($\sim$ 7000 km in a 5γ field). It should be noted that it is possible to construct models in which the electron intensity remains time invarient, but there is still appreciable scattering (see Lezniak and Webber, 1971). However, these models cannot account for the small magnitude of the observed gradient, 0-30%/AU (Webber and Lezniak, 1971) which is consistent with little scattering in the inner solar system.

Although 4-12 MeV electrons do not appear to suffer appreciable modulation in the inner solar system, this does not mean necessarily that they suffer little modulation throughout the solar cavity. There could exist a modulating region remotely far beyond the orbit of earth that controls the emission of particles to the inner solar system, permitting more electrons to enter during a quiet-time increase. Presumably, the behavior of the electrons in such a modulating region can be described by a diffusion process with an appropriate diffusion coefficient parallel and perpendicular to the mean field direction. We are clearly not in a position to observe directly changes in the parallel diffusion coefficient that could result in a quiet-time increase since this parameter is determined by irregularities generated locally in the modulating region. However, we may be able to observe directly changes in the perpendicular diffusion coefficient. Jokipii and Parker (1969) have shown that particles

are transported across the mean field direction principally as a result of the stocastic nature of the fields; the particles follow field lines that are random walking about the mean field direction. At the orbit of earth most of the random walk of interplanetary field lines appears to be produced by photospheric turbulence (Jokipii and Parker, 1969). Suppose that photospheric turbulence is the main source of the random walk beyond the orbit of earth, out to and including at least part of the proposed modulating region. Then, when field lines that have experienced an unusually large random walk in the photosphere are carried by the solar wind to the modulating region, more 4-12 MeV electrons (and perhaps other particles) will diffuse across this region, gaining access to the inner solar system and producing a quiet-time increase at earth. Note that since the mean field direction in the modulating region is presumably mainly azimuthal about the Sun, field line random walk will be particularly important for diffusion in the heliocentric radial direction. Clearly we can test the above hypothesis by seeing whether periods of usually large random walk are observed before quiet-time increase, with a delay which is then a measure of the transit time of the solar wind out to the modulating region.

3. Supporting Observational Evidence

In order to establish that there exists a correlation between the occurrence of quiet-time increases and of periods of large field line random walk, we obviously must have a reliable and sensitive measure of how much random walk is taking place. The only direct measure of the random walk is the power at zero frequency in the power spectrum of magnetic field fluctuations (Jokipii and Parker, 1969). However, the errors involved in determining the power at low frequencies are quite large and there is the practical difficulty that power spectra are not available for all the time periods we consider. We suggest instead that a useful measure of the random walk is the amplitude of the diurnal anisotropy, as is observed by neutron monitors. The formula for this amplitude, ξ, during quiet-periods, assuming that there is appreciable diffusion perpendicular to the mean field direction is (Krimsky, 1965; Parker, 1967):

$$\xi = \frac{3CV_{sw}}{v} \frac{(1 - K_\perp/K_\parallel)\tan\Psi}{(1 + K_\perp/K_\parallel \tan^2\Psi)} \qquad (1)$$

Here, $K_\parallel$ and $K_\perp$ are the diffusion coefficients parallel and perpendicular to the mean field direction, respectively, and Ψ defines the angle between the the mean field direction and the heliocentric radial direction. The solar wind speed is given by V_{sw}, the particle speed by v, and $C = (2 + \mu)/3$ is the Compton-Getting factor with μ the spectral index (Gleeson and Axford, 1968). During periods of large random walk, the ratio $K_\perp/K_\parallel$ increases over its average value ~ 0.2 (Jokipii and Parker, 1969). $K_\perp$ depends directly, while $K_\parallel$ inversely, on the power at low frequencies in the power spectra of field fluctuations. Thus, there should exist a direct correspondence between periods of low diurnal anisotropy and periods of large field line random walk.

Using a simple harmonic analysis, we have computed the amplitude of the diurnal anisotropy from the pressure-corrected hourly averages of the counting-rate of the Deep River neutron monitor. We have performed this analysis using the data from the 24 hour period centered on every 12 hours during 1967-1968. The average amplitude during this period was $\sim 0.4\%$ (VanHollebeke, 1971). We consider as low any amplitude $< 0.3\%$. Although continuous data is available

for these years, not all the computed anisotropies are a reliable measure of the random walk. We have eliminated from consideration any amplitude computed when the daily average of the monitor rate varied from day to day by more than 1%, or whose direction was inconsistent with the lack of significant radial streaming assumed in deriving (1).

In Figure 2 we have plotted the amplitudes of the diurnal anisotropy (in %) that are a reliable measure of the random walk during the period January 1967 through April 1968. The plot is divided into Bartels solar rotation periods of 27 days. Shown also in the figure is the sector structure of this interplanetary magnetic field (Fairfield, private communication). Light-shading indicates a sector with fields directed mainly away from the Sun; dark shading, mainly toward. The times when quiet-time increases occur are marked with brackets identical to those shown in Figure 1. The horizontal dashed line markes an amplitude of 0.3%. Any amplitude less than this is considered to indicate a large field line random walk. Note in Figure 2 that quiet-time increases are well-correlated with sector structure in that they do not generally extend over more than one sector. There is one notable exception to this rule, the event of 28 August - 6 September 1967. The main conclusion to draw from Figure 2, however, is that quiet-time increases and periods of low amplitude occur in a pattern. If we trace the sector containing a well-defined quiet-time increase back five solar rotations, then within the sector on the fifth rotation there is an extended period of low amplitude diurnal anisotropy. We do not contend that this pattern is obvious, but rather it can be seen only after considerably study. The eleven quiet-time increases shown in Figure 2 can be divided into categories: (i) for seven of the events there is an extended period of low amplitude anisotropy five rotations earlier, (ii) two of the events are questionable quiet-time increases and have no associated low amplitude period, and (iii) for two of the events we cannot trace the sector back five rotations. In Table 1 we have listed the events in category (i), together with their associated low amplitude periods. Listed also for each of the low amplitude periods are the ratio of the number of amplitudes < 0.3% to the number of amplitudes that are a reliable measure of the random walk, and the number of reliable amplitudes to the total possible amplitudes (2/day for each day of the period).

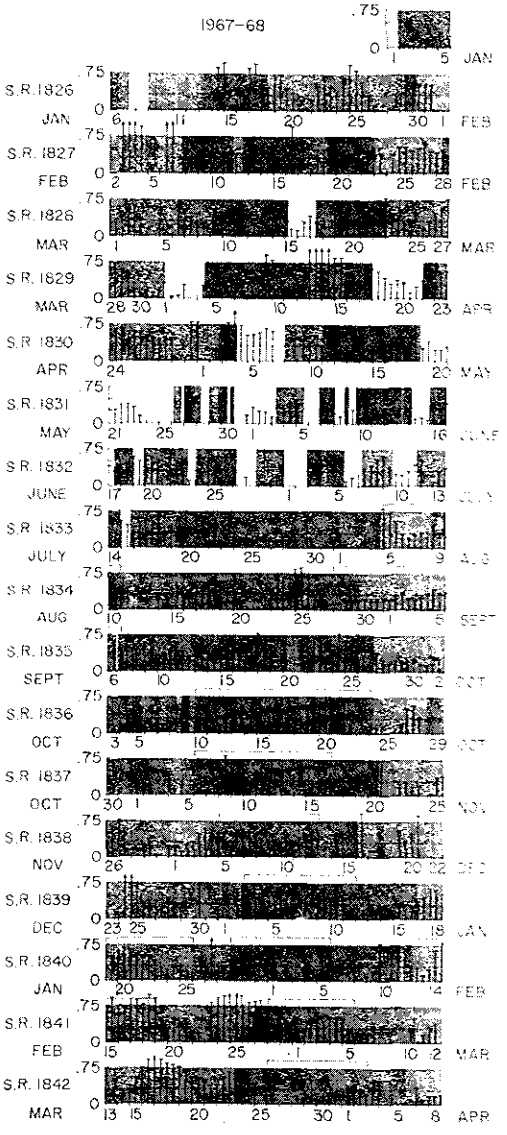

FIG. 2

TABLE 1

Quiet Time Increases	Low Amplitude Periods	Ampl <0.3% / Reliable Ampl.	Reliable Ampl. / Total Ampl.
10-23 Oct. 1967	31 May-9 June 1967	71(%)	70(%)
6-16 Nov. 1967	26 June-7 July 1967	100	30
5-12 Dec. 1967	23 July-3 Aug. 1967	100	54
19-25 Jan. 1968	30 Aug.-4 Sept. 1967	83	100
13-18 Feb. 1968	28 Sept.-3 Oct. 1967	91	91
28 Feb.-5 March 1968	10-17 Oct. 1967	71	87
26 March-2 April 1968	10-20 Nov. 1967	73	68

Only for the second event is there insufficient data to establish convincingly that there is an associated low amplitude period, although all the data available for the period have an amplitude $< 0.3\%$. On averaging over the remaining six events, 82% of the reliable amplitudes are $< 0.3\%$. Compare this with the percentage of reliable amplitudes $< 0.3\%$, computed using the data from the entire period January 1967-April 1968, of only 41%. The two events in category (ii) are 3-11 January 1968 and 29 January-5 February 1968. If these events are in fact due to an increase in the flux of galactic electrons, as opposed to solar electrons, we suggest that they are only the remnants of the well-defined increases that occurred in the same sector on the three previous rotations. The two events in category (iii) are 5-10 August 1967 and 28 August-6 September 1967. Although the sector containing these increases cannot be traced back to locate the associated low amplitude period, we can establish, by examining solar magnetogram data, that the sector probably existed for the required five rotations, lying out of the ecliptic.

4. Interpretation

These observations support the contention made in Section 2, viz., when field lines that have experienced an unusually large random walk in the photosphere are carried by the solar wind out to a modulating region beyond the orbit of earth, more 4-12 MeV electrons penetrate this region and propagate into the inner solar system, producing a quiet-time increase at earth. The transit time of the solar wind from the orbit of earth to the location of the modulating region accounts for most of the delay of five rotations between the occurrence of the low amplitude period and of the quiet-time increase. The modulating region, then, must lie at $\sim$ 30 AU from the Sun, assuming that the average solar wind speed is constant over this distance at $\sim$ 400 km/sec. The transit time of the electrons in from $\sim$ 30 AU must be short compared with one solar rotation, since within this time the electron intensity seen at earth appears to respond to changes in the modulating region. These observations imply, of course, that interplanetary field lines (at least those on which quiet-time increases occur) are continuous out to $\sim$ 30 AU. They can also be used to show that sector structure is essentially preserved out to $\sim$ 30 AU. The limit we can place on the random walk of field lines due to interplanetary turbulence, by noting that this random walk must always be less than that due to photospheric turbulence, suggests that interplanetary turbulence is not sufficient out to $\sim$ 30 AU to destroy the overall sector pattern.

Finally, consider the observed anti-correlation between quiet-time increases and increases in the low energy solar proton intensity (McDonald et al., 1971). The electron increases should occur independently of any proton increase. A quiet-time increase depends on solar conditions five solar rotations preceding the observed event, whereas an increase in the proton flux depends on concurrent solar conditions. However, the interplanetary magnetic field during the large proton increases in late 1967, the period when the anti-correlation is most evident (see McDonald et al., 1971) are quite disturbed and show evidence for loop structures. Thus, electrons propagating in from ~ 30 AU may be excluded from connecting onto the field lines where the proton increases occur.

5. References

Gleeson, L. J., and W. I. Axford. 1968. Astrophys. Space Sci., 2, 431.

Jokipii, J. R., and Parker, E. N. 1969. Astrophys. J., 155, 777.

Krimsky, G. F. 1965. Proc. 9th Internat. Conf. Cosmic Rays 1, 197.

Lezniak, J. A., and Webber, W. R. 1971. J. Geophys. Res., 76, 1605.

McDonald, F. B., Cline, T. L., and Simnett, G. M. 1971. Proc. 12th Internat. Conf. Cosmic Rays.

Parker, E. N. 1967. Planet Space Sci., 15, 1723.

VanHollebeke, M. 1970. Etude de la Variation Diurne Renforcee du Rayonnement Cosmique, Ph.D. Thesis, University of Paris.

Webber, W. R., and Lezniak, J. A. 1971. Bull. Am. Phys. Soc., 16, 566.